2017

Nanomaterials based electrochemical approaches for biosensing and bacterial disinfectio

Adhikari, Bal Ram

Nanomaterials Based Electrochemical Approaches for Biosensing and Bacterial Disinfection

By

Bal Ram Adhikari

A thesis submitted in conformity with the requirements for the Degree of
Doctor of Philosophy in Biotechnology
Faculty of Science and Environmental Studies
Lakehead University

Abstract

Electrochemical approaches to myriad medical and environmental challenges are highly attractive due to their strong potential for extensive and green applications. Point of care diagnostics through the electrochemical monitoring of clinically and environmentally relevant molecules are gaining attraction due to their low cost and simple fabrication procedures. The development of highly stable and sensitive electrochemical sensors/biosensors, for a wide variety of biomolecules in actual samples, makes these methods alternative analytical tools in different pharmaceutical and hospital laboratories. Electrochemical biocatalysis is an additional promising area to address the removal of bacteria for the generation of safe potable water. As the world's population is dealing with lack of access to safe drinking water, photoelectrocatalysis has been investigated as a very efficient technique for the destruction of pathogenic bacteria in water. Nanomaterials with dimensions of less than 100 nm have great potential to enhance the performance of electrochemical methods, due to their excellent electronic, mechanical, and thermal properties. These materials have the capacity to greatly enhance biocatalytic activity, and thus greatly improve the performance of electrochemical sensors/biosensors. This remarkable improvement in bacterial catalysis has been studied using a novel synergistic approach, which incorporates both photocatalysts and electrocatalysts.

For my PhD thesis, we designed a high-performance electrochemical sensor based on graphene for the sensitive detection of acetaminophen, valacyclovir, and mixtures thereof. This sensor was fabricated through the concurrent electrochemical reduction and deposition of graphene oxide (GO) onto a glassy carbon electrode (GCE) using cyclic voltammetry (CV). The electrocatalytic properties of the electrochemically reduced graphene (ERG) for the oxidation of acetaminophen were analyzed via cyclic voltammetry (CV), differential pulse voltammetry, (DPV) and chronoamperometry. For comparison, various ERG/GCEs were prepared under different electrodeposition cycles to optimize the required quantity of ERG. Our experimental results indicated that the optimized ERG/GCE possessed robust activity toward the electrochemical oxidation of acetaminophen, valacyclovir, and their mixture, leading to the development of a highly sensitive electrochemical sensor for its detection. An extremely low detection limit of 2.13 nM for acetaminophen, and 1.34 nM for the exclusive detection of valacyclovir was achieved. A wide linear detection range of from 5.0 nM to 800 μM was

achieved via the combination of an amperometric technique and DPV. The developed electrochemical sensor was further employed for the determination of acetaminophen, valacyclovir, and their mixture in human serum, with excellent recovery, ranging from 96.08% to103.2%. The fabricated electrochemical sensor also demonstrated high selectivity, stability and reproducibility.

We investigated a novel enzyme entrapment approach utilizing a cationic polymer for the detection of ethanol. Entrapment is one of the primary approaches for enzyme immobilization; however, it suffers from a few critical drawbacks, including leakage and high mass transfer resistance to substrates. To address these challenges, herein we report on a new facile and effective enzyme entrapment platform utilizing a special cationic polymer, poly(2-(dimethylamino)ethyl methacrylate) (MADQUAT) on a nanohybrid single-wall carbon nanotube/reduced graphene oxide (SWCNT–rGO) thin film. The ethanol biosensor developed in this study exhibited rapid response, wide linearity range, high sensitivity (26.27 μA mM^{-1} cm^{-2}), a remarkably low limit of detection (0.16 μM), high selectivity, and high stability. The optimized biosensor was further tested with actual samples including wine, beer, and blood alcohol, and demonstrated promising analytical and biomedical applications.

The increasingly serious issue of lack of access to clean potable water globally is of great concern. The high costs associated with the purchase and operation of water treatment facilities hinders access to clean water for entire populations. Herein, we report on an efficient and cost-effective approach for the remediation of *E. coli* (as model organism), through a combination of photochemistry and electrochemistry enabled by a bifunctional electrode. The bifunctional electrode utilizes titanium (Ti) as the substrate, nanoporous TiO_2 as a photocatalyst, and RuO_2 nanoparticles as an electrocatalyst. A high disinfection rate at 0.62 min^{-1}, with >99.999% of bacterial removal within 20 min has been achieved using this TiO_2/Ti/RuO_2 bifunctional electrode. Complete bacterial disinfection was attained within a 30 min electrochemical treatment, as assessed by a spread plate method. Further, the bifunctional disinfection mechanism was investigated through protein concentration leakage, total organic carbon mineralization, and metabolomics analysis. A major loss of vital metabolites occurred over a period of 20 to 30 min, which suggested the mass inactivation of *E. coli* within this treatment duration. The novel strategy for the integration of advanced electrochemical oxidation and photochemical degradation via the bifunctional electrode system developed in this study has

strong potential to be utilized as an environmentally compatible technology for water purification and wastewater treatment.

Simple and robust electrochemical approaches utilizing novel nanomaterials have been developed for the sensing of biomolecules and water disinfection. Carbon based nanomaterials and nanocomposites were employed to develop sensitive electrochemical sensor/biosensors, and nanoporous TiO_2/RuO_2 bifunctional materials were utilized for the design of a high-performance bacterial disinfection technology.

This thesis is dedicated to my parents *Bishnu Prasad Adhikari* and *Narmada Adhikari,* my beautiful wife *Trishna Kandel* and my adorable daughter *Prajna Adhikari*

Acknowledgements

First of all, I would like to express my sincere gratitude to my supervisor Dr. Aicheng Chen for his continuous guidance, help and efforts put on me to complete this thesis. I would not able to carry out this level of work without his wisdom and insight. I have not only learned from him to be a better PhD scholar but also a better human being. He has enlightened me through his immense knowledge in electrochemistry and its utilization in biology during my research work. I highly appreciate all his contributions, ideas, and funding to complete my Ph.D. I would like to express my equal gratitude to my co-supervisor Dr Heidi Schraft for her immense help and guidance to complete my thesis. I would not able to carry out all biology work and compilation of electromicrobiology without her understandings and insight. Besides my supervisors, I would like to thank my thesis committee member: Dr. Neelam Khaper for her encouragement and insightful comments. I also would like to thank Dr. Wely Floriano, the coordinator of PhD Biotechnology programme for her great help.

I also thankful to all the current and former lab members of Dr. Aicheng Chen's research group, Dr. Guosheng Wu, Dr. Sapanbir Thind, Jiali Wen, Dr Maduraiveeran Govindhan, Md. Nur Hossain, Dr Boopathi Sidhureddy, Dr. Zhonggang Liu, Venkateshsubramanian Manikandan, Brennan Mao, Antony Raj Thiruppathi for their friendship and collaborations. I also would like to thanks Michael Moore from Department of Biology for his support during my lab work and Dr. Brenda Magajna, programm facilitator, from Science and Environmental Studies PhD Programs for her administrative support. I am equally thankful to all faculty and the staff members of Department of Chemistry, Department of Biology and Instrumentation Lab for their support and encouragement.

Finally, I am thankful to my loving parents for their unconditional love and encouragement. I am equally thankful to my elder sister and brother for their encouragement and inspiration. Last but not least, my biggest thanks to my wife and beautiful daughter for their love and support.

Table of Contents

List of Figures

List of Tables

List of Abbreviations and Symbols

Ar	Argon
ERG	Electrochemically reduced graphene
rGO	Reduced graphene oxide
CV	Cyclic voltammetry
DPV	Differential pulse voltammetry
ADH	Alcohol dehydrogenase
MADQUAT	poly(2-(dimethylamino)ethyl methacrylate)
SEM	Scanning electron microscopy
I	Current
I_{max}	Maximum current
I_p	Peak current
I_{ss}	Steady state current
K_m	Michaelis–Menten constant
DMSO	Dimethyl sulfoxide
EDS	Energy-dispersive X-ray spectroscopy
ATCC	American type culture collection
TOC	Total organic carbon
DNA	Deoxyribo nucleic acid
UV	Ultraviolet
UV-Vis	Ultraviolet visibile

Chapter 1: Introduction

The growing demands of an increasing global population have spurred the development of miniaturized environmentally compatible devices for the health care industry. Electrochemistry offers promising nanomaterials based green approaches for biosensing and the removal of contaminants to preserve human health and the environment. In recent decades, interest in electrochemical approaches has increased significantly due to their portability, simple operation, cost effectivenes, sensitivity, and easy in-situ procedures. Various electrochemical devices, such as amperometry, potentiometry, galvanometry, and electrochemical impedance spectroscopy provide broad applications for the detection and removal of targeted biological molecules.

1.1. Electrochemical approaches for biosensing and disinfection

Electrochemistry provides a powerful platform for sensing and biosensing environmentally and clinically relavant small molecules. The detection of vital biomarkers, including nucleic acids and proteins is key toward the elucidation and development of clinical diagnostics.[1] Clinical diagnosis in non-hospital settings are gaining increased popularity due to their low cost, easy operation, and onsite results. Non-hospital point of care (POC) diagnoses comprises one of the primary activities that may be readily performed by caregivers and patients in the home setting. Electrochemical methods ideally fulfill all of the POC diagnostic requirements in clinical, as well as environmental settings. Sensors are devices which capture the physical, chemical, and biological changes, and convert these changes into measurable signals. A variety of electrochemical methods have been explored for the sensing of chemical contaminants and biomolecules.[2-4] Typically, voltammetric techniques such as cyclic voltammetry (CV), linear sweep voltammetry (LSV), differential pulse voltammetry (DPV), square wave voltammetry

(SWV), amperometric and potentiometric techniques, and electrochemical impedance (EIS) techniques are utilized in the determination of analytes.

1.1.1. Electrochemical sensors/biosensors

Electrochemical sensors and biosensors have attracted considerable attention for the sensitive detection of a variety of biological and pharmaceutical compounds. Since the discovery of carbon-based nanomaterials, including carbon nanotubes, C60 and graphene, they have garnered tremendous interest for their potential in the design of high performance electrochemical sensor platforms due to their exceptional thermal, mechanical, electronic, and catalytic properties. Carbon nanomaterial-based electrochemical sensors have been employed for the detection of various analytes with rapid electron transfer kinetics.

Non-enzymatic electrochemical sensors have been widely employed for the determination of environmentally and clinically relevant compounds. Non-enzymatic electrocatalysis ensures the direct oxidation of analytes on the electrode surface. The sensor materials impart a physically powerful effect on the electrocatalytic properties of the electrodes and determine the performance of these sensors. Enzymatic biosensors are difficult to produce due to their complex modification procedures and specific microenvironment conditions while non-enzymatic electrochemical sensors are gaining popularity due to their simple modification procedures and high stability. Enzyme-free electrochemical sensors have been widely used for determining the presence of hydrogen peroxide, glucose, dopamine, and other drug molecules.[5,6]

Electrochemical biosensors contain biological recognition elements (e.g., enzymes, proteins, antibodies, whole bacterial cells, nucleic acids etc.), which react with target analytes to generate an electrical signal. Electrochemical enzymatic biosensors contain substrate-specific

enzymes that have very sensitive interactions with electrochemical transducers.[7] An ideal electrochemical biosensor should meet the following criteria.[8]

- The biocatalyst must be highly specific for the purposes of the analysis, be stable under normal storage conditions, and show a low variation between assays.
- The response should be accurate, reproducible, and linear over the concentration range of interest.
- If the biosensor is to be employed for invasive monitoring in clinical applications, the probe must be miniaturized and biocompatible; having no toxic or antigenic effects.
- The complete biosensor should be cost effective, small, portable, and capable of being used by semi-skilled operators.

Enzyme immobilization strategies comprise the major rate determining step toward the development of high-performance enzymatic biosensors, as they affect enzyme loading and bioactivity. To date, a variety of immobilization techniques have been investigated to achieve optimum enzyme activity, such as the covalent binding of enzymes with biological linkers, or enzyme entrapment via matrix or other conductive polymers. The development and orientation of nanomaterials provides excellent opportunities for decorating and enhancing enzyme activities; hence, their functionality and applications play a pivotal role in immobilization strategies.[7]

1.1.2. Electrochemical disinfection

Rapid and energy-efficient water disinfection strategies are urgently required to address the global challenges related to energy and water scarcity.[9-13] Electrochemical water disinfection may be defined as the eradication of microorganisms through the use of an electric current that is

passed through the water under treatment by means of suitable electrodes.[14] Traditional treatment methods such as chlorine disinfection have played an influential role in the removal of waterborne pathogens. However, disinfection by-products (DBPs) that are released during chlorination make the entire process undesirable for disinfection. Electrochemical water disinfection approaches provide green, by-product-free treatment methods that may quickly inactivate waterborne pathogens without altering the natural qualities of the water itself.

1.2. Application of nanomaterials

Remarkable achievements in nanotechnology and nanoscience have enabled the use of nanomaterials in diverse areas such as drug delivery, novel therapeutic treatments, tissue engineering, and small molecule detection.[15] Nanomaterials have the capacity to significantly enhance electrochemical signals, thereby increasing the sensitivity and selectivity of electrochemical sensors and biosensors. Nanoparticles and nanocomposite materials will play a critical role in the fabrication of high-performance electrochemical sensing platforms for the detection of target molecules. Functional nanomaterials may induce synergistic effects, involving catalytic activity, conductivity, and biocompatibility, which can accelerate signal transduction.

Recent design and use of carbon nanomaterials, primarily single-walled carbon nanotubes (SWCNTs), reduced graphene oxide (rGO), SWCNTs-rGO, Au nanoparticle-rGO nanocomposites, and buckypaper as sensing materials for the electrochemical detection of some representative biological and pharmaceutical compounds such as methylglyoxal, acetaminophen, valacyclovir, β-nicotinamide adenine dinucleotide hydrate (NADH), and glucose. Furthermore, the electrochemical performance of SWCNTs, rGO, and SWCNT-rGO for the detection of acetaminophen and valacyclovir was comparatively studied, revealing that SWCNT-rGO

nanocomposites possess excellent electrocatalytic activity in comparison to individual SWCNT and rGO platforms.[4]

Different nanostructured materials and composites, with myriad dimensions and morphologies have been synthesized and utilized in the fabrication of enzymatic and non-enzymatic sensors. The most important nanotechnology based clinical strategies include DNA detection, biomarker discovery, cancer diagnosis, and pathogen detection. Carbon based nanomaterials (e.g., carbon nanotubes, fullerenes, graphene) are the most widely used in electroanalytical and electrocatalytic sensing applications. The capacity for carbon based nanomaterials to enhance electron transfer during electrochemical reactions makes these materials an ideal choice for electroanalytical applications. Noble metal nanoparticles have already been proven to be one of the most important classes of nanomaterials for biosensing approaches, as well as in other biomedical applications.[16,17] The growing need for analytical devices that require smaller sample volumes, decreased power consumption, and improved performance, are potent incentives behind the rapid growth in nanomaterials research.[18]

Nanotechnology offers a variety of promising solutions to filter out contaminants such as organic and inorganic solutes; heavy metals such as mercury, lead, arsenic, and cadmium; and waterborne pathogens causing cholera and typhoid. Existing water purification technologies have many limitations, whereas nanotechnology contributes a scaffold for offering the rapid removal of contaminants at low cost. Nanophotocatalysts can chemically break down the organic contaminants and are self-regenerating; hence, they can be used repeatedly. Different nanomaterials such as ZnO, TiO_2, ZnO-CeO_2, Degussa P_{25}, and TiO_2 NPs play an important role in the photodegradation of contaminants, whereas photocatalysis and electrocatalysis have been gaining considerable attention due to their promising applications in water disinfection and the

remediation of hazardous waste.[19-21] When a photocatalyst absorbs light, it generates electron-hole pairs and thus generates electrons and holes that eventually react with water and dissolved oxygen to produce reactive oxygen species (ROS). These ROS, such as the hydroxyl radicals, peroxides, singlet oxygen and superoxides, are potent oxidizing agents, which can inactivate pathogens by damaging vital macromolecules.[22,23] For photocatalytic treatments, titanium dioxide (TiO_2) is considered as one of the most promising photocatalysts due to its low cost, high photocatalytic activity, and chemical stability.[24,25]

1.3. Dissertation rational and scope

The application of advanced electrochemical approaches in biomedical, pharmaceutical and environmental sensing and bacterial catalysis has increased as a result of their enhanced sensitivity, specificity and simple use, to provide quick, cost-effective and repeatable measurements using miniaturized and portable devices. The primary aim of this dissertation is to explore the different aspects of nanomaterials toward the development of sensitive electrochemical methods of biosensing and the removal of bacterial contaminants from water. In the following chapters, detailed work is discussed in regard to the synthesis of carbon-based nanomaterials and their primary applications for the sensing and biosensing of different biomolecules, followed by the development of a bacterial disinfection strategy. In Chapter 2, a comprehensive literature review is presented as relates to the evolution of nanomaterials based electrochemical sensors, as well as biosensors for different target biomolecules. Various electrochemical based bacterial disinfection strategies are also discussed. In Chapter 3, detailed electrochemical methodologies, electrode fabrication methodologies and characterization are discussed for biosensing and disinfection strategies.

The primary research objectives of this thesis were to:

(1) Study the synthesis, characterization and optimization of carbon based nanomaterials to design electrochemical sensors and biosensors targeting different biomolecules.

(2) Study the preparation and analytical performance of reduced graphene oxide (rGO) towards detection of acetaminophen

(3) Optimize graphene oxide concentration and deposition cycle for sensitive and simultaneous detection of valacyclovir and acetaminophen.

(4) Further explore the electrocatalytic behaviour of rGO and its nanocompoiste in combination with single walled carbon nanotubes (SWCNTs) to be used as a substrate for enzyme immobilization for the fabrication of a high-performance electrochemical biosensor.

(5) Investigate the synergistic effects of a photocatalyst (nanoporous TiO_2) and electrocatalyst (RuO_2) to construct a bifunctional electrode for a bacterial disinfection strategy.

We are attempting to develop electrochemical sensors/biosensors through the utilization of new approaches, reducing production costs while broadening application areas. Carbon based nanomaterials (e.g. graphene oxide and single walled carbon nanotubes) were selected in my research due to their exceptional thermal, mechanical and electronic properties. I have successfully developed a sensor for the detection of acetaminophen utilizing graphene nanomaterials. The detailed work of graphene based electrochemical sensor is discussed in chapter 4. The fabrication of sensors with graphene has been achieved through one step electrochemical reduction and the deposition of graphene oxide (GO) on an electrode surface, which is a green approach in contrast to chemical methods of reduction. This new approach allows us to fabricate novel sensors with a small volume of graphene for the detection of drug compounds in clinical settings.

In chapter 5, I studied the different parameters of graphene oxide for the selective and sensitive detection of valacyclovir and its mixture with acetaminophen. Focus was on different optimization parameters including concentration and electrodeposition cycle of graphne oxide to achieve optimum electrocatalytic acitivity on drug molecules. New and exciting properties of reduced graphene oxide (rGO), were explored further, and I have prepared a novel nanohybrid material with single walled carbon nanotubes (SWCNTs). I have studied the electrocatalytic behaviour of this rGO-SWCNTs nanohybrid film with acetaminophen and valacyclovir. The nanohybrid material showed a very high electrocatalytic response in comparison to individual rGO and SWCNTs. This work has been published as an invited feature article,[26] but is not included in the thesis.

The application of the rGO-SWCNTs nanohybrid has been further explored for its biocompatibility and biosensing properties, as described inchapter 6. The rGO-SWCNTs nanohybrid film was used for an enzyme immobilization strategy for the sensitive detection of ethanol. The enzyme immobilization strategy was based on a cationic polymer employing alcohol dehydrogenase (ADH) as model enzyme. We have studied biocompatibility properties of the rGO-SWCNTs nanohybrid through FTIR and found highly compatible without inducing any structural changes to the enzyme.

In an attempt to broadening the application of nanostructured materials, a new approach of combining two nanostructred materials (bifunctional) was studied to determine whether they would allow for synergistic enhancements. Chapter 7 discusses the fabrication of a bifunctional electrode constructed with nanoporous TiO_2 as the photocatalyst, and RuO_2 as the electrocatalyst and its application for efficient bacterial disinfection. SEM images of the TiO_2 revealed a highly ordered nanoporous structure. The bifunctional electrode exhibited very high activity in contrast

to individual nanoporous TiO_2 and RuO_2 which confirmed the synergistic electronic effect of the bifunctional electrode.

Finally, chapter 8 closes with the thesis conclusion and future prospectus.

References

(1) Labib, M.; Sargent, E. H.; Kelley, S. O. Electrochemical methods for the analysis of clinically relevant biomolecules. *Chem. Rev.* **2016,** *116* (16), 9001.

(2) Kirsch, J.; Siltanen, C.; Zhou, Q.; Revzin, A.; Simonian, A. Biosensor technology: recent advances in threat agent detection and medicine. *Chem. Soc. Rev.* **2013,** *42* (22), 8733.

(3) Tang, D.; Tang, J.; Su, B.; Chen, G. Ultrasensitive electrochemical immunoassay of staphylococcal enterotoxin B in food using enzyme-nanosilica-doped carbon nanotubes for signal amplification. *J.Agr. Food Chem.* **2010,** *58* (20), 10824.

(4) Xu, R.-X.; Yu, X.-Y.; Gao, C.; Liu, J.-H.; Compton, R. G.; Huang, X.-J. Enhancing selectivity in stripping voltammetry by different adsorption behaviors: the use of nanostructured Mg–Al-layered double hydroxides to detect Cd (II). *Analyst* **2013,** *138* (6), 1812.

(5) Chen, X.; Wu, G.; Cai, Z.; Oyama, M.; Chen, X. Advances in enzyme-free electrochemical sensors for hydrogen peroxide, glucose, and uric acid. *Microchim. Acta* **2014,** *181* (7-8), 689.

(6) Miao, Y.; Ouyang, L.; Zhou, S.; Xu, L.; Yang, Z.; Xiao, M.; Ouyang, R. Electrocatalysis and electroanalysis of nickel, its oxides, hydroxides and oxyhydroxides toward small molecules. *Biosens. Bioelectron.* **2014,** *53*, 428.

(7) Zhu, C.; Yang, G.; Li, H.; Du, D.; Lin, Y. Electrochemical sensors and biosensors based on nanomaterials and nanostructures. *Anal. Chem.* **2014,** *87* (1), 230.

(8) Grieshaber, D.; MacKenzie, R.; Voeroes, J.; Reimhult, E. Electrochemical biosensors-sensor principles and architectures. *Sensors* **2008,** *8* (3), 1400.

(9) Shannon, M. A.; Bohn, P. W.; Elimelech, M.; Georgiadis, J. G.; Marinas, B. J.; Mayes, A. M. Science and technology for water purification in the coming decades. *Nature* **2008,** *452* (7185), 301.

(10) Schwarzenbach, R. P.; Escher, B. I.; Fenner, K.; Hofstetter, T. B.; Johnson, C. A.; Von Gunten, U.; Wehrli, B. The challenge of micropollutants in aquatic systems. *Science* **2006,** *313* (5790), 1072.

(11) Logan, B. E.; Elimelech, M. Membrane-based processes for sustainable power generation using water. *Nature* **2012,** *488* (7411), 313.

(12) Liu, C.; Xie, X.; Zhao, W.; Yao, J.; Kong, D.; Boehm, A. B.; Cui, Y. Static electricity powered copper oxide nanowire microbicidal electroporation for water disinfection. *Nano lett.* **2014,** *14* (10), 5603.

(13) Liu, C.; Xie, X.; Zhao, W.; Liu, N.; Maraccini, P. A.; Sassoubre, L. M.; Boehm, A. B.; Cui, Y. Conducting nanosponge electroporation for affordable and high-efficiency disinfection of bacteria and viruses in water. *Nano Lett.* **2013,** *13* (9), 4288.

(14) Kraft, A. Electrochemical water disinfection: a short review. *Platin. Met. Rev.* **2008,** *52* (3), 177.

(15) Smith, D. M.; Simon, J. K.; Baker Jr, J. R. Applications of nanotechnology for immunology. *Nat. Rev. Immunol.* **2013,** *13* (8), 592.

(16) Kwon, S. J.; Bard, A. J. DNA analysis by application of Pt nanoparticle electrochemical amplification with single label response. *J. Am. Chem. Soc.* **2012,** *134* (26), 10777.

(17) Arvizo, R. R.; Bhattacharyya, S.; Kudgus, R. A.; Giri, K.; Bhattacharya, R.; Mukherjee, P. Intrinsic therapeutic applications of noble metal nanoparticles: past, present and future. *Chem. Soc. Rev.* **2012,** *41* (7), 2943.

(18) Chen, A.; Chatterjee, S. Nanomaterials based electrochemical sensors for biomedical applications. *Chem. Soc. Rev.* **2013,** *42* (12), 5425.

(19) Yang, S.; Li, J.; Shao, D.; Hu, J.; Wang, X. Adsorption of Ni (II) on oxidized multi-walled carbon nanotubes: effect of contact time, pH, foreign ions and PAA. *J Hazard. Mater.* **2009,** *166* (1), 109.

(20) Humplik, T.; Lee, J.; O'hern, S.; Fellman, B.; Baig, M.; Hassan, S.; Atieh, M.; Rahman, F.; Laoui, T.; Karnik, R. Nanostructured materials for water desalination. *Nanotechnology* **2011,** *22* (29), 292001.

(21) Doroodmand, M. M.; Tahvildar, Z.; Sheikhi, M. H. Multi-Walled Carbon Nanotubes/Polyacrylonitrile Composite as Novel Semi-Permeable Filter for Water Treatment Process. *Sci. Adv. Mater.* **2012,** *4* (10), 1085.

(22) Malato, S.; Fernández-Ibáñez, P.; Maldonado, M. I.; Blanco, J.; Gernjak, W. Decontamination and disinfection of water by solar photocatalysis: recent overview and trends. *Catal. Today* **2009,** *147* (1), 1.

(23) Chong, M. N.; Jin, B.; Chow, C. W.; Saint, C. Recent developments in photocatalytic water treatment technology: a review. *Water Res.* **2010,** *44* (10), 2997.

(24) Fujishima, A.; Rao, T. N.; Tryk, D. A. Titanium dioxide photocatalysis. *J. Photochem. Photobiol. C: Photochem. Rev.* **2000,** *1* (1), 1.

(25) Amano, F.; Yamaguchi, T.; Tanaka, T. Photocatalytic oxidation of propylene with molecular oxygen over highly dispersed titanium, vanadium, and chromium oxides on silica. *J. Phys. Chem. B* **2006,** *110* (1), 281.

(26) Adhikari, B.-R.; Govindhan, M.; Chen, A. Carbon nanomaterials based electrochemical sensors/biosensors for the sensitive detection of pharmaceutical and biological compounds. *Sensors* **2015**, *15*, 22490.

Chapter 2: Literature Review

2.1. Introduction

Since the development of the first amperometric enzymatic biosensors by Clark and Updike in the 1960s, electrochemical glucose oxidase (GOx) based glucose sensors have been widely investigated.[1-3] Electrochemical sensors and biosensors have attracted considerable attention for the sensitive detection of a variety of biological and pharmaceutical compounds due to their high sensitivity, specificity, and low detection limit.[4] Since the discovery of carbon-based nanomaterials, including carbon nanotubes, C_{60}, and graphene, they have garnered tremendous interest as relates to their potential for the design of high performance electrochemical sensor platforms due to their exceptional thermal, mechanical, electronic, and catalytic properties. Carbon nanomaterial-based electrochemical sensors have been employed for the detection of various analytes with rapid electron transfer kinetics. Owing to the advantages of instrumental simplicity, moderate cost, and portability, electroanalytical techniques offer a powerful sensing strategy, which is superior to various traditional analytical methods.[5] The development of active electrocatalysts plays a key role in the design of efficient, reliable, stable, and innovative sensing devices.[6] Numerous electrochemical sensor platforms have been developed for the detection and quantification of medically and pharmaceutically important compounds such as glucose, methylglyoxal, nicotinamide adenine dinucleotide (NADH), acetaminophen, and valacyclovir. Moreover, recent developments in the field of nanotechnology and materials science have paved the way for the synthesis of many novel materials with desired morphologies and unique physicochemical properties.[7]

2.2. Electrochemical sensing methods

Electrochemical sensors are devices which capture the physical, chemical and biological changes and convert these changes into measurable signal. A variety of electrochemical methods have been explored for the detection of chemical contaminants and biomolecules.[5,8,9] Typically in electrochemistry, the reaction under investigation would either generate a measurable current *(*amperometric*),* a measurable potential or charge accumulation *(*potentiometric*)* or measurably alter the conductive properties of a medium *(*conductometric*)* between electrodes.[10] Other types of electrochemical detection techniques, such as impedimetric*,* which measures impedance (both resistance and reactance) through electrochemical impedence spectroscopy method.[11,12] Amperometric devices are a type of electrochemical sensor, which measure current generating from the oxidation or reduction of an electroactive species in a biochemical reaction.[13,14] Clark oxygen electrodes are the first simplest forms of amperometric biosensors, where a current is produced in proportion to the oxygen concentration. This is measured by the reduction of oxygen at a platinum working electrode in reference to a Ag/AgCl reference electrode at a given potential.[15] Voltammetry belongs to a category of electro-analytical methods, through which information about an analyte is obtained by varying a potential and then measuring the resulting current. It is, therefore, an amperometric technique. Since there are many ways to vary a potential, there are also many forms of voltammetry, such as: polarography (DC Voltage),[16] linear sweep, differential staircase, normal pulse, reverse pulse, differential pulse and more.[17] Typically, voltammetric techniques such as cyclic voltammetry (CV), linear sweep voltammetry (LSV), differential pulse voltammetry (DPV), square wave voltammetry (SWV) techniques are utilized in the determination of analytes.

2.2.1. Cyclic Voltammetry (CV)

It is one of the most widely used forms and is useful to obtain information about the redox potential and electrochemical reaction rates (e.g. the chemical rate constant) of analyte solutions. In this case, the voltage is swept between two values at a fixed rate, however, when the voltage reaches V_2 the scan is reversed and the voltage is swept back to V_1, as is in Figure 2.1. The scan rate, $(V_2 - V_1)/(t_2 - t_1)$, is a critical factor, since the duration of a scan must provide sufficient time to allow for a meaningful chemical reaction to occur. Varying the scan rate, therefore, yields correspondingly varied results.[18]

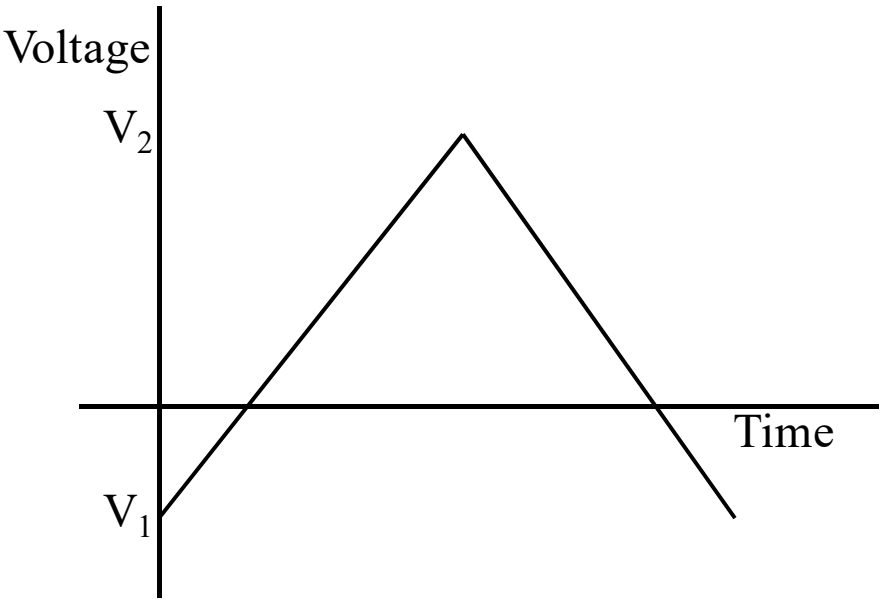

Figure 2. 1. Single seep segment of cyclic voltammograms

2.2.2. Differential Pulse Voltammetry (DPV)

This technique is very sensitive for the detection of trace amount of analytes. The potential applied through the technique consists of small pulses superimposed upon a staircase wave form. The current is measured twice in each pulse period (once before the pulse, and at the

end of the pulse), and the difference between these two current values is recorded and displayed. The current is measured at points S1 and S2. The typical value of T ranges from 0.5 to 5.0 s, while the value of t_p is on the order of 50 ms. If we consider current at points S1 and S2 as I_1 and I_2, respectively, the difference of I_2- I_1 represents the current due to the application of pulse.[19]

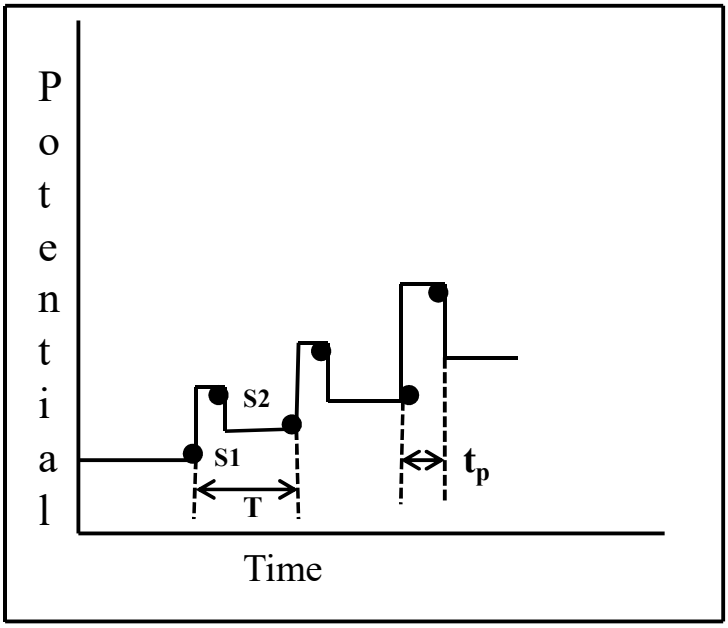

Figure 2. 2. Waveform current sampling time for differential pulse voltammetry

2.2.3. Chronoamperometry

Chronoamperometry (CA) is one of the simplest wave form potentiostat. As shown in Figure 3.3, the potential is changed directly from the initial potential to the first step potential, and it is held at this value for the first step time.[20] This is a single potential step experiment. In a double potential step experiment, the potential is changed to the second step potential after the first step time, and it is then held at this value for the second step time.[21] In chronoamperometry, the current is monitored as a function of time.

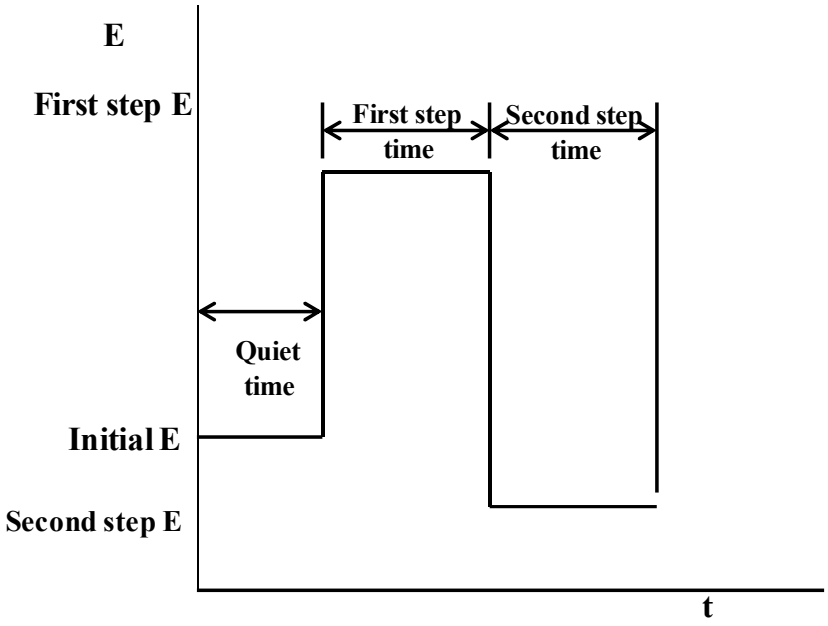

Figure 2. 3. Waveform of chronoamperommetry

An electrochemical sensor consists of two major components: (i) a chemical or biological recognition element; and (ii) a physical transducer (electrode) that transduces the analytical signal of the sensing event to an electronic circuit. Interactions between the substrate resident sensing element and the analytes are determined via the sensitivity, selectivity, speed of response, and reversibility of the designed sensors.[22] Strong interactions are typically associated with higher sensitivity and selectivity, whereas perfect reversibility requires weak interactions. The critical parameters of electrochemical sensors are sensitivity, detection limit, dynamic range, selectivity, linearity, response time, and stability.[23] Figure 2.4. displays a schematic illustration of an electrochemical sensor system, which exemplifies the three primary elements (e.g., sample (or analyte), transduction platform, and signal processing step).[24]

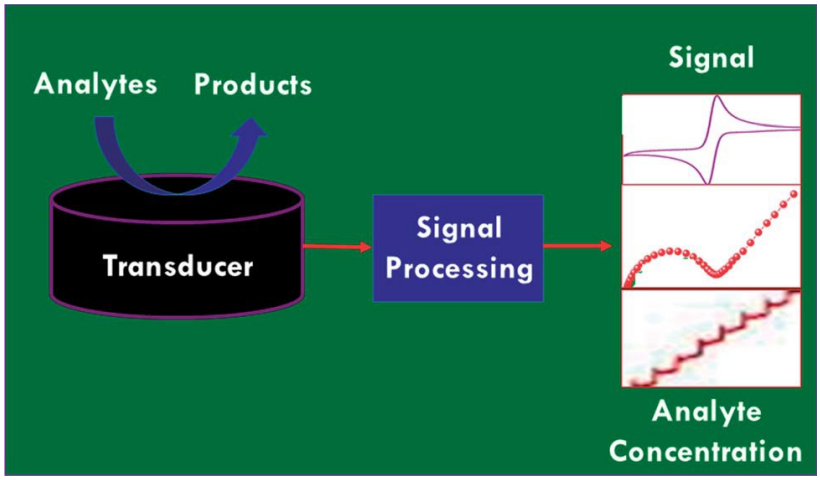

Figure 2. 4. Operation of a model electrochemical sensor [24]

Electrochemistry based analytical methods have impacted multiple fields, including medical diagnostics, environmental analysis, food sciences, enzymatic kinetics, and pharmacology.[25] Miniaturized electroanalytical systems and their incorporation into microfluidic devices for point of care (POC) applications has been studied for environmental analysis, and genetic testing.[26] Graphene oxide-ionic liquid based miniaturized electrochemical devices has been demonstrated for the very sensitive electrochemical detection of wide variety of electroactive targets of importance in food analyses, environmental monitoring, and clinical diagnoses.Several graphene based electrochemical sensor for the detection organophosphorus (OP) pesticides and nerve agents has been studied with very sensitive signal.[27,28] Our research group has recently surveyed the design and development of electrochemical sensors based on nanomaterials for biomedical applications,[29] and the applications of SWV in electrochemical sensing, [21] In the present review, we focus on the development of nanomaterials based electrochemical sensors and biosensors for the detection of pharmaceutical compounds and clinically relevant compounds.

2.3. Nanomaterials based electrochemical sensing platforms for pharmaceutical and biological compounds

Any particle size in between 1-100 nm regarded as nanomaterials. With remarkable development in nanotechnology and nanoscience, nanomaterials based electrochemical signal amplifications have great potential to improve both sensitivity and selectivity of electrochemical sensors and biosensors.[30] The nanomaterials used in working electrode for the construction of electrochemical sensor has crucial role for sensitive detection of target molecules. These nanomaterials further increase the synergistic effect on catalytic activity, conductivity and biocompatibility to accelerate the signal transduction.[30] Among the nanomaterials used in electrochemical sensor/biosensor, carbon based nanomaterials are well studied for electrochemical sensor targeting variety of biomolecules as shown in Figure 2.5.

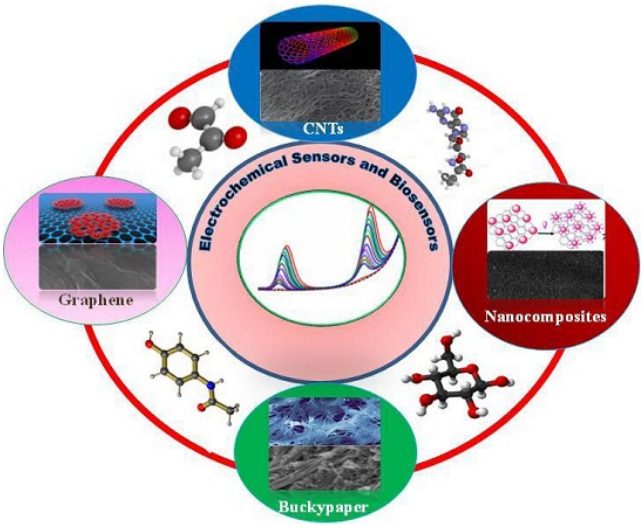

Figure 2. 5. Carbon nanomaterials based electrochemical sensors/biosensors[4]

Owing to the advantages of instrumental simplicity, moderate cost, and portability, electroanalytical techniques provide a powerful sensing strategy, superior to various traditional analytical methods.[31] Assorted electroanalytical techniques have been employed for the development of electrochemical sensors and biosensors for the detection and quantification of myriad biomarker species, chemical compounds, and minerals in environmental and biological samples.[32-34] The development of active electrocatalysts plays a key role in the design of efficient, reliable, stable, and innovative sensing devices.[35] Numerous electrochemical sensor platforms have been developed for the detection and quantification of medically and pharmaceutically important compounds such as glucose, methylglyoxal, nicotinamide adenine dinucleotide (NADH), acetaminophen, and valacyclovir. Moreover, recent developments in the field of nanotechnology and materials science have paved the way for the synthesis of many new materials with desired morphologies and unique physicochemical properties.[36]

Carbon-based nanomaterials such as carbon nanotubes, graphene, buckypaper, and nanohybrids among various other types of engineered nanomaterials have received enormous attention due to their promising sensor applications, which are most widely used in the electrochemical sensing of various compounds.[37-39] Carbon nanomaterials offer diverse advantages with their unique properties, such as a high surface-to-volume ratio, high electrical conductivity, chemical stability, biocompatibility, and robust mechanical strength.[40-42] Carbon possesses the capacity to hybridize into sp, sp^2 and sp^3 configurations with narrow gaps between their 2s and 2p electron shells. These unique properties are responsible for enabling the design of versatile carbon-based nanomaterials for the sensitive detection of biological compounds.[43-45] Carbon nanotubes may be comprised of a single graphitic layer, or multiple coaxial layers, resulting in the formation of single-walled carbon nanotubes (SWCNTs) and multiple-walled

carbon nanotubes (MWCNTs). SWNTs are seamlessly wrapped into cylindrical tubes, having diameters of between 0.4 nm and 2.5 nm. These materials offer excellent physical and chemical properties that enable a wide range of applications in biomedicine.[46]

Methylglyoxal is a predictor in type 2 diabetes mellitus of intima-media thickening, vascular stiffening, and the elevation of systolic blood pressure, suggesting its clinical usefulness as a biomarker for diabetic macroangiopathy.[47] In view of the prominence of methylglyoxal in clinical applications, there are many methods reported for its determination. The use of SWCNTs as a sensing material dramatically decreases the overpotential, which makes a promising carbon nanomaterial for the detection of variety of biological compounds. Chen and co-workers have demonstrated a SWCNT based sensor platform for the quantitative determination of methylglyoxal in 0.1 M PBS (pH 7.4), showing that the sensor system was highly specific and sensitive for the detection of plasma levels of methylglyoxal in healthy individuals and diabetic patients.[48]

Valacyclovir is the drug of choice for the treatment of herpes zoster and cold sores, and is an Lvalyl ester and prodrug of the antiviral drug acyclovir. Subsequent to absorption, valacyclovir is rapidly and almost completely hydrolyzed to acyclovir and L-valine, which is an essential amino acid. It is also effective for the suppression or treatment of genital herpes in immunocompetent individuals. SWCNTs have been utilized to modify GCE for the sensitive detection of valacyclovir.[49]

Graphene is a much newer member in the family of carbon materials in comparison to fullerenes. Graphene is an atomically thin film that consists of hexagonally arranged carbon atoms with sp^2 hybridization in two dimensions.[45] The combination of attributes such as a high surface area, enhanced mobility of charge carriers, and high stability makes graphene an ideal

platform for the anchoring of metal nanoparticles for electrochemical sensing applications.[50-52]NADH/NAD+ is an important co-enzyme couple that plays a significant role in energy production/consumption within the cells of living organisms, which participates in a variety of enzymatic reactions involving more than 300 dehydrogenases.[53] Acetaminophen is a widely used analgesic (pain reliever) and fever reducer, and is considered to be very safe when administered at recommended dosages; however, it causes hepatotoxicity at higher doses.[54] Recently, graphene and Au nanoparticle-rGO nanocomposite based electrochemical sensors have been fabricated by Chen and co-workers[55] via an electrochemical method for the sensitive detection of NADH and acetaminophen.

Buckypaper is a thin film (5–25 μm) comprised of lateral arranged networks of nanotubes, which constitute a promising platform for the fabrication of highly concentrated and aligned nanotube-reinforced composites. Recently, much attention has been given to macroscopic assemblies of carbon nanotubes, which include carbon buckypapers, in order to exploit the characteristic properties of single carbon nanotubes at macroscopic scales.[56] Buckypapers and composites thereof are innovative materials with intriguing physical and chemical properties that have strong potential for pharmacological and prosthetic applications. Buckypaper has been incorporated into the design of a mediator-free glucose sensor with high sensitivity, stability, selectivity, and reproducibility.[57]

Carbon nanotubes and graphene nanocomposite based electrochemical sensing platforms have been widely explored for the detection of various biological and pharmaceutical compounds including glucose,[58-60] lactate,[61] dopamine,[62-64] rutine,[65] human serum albumin ,[66] DNAs,[68] epinephrine,[69,70] cholesterol,[71,72] methimazole,[73] sumatriptan,[74] and paracetamol .[75] The electrode

materials, electrochemical methods, the linear range and the detection limit for the detection of pharmaceutical drugs and clinically relevant compunds are compared in table below

Carbon Based Nanomaterials	Analytes	Methods	Linear Range	Detection Limit	Reference
SWNT-Nafion-GOx	Glucose	Amperometry	2 mM to 20 mM	-	Wang et al., 2003
SWNT-GOx	Glucose	Amperometry	Up to 40 mM	-	Wang et al., 2003
Pt-Nafion-SWCNTs-GOx	Glucose	Amperometry	0.5 μM to 5 mM	0.5 μM	Hrapovic et al., 2004
SWNT-mineral-oil paste	Lactate	Amperometry	Up to 7.0 mM	0.3 mM	Rubianes et al., 2005
Nafion-SWNT	Dopamine	DPV	0.02 μM to 6.0 μM	5.00 nM	Wang et al., 2006
SWNT polymer composite	Dopamine	CV	16 nM to 600 μM	8 nM	Zhang et al., 2006
SWCNTs	Dopamine	DPV	3 μM to 200 μM	48 nM	Habibi et al., 2011
SWCNTs	Rutine	CV	20 nM to 5 μM	10 nM	Zeng et al., 2006
SWCNTs	Albumin	CV	0.075 nM to 7.5 nM	75 pM	Yu et al., 2005
SWCNTs	DNAs	DPV	5 μM to 30 μM	1.43 μM	Li et al., 2009
MWCNTs-Nafion	Epinephrine	CV and DPV	0.06 mM to 0.24 mM	0.02 mM	Yogeswaran et al.,2007
MWNT nanocomposite	Epinephrine	LSV	50 nM to 10 μM	10 nM	Yi et al., 2008
MWCNTs	Cholesterol	Amperometry	Up to 6.0 mM	0.2 mM	Guo et al., 2004
MWCNTs	Cholesterol	Amperometry	100 mg/dL to 400 mg/dL	-	Li et al., 2005
MWCNTs	Methimazole	Amperometry	0.074 μM to 63.5 μM	0.056 μM	Martinez et al., 2008
MWCNTs-silver nanoparticles	Sumatriptan	CV	80 nM to 100 μM	40 nM	Ghalkhani et al., 2009
MWCNTs	Paracetamol	ASV	0.01 μM to 20 μM	10 nM	Kachoosangi et al., 2008
SWCNTs	Methylglyoxal	SWV	0.1 μM to 100 μM	-	Chattergee et al., 2013
SWCNTs	Valacyclovir	DPV	5 nM to 55 nM	1.8 nM	Shah et al., 2013
SWCNTs	Acetaminophen	DPV	5 nM to 80 μM	4.3 nM	Adhikari et al., 2015
Graphene-ppy	Glucose	Amperometry	-	3 μM	Alwarappan et al., 2010
Graphene-Pt	Ascorbic acid	DPV	0.03 μM to 8.13 μM	0.03 μM	Sun et al., 2011
Graphene	Norepinephrine	Amperometry	0.04 μM to 100 μM	0.84 nM	Raj et al., 2014
Reduced GO	NADH	Amperometry	10 μM to 600 μM	0.33 μM	Tabrizi et al., 2014
Graphene-Au nanorod	NADH	Amperometry	5 μM to 337 μM	1.5 μM	Li et al., 2013
Au-TiO_2/graphene	NADH	Amperometry	10 μM to 240 μM	0.2 μM	Fan et al., 2012
Graphene-TiO_2	NADH	Amperometry	10 nM to 2 mM	3×10^{-9} M	Wang et al., 2012
AuNPs-rGO	NADH	Amperometry	50 nM to 500 μM	1.13 nM	Govindhan et al., 2015
Nitrogen doped Graphene	Uric acid	DPV	0.1 μM to 20 μM	0.045 μM	Sheng et al., 2012
Graphene	Uric acid	Amperometry	0.19 μM to 49.68 μM	0.132 μM	Du et al., 2013
Nafion-AgNPs-rGO	Uric acid	LSV	10 μM to 800 μM	8.2 μM	Kaur et al., 2013
Pt-rGO	Uric acid	DPV	10 μM to 130 μM	0.45 μM	Raj et al., 2013

ERGO	Serotonin	DPV	5 µM to 300 µM	0.11 µM	Raj et al., 2013
ERG/Ni_2O_3-NiO	acetaminophen	DPV	0.04 µM to 100 µM	0.02 µM	Liu et al., 2014
Graphene-chitosan	Acetaminophen	DPV	1 µM to 100 µM	0.3 µM	Zheng et al., 2013
Graphene	Acetaminophen	SWV	0.1 µM to 20 µM	0.032 µM	Kang et al., 2010
rGO	Acetaminophen	DPV	5 nM to 800 µM	2.13 nM	Adhikari et al., 2015
SWCNTs-GNS	Acetaminophen	DPV	0.05 µM to 64.5 µM	0.038 µM	Chen et al., 2012
MWCNT-graphene nanosheets	Acetaminophen	DPV	0.8 µM to 110 µM	0.1 µM	Arvand et al., 2013
MWCNT/GO	Acetaminophen	DPV	0.5 µM to 400 µM	47 nM	Cheemalapati et al., 2013
SWCNTs-rGO	Acetaminophen	DPV	5 nM to 80 µM	1.4 nM	Adhikari et al.,2015
MWCNT/GONR	Dopamine	DPV	0.15 µM to 12.15 µM	0.08 µM	Sun et al., 2011
Buckypaper-SWCNTs	Glucose	Amperometry	0 mM to 10 mM	0.022 mM	Papa et al., 2014
Buckypaper-GOx-HRP	Glucose	Amperometry	Up to 9 mM	0.01 mM	Ahmadalinezhad et al., 2011

2.4. Electrochemical sensors and biosensors: classification

Electrochemical sensors/biosensors have been classified according to bioreceptor molecules attached on the electrode surface. The selection of bioreceptor molecule for the design of electrochemical biosensor has great impact on its sensitivity and selectivity.[76] A variety of bioreceptor molecules can be utilized for the fabrication of electrochemical biosensors as shown in Figure 2.6.

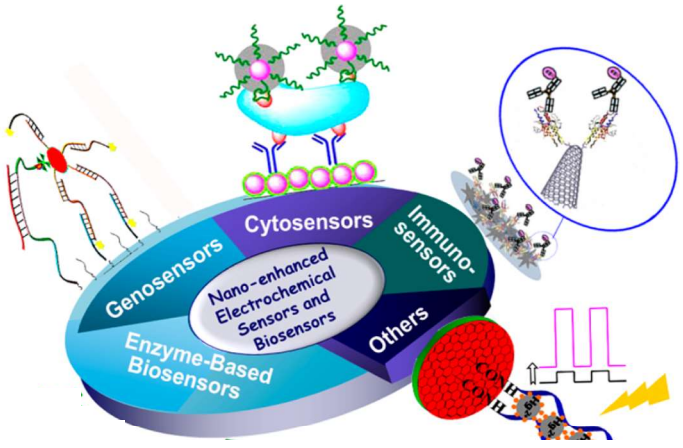

Figure 2. 6. Schematic diagram of classification of electrochemical sensors and biosensors. Adapted from reference [76] with permission. Copyright 2014 American Chemical Society.

2.4.1. Non-enzymatic sensors

Electrochemical methods for bimolecular detection have garnered significant attention over the last two decades. Enzymatic sensors possess high selectivity; however, they suffer from limitations such as instability, complex modification procedures, and vital microenvironmental factors.[76] These limitations have spurred the development of non-enzyme sensors that involve simple modification procedures without any bioreceptor molecules and have good stability.[77] Enzyme-free electrochemical sensors have been widely used for determining the presence of hydrogen peroxide, glucose, dopamine, uric acid, acetaminophen, and valacyclovir.[4] The perspectives and current challenges of enzyme-free electrochemical sensors have been discussed.[78] Nickel and its oxides, hydroxides and oxyhydroxides were studied for the electrocatalysis and electroanalysis properties for small molecules detection.[79] Several examples of non-enzymatic sensors for the detection of small molecules are discussed here.

The most studied and cited work in the literature is glucose biosensor. Glucose plays a critical role in human metabolism, and glucose biosensors have significantly contributed to clinical monitoring [80,81]. The most recent advances in non-enzymatic glucose sensors have been gaining popularity due to its fast reaction and stable performance. Various nanomaterials with different morphologies and compositions were synthesized toward the construction of novel non-enzymatic electrochemical sensors for glucose detection.[82] Electrochemical sensors comprised of PtCu nanomaterials are very sensitive and specific for glucose detection due to the wiring of dispersed crystals, porous nanostructure, clean surface, and synergetic electronic effects of alloyed atoms. The performance of the resulting sensor showed the very sensitive detection of glucose in serum samples.[83] Reduced graphene oxide (rGO) modified with platinum nanocubes and copper oxide nanoflowers have been used to construct electrochemical non-enzymatic sensor

for glucose monitoring. The developed sensor was suitable to be used as point of care glucose monitoring. [84] These sensors were highly specific to glucose in the presence of commonly interfering species like ascorbic acid (AA), dopamine (DA), uric acid (UA), and acetaminophen. Ni/CdS bifunctional Ti@TiO_2 core-shell nanowire based electrochemical sensor exhibited high sensitivity for the electrochemical detection of glucose oxidation.[85] Several nanostructure materials have been studied to construct the high performance non enzymatic electrochemical sensor based on Ni NPs, CdS under visible light irradiation. The ability to combine the unique properties of individual nanomaterial provides a new and exciting frontier for the formation of novel electrodes. A photoelectrochemical approach in the application of the glucose sensor was also investigated. A photoelectrochemical glucose detection system based on a non-enzyme catalytic oxidation reaction demonstrated promising results with high sensitivity and rapid response.

Another widely used electrochemical non-enzymatic sensor for the quick and sensitive detection of hydrogen peroxide (H_2O_2) has been investigated in the field of bioanalytics, food safety, and environmental protection.[86,87] The sensor was based on the electrochemical deposition of Pd−Pt and Pd−Au nanoparticles on spectrographic graphite. The sensitivity was derived from the co-deposition of Pd with either Pt or Au, which enhanced the electrocatalytic activity for the reduction of H_2O_2.[88] An additional powerful sensor utilizing graphene oxide (GO), carbon nanotubes (CNTs), and Pt nanocatalysts was developed for H_2O_2 dtection.[89] The GO−CNT−Pt nanocomposites exhibited biomimetic properties exhibited peroxidase-like catalysis on H_2O_2 which able to detect a very potent electrochemical signal. The non-enzymatic sensosr utilizing these biomimetic nanomaterials has great potential for extensive catalysis applications in environmental, medical and food safety.

2.4.2. Electrochemical enzyme based biosensors

Electrochemical enzyme based biosensors, a subclass of chemical sensors, combine the high specificity of enzymes with the sensitivity of electrochemical transducers.[90] Enzyme electrodes comprise electrochemical probes with a thin layer of immobilized enzymes on the surface of the working electrode (transducer) as shown in Figure 2.7. Enzymes constitute the most critical component of enzyme electrodes since they provide the selectivity for the sensor and catalyze the formation of electroactive products for detection.[91] The chronological development of enzyme based biosensors using various materials and techniques have been reported in the literature. The enzymatic glucose biosensor is the most studied enzyme based electrochemical biosensor. Electrochemical glucose biosensors based on glucose oxidase (GOx) has been discussed frequently in literatures for amperometric glucose sensing.[92] Enzyme immobilization strategy is the most crucial part of biosensor fabrication. Current trends in enzymatic immobilization, for lactate and uric acid biosensors were discussed.[93-95] Improvements in immobilization strategies and the study of recent achievements in this area

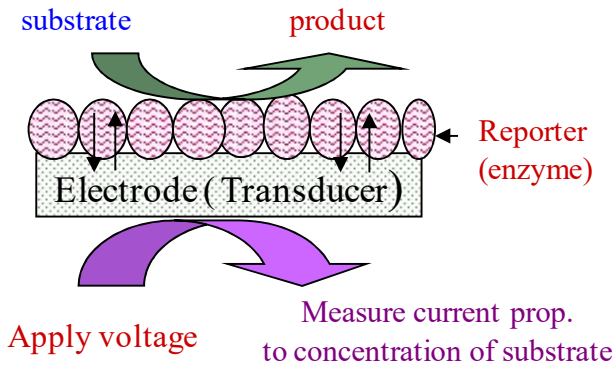

Figure 2. 7. Schematic diagram of typical electrochemical biosensor

have focused on the development of novel immobilization strategies and the study of direct electron transfer with the assistance of functional nanomaterials. Immobilization strategies comprise key steps in the development of high-performance biosensors, since they affect the loading as well as the bioactivity of enzymes. To date, different techniques have been utilized to achieve efficient enzyme immobilization, such as the covalent binding of enzymes onto the substrate surface, or the incorporation of enzymes into different matrices. The development of nonmaterials provide a substrate for enhancing their functionality and applications in the immobilization of enzymes.[96] A vast number of nanostructured materials with different morphologies, dimensions, and compositions have been synthesized and utilized as novel electrode materials for the immobilization of desired enzymes. Graphite nanoparticles composed of multiple stacked graphene sheets have attracted many researchers due to their homogeneous spherical shapes, high conductivity, and large surface area for biomolecular catalysis; graphene based enzyme biosensors have been reported to detect glucose in actual samples.[97] Subsequent to modification, GOx was linked with graphite nanoparticles through amide bonds, and this novel cost effective approach might be applied to other electrochemical biosensors. A novel sensing platform for H_2O_2 and glucose based on the palladium helical carbon nanofiber (Pd-HCNF) hybrid nanostructures with the immobilization of glucose oxidase have been studied.[98] The diminutive size and uniform distribution of the Pd NPs, in conjunction with the excellent conductivity and large surface area of the HCNFs drastically reduced the overpotential, and increased the electron transfer rate. Novel nanomaterials such as $NiFe_2O_4$,Tm_2O_3,and Cu_2O,for the detection of cholesterol with the immobilization of cholesterol esterase (ChEt) and cholesterol oxidase (ChOx) have been studied by several authors.[99,100] These biosensors revealed evidence of largely improved analytical performance toward cholesterol.

2.4.2.1. Direct substrate-enzyme electron transfer

The chronological development of enzyme-based electrochemical biosensors through first generation to third generation, a great improvement have been achieved in substrate enzyme electron transfer. The first generation biosensor is the first developed enzyme biosensor, where product of the reaction diffuses to the electrode (transducer) and generates electrical response. This type of reaction is very non-specific and suffers from sluggish electron transfer. The second generation biosensor involves specific mediator between transducer and reaction to generate signal. The third-generation biosensors are mediator less where reaction itself generate sufficient electrical signal through substrate-enzyme electron transfer.[101] There have been several attempts to understand the direct electrochemistry of enzymes in order to reduce long electron-tunneling distances between the enzymes and transducers.[102] A whole cell based glucose oxidase (GOx)-yeast/CNTs biosensor has been developed for the electrochemical glucose sensing platform.[103] Direct electron transfer (DET) was achieved through recombinant GOx without any adverse effects of the host yeast on the electrocatalytic activity. Several other approaches have been utilized by several authors to develop a DET glucose biosensor that was based on self-assembled GOx on electrochemically reduced graphene oxide, MnO_2 decorated rGO and functionalized CNTs.[104-106] Although well-defined voltammetric peaks of the direct electrochemistry of GOx have been achieved in previous reports, the detection of glucose based on the direct GOx electron transfer has rarely been realized. However, glucose detection theoretically belongs to the first-generation amperometric glucose biosensors, rather than the third-generation. These issues have been tried to address by systematically investigated the signal transduction and enzyme activity in biosensors that were based on GOx and CNTs embedded within a bioadhesive chitosan (CHIT) film.[107] They studied the role of DET in glucose sensing using a GOx/CNT

hybrid, supported by CHIT at the electrode surface. Two primary issues were investigated, including the role of the reactions that were relevant to electrochemical glucose sensing, and the effects of CNT on the retention and enzymatic activity of GOx in CHIT films and in aqueous suspensions. Well-defined voltammetric peaks of direct GOx electrochemistry were observed, regardless of the CHIT. However, the DET was not the mechanistic basis for glucose sensing at a GOx/CNT-based biosensor, which indicated that the GOx molecules within the electron tunneling distance from CNT were not enzymatically active toward glucose. To address this issue, Cui and co-workers designed a functionalized planar boron-doped diamond (BDD) electrode as a biosensing platform for biomolecule immobilization, with GOx as a model bioreceptor molecule.[107] BDD was treated with KOH and functionalized with 3-aminopropyltriethoxysilane. The free amino GOx groups and aminopropyltriethoxysilane were crosslinked by glutaraldehyde. The DET between the flavin adenine dinucleotide (FAD) on GOx and the electrode was investigated by using the aminopropyltriethoxysilane-glutaraldehyde conjugate as a molecular wire to facilitate electron tunneling between the FAD and BDD.

2.4.3. Electrochemical genosensors

Recent advances in the electrochemical detection of nucleic acids have allowed for the development of new types of genosensors. In electrochemical genosensors, single stranded DNA (ssDNA) fragments are utilized as recognition probes through immobilization onto the electrode surface, which recognizes target DNA through hybridization as depicted in Figure 2.8.[108]

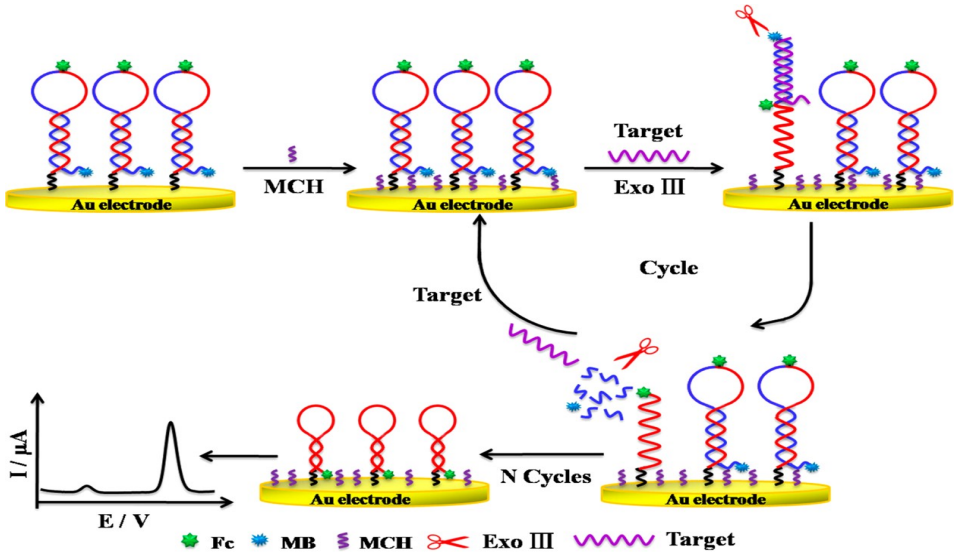

Figure 2. 8. Schematic illustration of the voltammetric approach of electrochemical genosensors. Adapted from reference [108] with permission. Copyright 2015 American Chemical Society.

The electrochemical genosensors contain DNA and capture probes that are immobilized on the transducer for the capture of targets, and signal probes for electrochemical signal generation.[109] These hybridization signals are captured through several electrochemical methods. According to electrochemical detection principles, several critical factors should be considered for the achievement of good sensitivity and selectivity in biodetection. Novel methods and new signal amplification techniques generated through DNA and RNA assays have been studied in the acquisition of electrochemical signals.

2.4.4. Electrochemical immunosensors

Immunoassays comprise standardized biodetection methods that are based on specific antigen-antibody reactions that are used in clinical laboratories for disease diagnosis and for environmental contamination monitoring.[110-113] Due to the combination of specific antigen-antibody recognition with the high sensitivity of electrochemical methods, electrochemical

immunosensors (EIs) have attracted considerable interest, and significant progress has been achieved in the early diagnosis and clinical analysis of disease, food safety, environmental monitoring, public security and home-health care.[114] A typical electrochemical immunosensor presented in Figure 2.9 where capture antibody attached on carbon electrode through functionalized magnetic bead where specific analyte (antigen) is detected by capture antibody tagged with enzyme[115]Electrochemical immunosensors are attractive due to their rapid response and portability with an excellent lower detection limit. Voltammetry and amperometry such as linear sweep, differential pulse, square-wave, and stripping, are the most commonly used electrochemical methods for immunoassays.

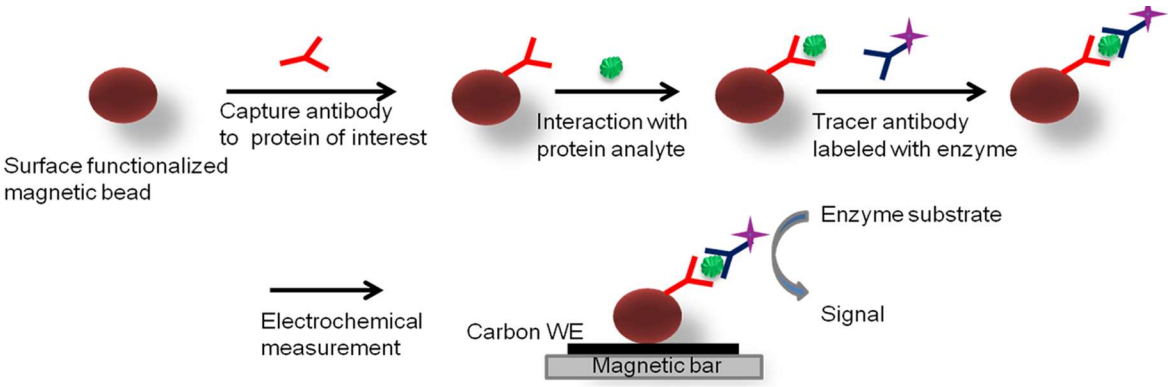

Figure 2. 9. Schematic representation of electrochemical immunosensor. Adapted from reference [115] with permission. Copyright 2012 American Chemical Society.

2.5. Immobilization of bioreceptor molecules on electrode surface

Various biosensors use different biomolecules as biorecptors and signalling molecules, such as nucleic acids, antibodies, whole cells, or enzymes. The immobilization of the bioreceptor onto the transducer is critical for biosensor performance.[116] Biomolecules have been immobilized not only on transducers to act as bioreceptors, but also on other surfaces such as magnetic, gold

or latex particles, and recently, on a wide variety of nanomaterials that enhanced the analytical performance of the biosensors. Among the wide range of immobilization strategies for transducer surfaces, irreversible (covalent binding, crosslinking, entrapment or micro-encapsulation) and reversible (adsorption, bioaffinity, chelation or metal binding and formation of disulfide bonds) immobilization methods have been studied in detail as shown in Figure 2.10.[117]

Covalent binding is the immobilisation of bioreceptor molecules with covalent bonds which are most widely used method during biosensor fabrication. The vast majority of chemical modification techniques include

Primary amines ($–NH_2$): The most specific and efficient reagents are those that use the N-hydroxysuccinimidyl ester (NHS ester) reactive group.

Carboxygroups (–COOH): This group exists at the C-terminus of each polypeptide chain and in the side chains of aspartic acid (Asp, D) and glutamic acid (Glu, E).

Thiols (–SH): This group exists in the side chain of cysteine (Cys, C). Cysteines are joined together between their side chains via disulfide bonds (–S–S–). These must be reduced to thiols to make them available for binding. Reagents that are activated with maleimide or iodoacetyl groups are the most effective for thiol-directed conjugation.

Carbonyls (–CHO): Ketone or aldehyde groups can be created in glycoproteins by oxidising the polysaccharide post-translational modifications (glycosylation).

Carbohydrates (sugars): Glycosylation occurs primarily in the constant fragment (Fc) region of antibodies (IgG). Component sugars in these polysaccharide moieties that contain *cis*-diols can be oxidised to create active aldehydes (–CHO) for coupling. Labelling carbohydrates requires more steps than labelling amines because the carbohydrates must first be oxidised to create

reactive aldehydes; however, the strategy generally results in antibody conjugates with high activity due to the location of the carbohydrate moieties. Aldehyde-activated (oxidised) sugars can be reacted directly to primary amines through reductive amination (mentioned above) or to reagents that have been activated with hydrazide groups.[117]

Cross-linking is the process of chemically joining two or more molecules by a covalent bond. Cross-linking reagents (or cross-linkers) are molecules that contain two or more reactive ends capable of chemically attaching to specific functional groups (primary amines, thiols, etc.) on proteins or other biomolecules.[118].

Entrapment is one of the major approaches for enzyme immobilization; however, it suffers a few critical drawbacks including leakage and high mass transfer resistance to substrates. The entrapment method is based on the holding biomolecules, mostly enzymes, within a polymeric network through electrostatic forces. There are different approaches to entrapping enzymes such as gel or fibre entrapping and micro-encapsulation. The practical use of these methods is limited by mass transfer limitations through membranes or gels.

Adsorption is the simplest immobilisation method wtih non-specific adsorption mainly based on physical adsorption or ionic binding. In physical adsorption, the bioreceptors are attached to the surface through hydrogen bonding, van der Waals forces or hydrophobic interactions, whereas in ionic binding, the enzymes are bound through salt linkages.[119]. The limitations of the adsorption mechanism are the random orientation and weak attachment, which produce desorption and poor reproducibility.[120]

Bioaffinity the affinity based technique between complementary biomolecules such as lectin–sugar, antibody–antigen and biotin–avidin applied to biomolecule immobilisation.[121,122] The remarkable selectivity of the interaction is a major benefit of the method. However, the

procedure often requires the covalent binding of a costly affinity ligand (e.g. antibody or lectin) to the support. The most established procedures are the (strept)avidin–biotin interaction and the use of Protein A or G for antibody immobilisation:

Chelation or metal binding this method is known as 'metal link immobilisation'. The metal salt or hydroxide, mainly titanium and zirconium salt, is precipitated and bound by co-ordination with nucleophilic groups on the surface (e.g. cellulose-, chitin-, alginic acid- and silica-based carriers) by heating or neutralisation.

Disulfide bonds are a unique stable covalent bond formed between the support and bioreceptor molecule, it can be broken by reaction with a suitable agent such as dithiothreitol (DTT) under mild conditions. The reactivity of the thiol groups can be modulated via pH alteration, the activity yield of the methods involving disulfide bond formation is usually high, provided that an appropriate thiol-reactive adsorbent with high specificity is used.[123]

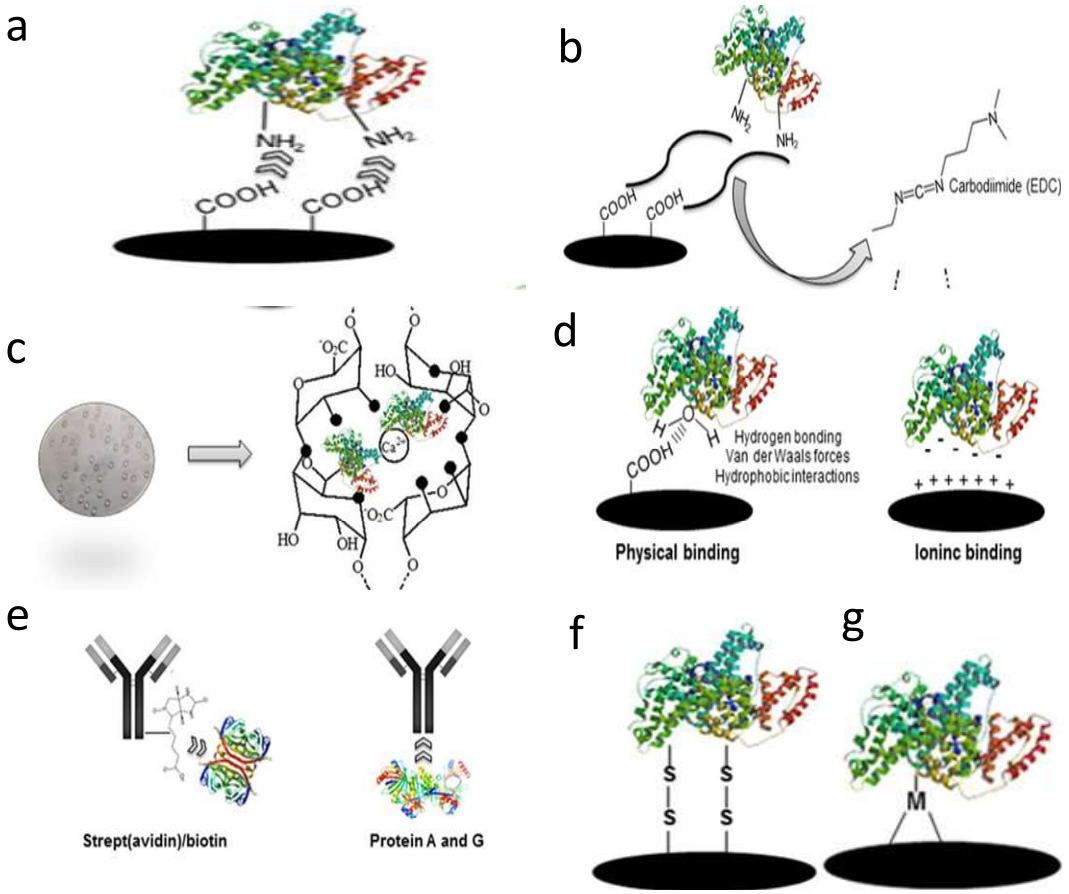

Figure 2. 10. Schematic representation of (a) covalent binding through primary amines, (b) cross-linking using carbodi-imide, and (c) entrapment on beads or fibres (d) adsorption, physical and ionic binding, (e) bioaffinity with streptavidin/biotin and Protein A/G, (f) metal binding, and (g) disulfide bonds. Reproduced from refrence [117] with permission.

The immobilization of bioreceptor molecules on electrode surfaces is critical, as it determines the sensitivity, limit of detection, reproducibility, and stability of biosensor. When working with the immobilization of biomolecules, an optimization method for one type of biomolecule may not necessarily translate to another. Recent advances in bioconjugation techniques are widely described in the literature.[124] The different strategies may be classified according to various levels of selectivity and difficulty, ranging from random methods (e.g., adsorption) to more

advanced techniques that are based on protein engineering, which are employed to facilitate directional immobilization.[125]

2.6. Electrochemical methods of bacterial disinfection

Disinfection is a strategy for the removal of pathogenic microorganisms from drinking water. Traditional disinfection methods incorporate chlorine, monochloramine, chlorine dioxide, ozone, hydrogen peroxide, and ultraviolet (UV) irradiation. Chlorination is the oldest method of disinfection; but the disinfection byproducts (DBPs) generated through chlorination have raised increasing concerns.[126] Ozone is a potent oxidant that may have the capacity to effectively inactivate many types of microorganisms, with limited ozone production.[127,128] Among all methods, electrochemical processes in both chloride and chloride-free electrolytes have proven to be highly-efficient for disinfection of most waterborne pathogens such as: *Cryptosporidium parvum* oocysts and *Clostridium perfringens* spores which are resistant to chlorine.[129] Electrochemical methods have garnered increasing interest due to strongly reactive oxygen molecules (ROS) that are ingenerated via electrolysis. It is vital to understand the mechanisms of different inactivation methods, which might be helpful in the identification of rate-limiting steps during disinfection, toward the development of more effective strategies in practical disinfection applications. Ozone was proven to be superior to chlorine and monochloramine for the inactivation of *Cryptosporidium parvum* oocysts and *Bacillus subtilis* spores.[130,131] Cho et al.[132] compared disinfection efficiencies of ozone and free chlorine along with the detection of protein release, lipid peroxidation and alterations in cell permeability, using *E. coli* as a representative microorganism. It was observed that ozone initiated the highest level of cellular damage over free chlorine. Ozone possesses a more potent oxidizing ability to react with the organics on cell

walls prior to penetrating into the cytoplasm, which imparts severe cell damage. For chlorine, with a weaker oxidizing ability, the reaction with organics on the cell wall was limited, and the inactivation of cells was realized through its interaction with intracellular components.[153] There are many indications that electrolyzed water has a higher disinfecting activity compared to normal commercially available hypochlorite solutions.[133] A number of electrochemical disinfection studies using *E. coli* as the indicator microorganism have been studied and compared its responses on exposure to ozonation and chlorination.[134,135] The SEM observations of *E. coli* following these disinfection strategies suggested that bacteria in the electrochemical treatment were severely damaged, similar to the damage imparted by ozone, and much stronger than chlorine. Bergmann et al.[136] indicated that electrolyzed water (50 mg L^{-1} Cl^{-}) had a higher lethal efficiency than Ca $(OCl)_2$ of the same measured active chlorine concentration. *E. coli* is a widely utilized indicator microorganism for bacteriologic water quality. However, the inactivation of *E. coli* cannot automatically be taken as being representative of the responses of all microorganism species. Nakajima et al.[137] and Delaedt et al.[138] showed that the complete eradication of a bacterial suspension following 5 min of electrolysis was obtained with 20 mA in the case of *E. coli*; however, 30 mA was required when treating *Legionella Pneumophila* (*L. pneumophila*). Different microorganisms *E. coli*, *Bacillus subtilis*, and *Saccharomyces cerevisiae* Kolin cells to have been studied for the effects of chlorination, ozonation, and electrochemical disinfection. The results indicated that *E. coli* cells were more sensitive than *Bacillus subtilis* and *Saccharomyces cerevisiae*. Moreover, it was reported that gram-positive *Staphylococcus aureus* exhibited stronger drug-resistance than gram-negative bacillus due to their different peptidoglycan structures.[139] Tyrrell et al.[140] tested five indigenous populations (including fecal coliforms, enterococci, Clostridium perfringens, male-specific bacteriophages, and somatic

coliphage) in secondary sewage effluents using chlorine and ozone. Inactivation efficiencies differed significantly between species, which confirmed that a single bacterium indicator, such as the fecal coliform, is inadequate for predicting overall microorganism responses to disinfection treatments. Reactive oxygen species (ROS, primarily •OH) that are generated during electrochemical treatments, are considered to play a significant role in imparting bacterial cell wall damage, and ultimately contribute to bacterial disinfection.

2.6.1. TiO_2 based photocatalytic disinfection

The use of TiO_2 suspensions for water disinfection through photocatalysis involves an additional post-treatment step to segregate the particulates from the treated water, which typically increases the cost of treatment. An additional disadvantage of suspension systems is the recombination of charge carriers due to which the system yields very low levels of hydroxyl radicals. Electrochemical photocatalysis using TiO_2 photoanodes is a potential solution for improving charge carrier separation. The application of an external electrical potential to the TiO_2 anode may improve charge carrier separation, and thus reduce the recombination rate

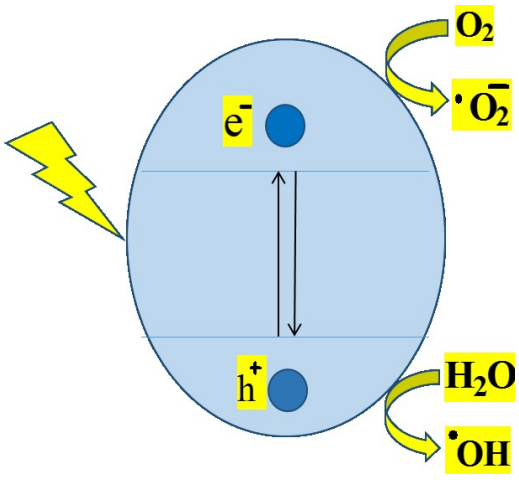

Figure 2. 11. Schematic illustration for energetics and principal reaction mechanism of TiO_2 photocatalysis.

The mechanism of photocatalysis may be explained as:

Photocatalyst + hv $\rightarrow h^+ + e^-$

$O_2 + e^- \rightarrow O_2 \bullet^-$

$H_2O + h^+ \rightarrow H^+ + OH\bullet$

Contaminant + $O_2 \bullet^-$ → products

Contaminant + OH• → products

Upon irradiation, photogenerated valence band holes migrate toward the semiconductor surface, where the generation of hydroxyl radicals (·OH) takes place due to water oxidation. The photogenerated conduction band electrons migrate to the supporting electrode, from where they transit to the counter electrode and are accepted onto molecular oxygen to create superoxide radical anions ($O_2 \cdot^-$). Subsequent reduction reactions yield hydrogen peroxide (H_2O_2) and ·OH. Electrochemical photocatalysis for water disinfection and organic pollutant degradation have been studied in the literature.[141-143] The major benefit of electrochemical photocatalysis for bacterial disinfection is the electro-migration of negatively charged bacteria to the positively biased photoanode.[144-146] There have been several investigations into the nanoengineering of titania (TiO_2) electrodes to improve the efficiency of photoelectrochemical bacterial disinfection. The potential use of TiO_2 nanotubes as photoanodes has been increasing due to their high ROS generation capacity. They exhibit improved photoelectrolytic properties, in contrast to nanoparticle films, due to the short diffusion path for photogenerated holes, and direct path for photogenerated electrons to the supporting electrodes.[147] These nanotubes may be prepared by the anodic oxidation of a Ti substrate in fluoride containing electrolytes. TiO_2 nanotubes remain attached to the substrate, and therefore may be directly used as photoanodes.[148,149]

Electrocatalytic oxidation offers promising approaches for the complete mineralization of pollutants without the generation of harmful byproducts. Contaminants are directly mineralized as the result of interactions of adsorbed hydroxyl radicals on the electrode surface during electrocatalytic oxidation. The most commonly employed electrodes for the electrocatalytic oxidation are boron doped diamond (BDD), platinum (Pt), antimony (Sb)-doped ruthenium oxide (RuO_2) / titanium dioxide (TiO_2), titanium-iridium oxide (Ti/IrO_2)– tin oxide (SnO_2)– Sb_2O_5, Ti–Pt/Pb–PbO_2, Ti/Sb–SnO_2, Ti/PbO_2, Ti/(IrO_2-Ta_2O_5), Ti/SnO_2–Sb_2O_5, Ti/SnO_2–Sb_2O_5–PtOx, Ti/SnO_2– Sb_2O_5–RuO_2, and Ti/RuO_2–IrO_2.[150-152]

2.7. Summary and perspectives

Electrochemical approaches have drawn a great attention as a green technology for the analysis and removal of chemical-biological toxins. Electrochemical sensors and biosensors based on nanostructured materials provide a critical analytical tool for the ultrasensitive, rapid, and selective determination of biomarkers and other clinically relevant molecules. The unique physicochemical and electrochemical properties of nanomaterials facilitate the fabrication of potentially robust electrochemical sensor systems with good biocompatibility and outstanding electrical conductivity. Well designed nanometric architectures assist with the creation of suitable environments for biomolecule immobilization, overpotential decreases, and improvements in sensitivity and long-term stability. The sensitive, reliable and rapid analysis of critical disease biomarkers and globally emerging pharmaceutical compounds may enable an extensive range of preemptive medical diagnostic applications. Rapid, energy efficient and green water disinfection technologies are key elements in addressing the immense challenges for the provision of clean potable water globally. Electrochemical water disinfection strategies working in conjunction with photo- and electrocatalysts have many advantages over the other

conventional disinfection strategies. The novel strategy of combining both photocatalysts and electrocatalysts for the removal of bacterial contamination in water demonstrates the vast potential of new generation technologies to benefit clean water-deprived regions on a global scale.

References

(1) Updike, S.; Hicks, G. The enzyme electrode. *Nature* **1967,** *214*, 986.

(2) Tsai, T.-W.; Heckert, G.; Neves, L. s. F.; Tan, Y.; Kao, D.-Y.; Harrison, R. G.; Resasco, D. E.; Schmidtke, D. W. Adsorption of glucose oxidase onto single-walled carbon nanotubes and its application in layer-by-layer biosensors. *Anal. Chem.* **2009,** *81* (19), 7917.

(3) Clark, L. C.; Lyons, C. Electrode systems for continuous monitoring in cardiovascular surgery. *Ann. N. Y. Acad. Sci.* **1962,** *102* (1), 29.

(4) Adhikari, B.-R.; Govindhan, M.; Chen, A. Carbon nanomaterials based electrochemical sensors/biosensors for the sensitive detection of pharmaceutical and biological compounds. *Sensors* **2015,** *15* (9), 22490.

(5) Kirsch, J.; Siltanen, C.; Zhou, Q.; Revzin, A.; Simonian, A. Biosensor technology: recent advances in threat agent detection and medicine. *Chem. Soc. Rev.* **2013,** *42* (22), 8733.

(6) Govindhan, M.; Adhikari, B.-R.; Chen, A. Nanomaterials-based electrochemical detection of chemical contaminants. *RSC Adv.* **2014,** *4* (109), 63741.

(7) Pandey, P.; Datta, M.; Malhotra, B. Prospects of nanomaterials in biosensors. *Anal. Let.* **2008,** *41* (2), 159.

(8) Xu, R.-X.; Yu, X.-Y.; Gao, C.; Liu, J.-H.; Compton, R. G.; Huang, X.-J. Enhancing selectivity in stripping voltammetry by different adsorption behaviors: the use of

nanostructured Mg–Al-layered double hydroxides to detect Cd (II). *Analyst* **2013,** *138* (6), 1812.

(9) Tang, D.; Tang, J.; Su, B.; Chen, G. Ultrasensitive electrochemical immunoassay of staphylococcal enterotoxin B in food using enzyme-nanosilica-doped carbon nanotubes for signal amplification. *J.Aagri Food Chem.* **2010,** *58* (20), 10824.

(10) Chaubey, A.; Malhotra, B. Mediated biosensors. *Biosens. Bioelectron.* **2002,** *17* (6), 441.

(11) Mirsky, V. M.; Riepl, M.; Wolfbeis, O. S. Capacitive monitoring of protein immobilization and antigen–antibody reactions on monomolecular alkylthiol films on gold electrodes. *Biosensors and Bioelectronics* **1997,** *12* (9), 977.

(12) Guiseppi-Elie, A.; Lingerfelt, L. Impedimetric detection of dna hybridization: Towards near-patient dna diagnostics. *Immobilisation of DNA on Chips I* **2005**, 161.

(13) Ronkainen, N. J.; Halsall, H. B.; Heineman, W. R. Electrochemical biosensors. *Chemical Society Reviews* **2010,** *39* (5), 1747.

(14) Luppa, P. B.; Sokoll, L. J.; Chan, D. W. Immunosensors—principles and applications to clinical chemistry. *Clinica chimica acta* **2001,** *314* (1), 1.

(15) Heyrovský, J. The development of polarographic analysis. *Analyst* **1956,** *81* (961), 189.

(16) Banica, F.-G. *Chemical sensors and biosensors: fundamentals and applications*; John Wiley & Sons, 2012.

(17) Katz, E.; Willner, I. Probing biomolecular interactions at conductive and semiconductive surfaces by impedance spectroscopy: routes to impedimetric immunosensors, DNA-sensors, and enzyme biosensors. *Electroanalysis* **2003,** *15* (11), 913.

(18) Pei, R.; Cheng, Z.; Wang, E.; Yang, X. Amplification of antigen–antibody interactions based on biotin labeled protein–streptavidin network complex using impedance spectroscopy. *Biosens. Bioelectron.* **2001,** *16* (6), 355.

(19) Gupta, V. K.; Jain, R.; Radhapyari, K.; Jadon, N.; Agarwal, S. Voltammetric techniques for the assay of pharmaceuticals—a review. *Anal. Biochem.* **2011,** *408* (2), 179.

(20) Uslu, B.; Ozkan, S. A. Electroanalytical methods for the determination of pharmaceuticals: a review of recent trends and developments. *Anal. Let.* **2011,** *44* (16), 2644.

(21) Chen, A.; Shah, B. Electrochemical sensing and biosensing based on square wave voltammetry. *Anal. Methods* **2013,** *5* (9), 2158.

(22) Hierlemann, A.; Gutierrez-Osuna, R. Higher-order chemical sensing. *Chem. Rev.* **2008,** *108* (2), 563.

(23) Bonizzoni, M.; Anslyn, E. V.; ACS Publications, 2009.

(24) Maduraiveeran, M.; Adhikari, B.-R.; Chen, A. Nanomaterials-based electrochemical detection of chemical contaminants. *RSC Adv*. **2014**, *4*, 63741.

(25) *To*h, H. S.; Tschulik, K.; Batchelor-McAuley, C.; Compton, R. G. Electrochemical quantification of iodide ions in synthetic urine using silver nanoparticles: a proof-of-concept. *Analyst* **2014,** *139* (16), 3986.

(26) Wang, J. Portable electrochemical systems. *Trends Anal. Chem; TrAC.* **2002,** *21* (4), 226.

(27) Brownson, D. A.; Banks, C. E. Graphene electrochemistry: an overview of potential applications. *Analyst* **2010,** *135* (11), 2768.

(28) Zhang, W.; Asiri, A. M.; Liu, D.; Du, D.; Lin, Y. Nanomaterial-based biosensors for environmental and biological monitoring of organophosphorus pesticides and nerve agents. *Trends Anal. Chem; TrAC* **2014,** *54*, 1.

(29) Chen, A.; Chatterjee, S. Nanomaterials based electrochemical sensors for biomedical applications. *Chem. Soc. Rev.* **2013,** *42* (12), 5425.

(30) Kirsch, J.; Siltanen, C.; Zhou, Q.; Revzin, A.; Simonian, A. Biosensor technology: Recent advances in threat agent detection and medicine. *Chem. Soc. Rev.* **2013**, *42*, 8733–8768.

(31) Xu, R.X.; Yu, X.Y.; Gao, C.; Liu, J.H.; Compton, R.G.; Huang, X.J. Enhancing selectivity in stripping voltammetry by different adsorption behaviors: The use of nanostructured Mg-Al-layered double hydroxides to detect Cd (II). *Analyst* **2013**, *138*, 1812–1818.

(32) Govindhan, M.; Lafleur, T.; Adhikari, B.-R.; C*hen, A.* **Elec**tr*och*emical sensor based on carbon nanotubes for the simultaneous detection of phenolic pollutants. *Electroanalysis* **2015**, *27*, 902–909.

(33) Hung, V.W.-S.; Kerman, K. Gold electrodeposition on carbon nanotubes for the enhanced electrochemical detection of homocysteine. *Electrochem. Commun.* **2011**, *13*, 328–330.

(34) Govindhan, M.; Adhikari, B.-R.; Chen, A. *Nanomaterials-based e***lect**ro*ch*emical detection of chemical contaminants. *RSC Adv.* **2014**, *4*, 63741–63760.

(35) Pandey, P.; Datta, M.; Malhotra, B.D. Prospects of nanomaterials in biosensors. *Anal. Lett.* **2008**, *41*, 159–209.

(36) Chen, A.; Chatterjee, S. Nanomaterials based electrochemical sensors for biomedical applications.*Chem. Soc. Rev.* **2013**, *42*, 5425–5438.

(37) Figueiredo-Filho, L.C.S.; Brownson, D.A.C.; Fatibello-Filho, O.; Banks, C.E. Exploring the origins of the apparent "electrocatalytic" oxidation of kojic acid at graphene modified electrodes. *Analyst* **2013**, *138*, 4436–4442.

(38) Ahmadalinezhad, A.; Wu, G.; Keeler, W.; Chen, A. Fabrication and electrochemical study of carbon modified TiO_2 nanowires. *Electrochem. Commun.* **2014**, *49*, 25–29.

(39) Goyal, R.N.; Chatterjee, S.; Rana, A.R.S. The effect of modifying an edge-plane pyrolytic graphite electrode with single-wall carbon nanotubes on its use for sensing diclofenac. *Carbon* **2010**, *48*, 4136–4144.

(40) Revin, S.B.; John, S.A. Electrochemical sensor for neurotransmitters at physiological pH using a heterocyclic conducting polymer modified electrode. *Analyst* **2012**, *137*, 209–215.

(41) Ahammad, A.; Lee, J.; Rahman, M. Electrochemical Sensors Based on Carbon Nanotubes. *Sensors* **2009**, *9*, 2289–2319.

(42) Chatterjee, S.; Chen, A. Functionalization of carbon buckypaper for the sensitive determination of hydrogen peroxide in human urine. *Biosens. Bioelectron.* **2012**, *35*, 302–307.

(43) Chatterjee, S.; Chen, A. Voltammetric detection of the dicarbonyl compound: Methylglyoxal as a flavoring agent in wine and beer. *Anal. Chim. Acta* **2012**, *751*, 66–70.

(44) Wanekaya, A.K. Applications of nanoscale carbon-based materials in heavy metal sensing and detection. *Analyst* **2011**, *136*, 4383–4391.

(45) Hong, G.; Diao, S.; Antaris, A.L.; Dai, H. Carbon nanomaterials for biological imaging and nanomedicinal therapy. *Chem. Rev.* **2015**, doi:10.1021/acs.chemrev.5b00008.

(46) Ogawa, S.; Nakayama, K.; Nakayama, M.; Mori, T.; Matsushima, M.; Okamura, M.; Senda, M.; Nako, K.; Miyata, T.; Ito, S. Methylglyoxal is a predictor in type 2 diabetic patients of intimamedia thickening and elevation of blood pressure. *Hypertension* **2010**, *56*, 471–476.

(47) Chatterjee, S.; Wen, J.; Chen, A. Electrochemical determination of methylglyoxal as a biomarker in humanplasma. *Biosens. Bioelectron.* **2013**, *42*, 349–354.

(48) Shah, B.; Lafleur, T.; Chen, A. Carbon nanotube based electrochemical sensor for the sensitive detection of valacyclovir. *Faraday Discuss.* **2013**, *164*, 135–146.

(49) Liu, M.; Chen, Q.; Lai, C.; Zhang, Y.; Deng, J.; Li, H.; Yao, S. A double signal amplification platform for ultrasensitive and simultaneous detection of ascorbic acid, dopamine, uric acid and acetaminophen based on a nanocomposite of ferrocene thiolate stabilized Fe_3O_4@Au nanoparticles with graphene sheet. *Biosens. Bioelectron.* **2013**, *48*, 75–81.

(50) Vedala, H.; Sorescu, D.C.; Kotchey, G.P.; Star, A. Chemical sensitivity of graphene edges decorated with metal nanoparticles. *Nano Lett.* **2011**, *11*, 2342–2347.

(51) Liu, F.; Xiang, G.; Yuan, R.; Chen, X.; Luo, F.; Jiang, D.; Huang, S.; Li, Y.; Pu, X. Procalcitonin sensitive detection based on grapheneGÇôgold nanocomposite film sensor platform and single-walled carbon nanohorns/hollow Pt chains complex as signal tags. *Biosens. Bioelectron.* **2014**, *60*, 210–217.

(52) Ali, I.; Khan, T.; Omanovic, S. Direct electrochemical regeneration of the cofactor NADH on bare Ti, Ni, Co and Cd electrodes: The influence of electrode potential and electrode material. *J. Mol. Catal. A Chem.* **2014**, *387*, 86–91.

(53) James, L.P.; Mayeux, P.R.; Hinson, J.A. Acetaminophen-induced hepatotoxicity. *Drug Metabol. Dispos.* **2003**, *31*, 1499–1506.

(54) Govindhan, M.; Amiri, M.; Chen, A. Au nanoparticle/graphene nanocomposite as a platform forthe sensitive detection of NADH in human urine. *Biosens. Bioelectron.* **2015**, *66*, 474–480.

(55) Adhikari, B.R.; Govindhan, M.; Chen, A. Sensitive detection of acetaminophen with graphene-based electrochemical sensor. *Electrochim. Acta* **2015**, *162*, 198–204.

(56) Endo, M.; Muramatsu, H.; Hayashi, T.; Kim, Y.A.; Terrones, M.; Dresselhaus, M.S. Nanotechnology: Buckypaper from coaxial nanotubes. *Nature* **2005**, *433*, doi:10.1038/433476a.

(57) Ahmadalinezhad, A.; Wu, G.; Chen, A. Mediator-free electrochemical biosensor based on buckypaper with enhanced stability and sensitivity for glucose detection. *Biosens. Bioelectron.* **2011**, *30*, 287–293.

(58) Wang, J.; Musameh, M.; Lin, Y. Solubilization of carbon nanotubes by nafion toward the preparation of amperometric biosensors. *J. Am. Chem. Soc.* **2003**, *125*, 2408–2409.

(59) Wang, J.; Musameh, M.; Lin, Y. Solubilization of carbon nanotubes by nafion toward the preparation of amperometric biosensors. *J. Am. Chem. Soc.* **2003**, *125*, 2408–2409.

(60) Wang, J.; Musameh, M. Enzyme-dispersed carbon-nanotube electrodes: A needle microsensor for monitoring glucose. *Analyst* **2003**, *128*, 1382–1385.

(61) Hrapovic, S.; Liu, Y.; Male, K.B.; Luong, J.H. Electrochemical biosensing platforms using platinum nanoparticles and carbon nanotubes. *Anal. Chem.* **2004**, *76*, 1083–1088.

(62) Rubianes, M.A.D.; Rivas, G.A. Enzymatic biosensors based on carbon nanotubes paste electrodes. *Electroanalysis* **2005**, *17*, 73–78.

(63) Wang, H.S.; Li, T.H.; Jia, W.L.; Xu, H.Y. Highly selective and sensitive determination of dopamine using a nafion/carbon nanotubes coated poly(3-methylthiophene) modified electrode. *Biosens. Bioelectron.* **2006**, *22*, 664–669.

(64) Zhang, Y.; Cai, Y.; Su, S. Determination of dopamine in the presence of ascorbic acid by poly (styrene sulfonic acid) sodium salt/single-wall carbon nanotube film modified glassy carbon electrode. *Anal. Biochem.* **2006**, *350*, 285–291.

(65) Habibi, B.; Jahanbakhshi, M.; Pournaghi-Azar, M.H. Simultaneous determination of acetaminophen and dopamine using SWCNT modified carbonGÇôceramic electrode by differential pulse voltammetry. *Electrochim. Acta* **2011**, *56*, 2888–2894.

(66) Zeng, B.; Wei, S.; Xiao, F.; Zhao, F. Voltammetric behavior and determination of rutin at a single-walled carbon nanotubes modified gold electrode. *Sens. Actuators B Chem.* **2006**, *115*, 240–246.

(67) Yu, X.; Kim, S.N.; Papadimitrakopoulos, F.; Rusling, J.F. Protein immunosensor using singlewall carbon nanotube forests with electrochemical detection of enzyme labels. *Mol. Biosyst.* **2005**, *1*, 70–78.

(68) Li, J.; Zhang, Y.; Yang, T.; Zhang, H.; Yang, Y.; Xiao, P. DNA biosensor by self-assembly of carbon nanotubes and DNA to detect riboflavin. *Mater. Sci. Eng. C* **2009**, *29*, 2360–2364.

(69) Yogeswaran, U.; Thiagarajan, S.; Chen, S.M. Nanocomposite of functionalized multiwall carbon nanotubes with nafion, nano platinum, and nano gold biosensing film for simultaneous determination of ascorbic acid, epinephrine, and uric acid. *Anal. Biochem.* **2007**, *365*, 122–131.

(70) Yi, H.; Zheng, D.; Hu, C.; Hu, S. Functionalized multiwalled carbon nanotubes through *in situ* electropolymerization of brilliant cresyl blue for determination of epinephrine. *Electroanalysis* **2008**, *20*, 1143–1146.

(71) Guo, M.; Chen, J.; Li, J.; Nie, L.; Yao, S. Carbon nanotubes-based amperometric cholesterol biosensor fabricated through layer-by-layer technique. *Electroanalysis* **2004**, *16*, 1992–1998.

(72) Li, G.; Liao, J.M.; Hu, G.Q.; Ma, N.Z.; Wu, P.J. Study of carbon nanotube modified biosensor for monitoring total cholesterol in blood. *Biosens. Bioelectron.* **2005**, *20*, 2140–2144.

(73) Martinez, N.A.; Messina, G.A.; Bertolino, F.A.; Salinas, E.; Raba, J. Screen-printed enzymatic biosensor modified with carbon nanotube for the methimazole determination in pharmaceuticals formulations. *Sens. Actuators B Chem.* **2008**, *133*, 256–262.

(74) Ghalkhani, M.; Shahrokhian, S.; Ghorbani-Bidkorbeh, F. Voltammetric studies of sumatriptan on the surface of pyrolytic graphite electrode modified with multi-walled carbon nanotubes decorated with silver nanoparticles. *Talanta* **2009**, *80*, 31–38.

(75) Kachoosangi, R.T.; Wildgoose, G.G.; Compton, R.G. Sensitive adsorptive stripping voltammetric determination of paracetamol at multiwalled carbon nanotube modified basal plane pyrolytic graphite electrode. *Anal. Chim. Acta* **2008**, *618*, 54–60.

(76) Zhu, C.; Yang, G.; Li, H.; Du, D.; Lin, Y.; Electrochemical sensors and biosensors based on nanomaterials and nanostructures. *Anal. Chem.* **2014**, *87* (1), 230-249.

(77) Zhu, H.; Li, L.; Zhou, W.; Shao, Z.; Chen, X. Advances in non-enzymatic glucose sensors based on metal oxides. *J. Mater.Chem.* ***B*** **2016,** *4* (46), 7333.

(78) Chen, X.; Wu, G.; Cai, Z.; Oyama, M.; Chen, X . Advances in enzyme-free electrochemical sensors for hydrogen peroxide, glucose, and uric acid. *Microchim. Acta* 2014, 181, 689.

(79) Miao, Y.; Ouyang, L.; Zhou, S.; Xu, L.; Yang, Z.; Xiao, M.; Ouyang, R. Electrocatalysis and electroanalysis of nickel, its oxides, hydroxides and oxyhydroxides toward small molecules. *Biosens.Bioelectron.* **2014,** *53*, 428.

(80) Lin, Y.; Yu, P.; Hao, J.; Wang, Y.; Ohsaka, T.; Mao, L. Continuous and simultaneous electrochemical measurements of glucose, lactate, and ascorbate in rat brain following brain ischemia. *Anal. Chem.* **2014,** *86* (8), 3895.

(81) Freeman, M. H.; Hall, J. R.; Leopold, M. C. Monolayer-protected nanoparticle doped xerogels as functional components of amperometric glucose biosensors. *Anal. Chem.* **2013,** *85* (8), 4057.

(82) Tian, K.; Prestgard, M.; Tiwari, A. A review of recent advances in nonenzymatic glucose sensors. *Mater. Sci. Eng.: C* **2014,** *41*, 100.

(83) Cao, X.; Wang, N.; Jia, S.; Shao, Y. Detection of glucose based on bimetallic PtCu nanochains modified electrodes. *Anal. Chem.* **2013,** *85* (10), 5040.

(84) Dhara, K.; Stanley, J.; Ramachandran, T.; Nair, B. G.; TG, S. B. Pt-CuO nanoparticles decorated reduced graphene oxide for the fabrication of highly sensitive non-enzymatic disposable glucose sensor. *Sens. Actuators B: Chem.* **2014,** *195*, 197.

(85) Guo, C.; Huo, H.; Han, X.; Xu, C.; Li, H. Ni/CdS bifunctional Ti@ TiO2 core–shell nanowire electrode for high-performance nonenzymatic glucose sensing. *Anal. Chem.* **2013,** *86* (1), 876.

(86) Wang, T.; Zhu, H.; Zhuo, J.; Zhu, Z.; Papakonstantinou, P.; Lubarsky, G.; Lin, J.; Li, M. Biosensor based on ultrasmall MoS2 nanoparticles for electrochemical detection of H2O2 released by cells at the nanomolar level. *Anal. Chem.* **2013,** *85* (21), 10289.

(87) Li, W.; Kuai, L.; Qin, Q.; Geng, B. Ag–Au bimetallic nanostructures: co-reduction synthesis and their component-dependent performance for enzyme-free H 2 O 2 sensing. *J. Mater. Chem. A* **2013,** *1* (24), 7111.

(88) Nagaiah, T. C.; Schäfer, D.; Schuhmann, W.; Dimcheva, N. Electrochemically deposited Pd–Pt and Pd–Au codeposits on graphite electrodes for electrocatalytic H2O2 reduction. *Anal. Chem.* **2013,** *85* (16), 7897.

(89) Wang, H.; Li, S.; Si, Y.; Zhang, N.; Sun, Z.; Wu, H.; Lin, Y. Platinum nanocatalysts loaded on graphene oxide-dispersed carbon nanotubes with greatly enhanced peroxidase-like catalysis and electrocatalysis activities. *Nanoscale* **2014,** *6* (14), 8107.

(90) Rocchitta, G.; Spanu, A.; Babudieri, S.; Latte, G.; Madeddu, G.; Galleri, G.; Nuvoli, S.; Bagella, P.; Demartis, M. I.; Fiore, V. Enzyme Biosensors for Biomedical Applications: Strategies for Safeguarding Analytical Performances in Biological Fluids. *Sensors* **2016,** *16* (6), 780.

(91) Sassolas, A.; Blum, L. J.; Leca-Bouvier, B. D. Immobilization strategies to develop enzymatic biosensors. *Biotechnol. Adv.* **2012,** *30* (3), 489.

(92) Chen, C.; Xie, Q.; Yang, D.; Xiao, H.; Fu, Y.; Tan, Y.; Yao, S. Recent advances in electrochemical glucose biosensors: a review. *Rsc Adv.* **2013,** *3* (14), 4473.

(93) Cipolatti, E. P.; Silva, M. J. A.; Klein, M.; Feddern, V.; Feltes, M. M. C.; Oliveira, J. V.; Ninow, J. L.; de Oliveira, D. Current status and trends in enzymatic nanoimmobilization. *J. Mol. Catal. B: Enzymatic* **2014,** *99*, 56.

(94) Rassaei, L.; Olthuis, W.; Tsujimura, S.; Sudhölter, E. J.; van den Berg, A. Lactate biosensors: current status and outlook. *Anal. Bioanal. Chem.* **2014,** *406* (1), 123.

(95) Erden, P. E.; Kılıç, E. A review of enzymatic uric acid biosensors based on amperometric detection. *Talanta* **2013,** *107*, 312.

(96) Kurbanoglu, S.; Ozkan, S. A.; Merkoçi, A. Nanomaterials-based enzyme electrochemical biosensors operating through inhibition for biosensing applications. *Biosens. Bioelectron.* **2017,** *89*, 886.

(97) Piao, Y.; Han, D. J.; Seo, T. S. Highly conductive graphite nanoparticle based enzyme biosensor for electrochemical glucose detection. *Sens. Actuators B: Chem.* **2014,** *194*, 454.

(98) Jia, X.; Hu, G.; Nitze, F.; Barzegar, H. R.; Sharifi, T.; Tai, C.-W.; Wågberg, T. Synthesis of palladium/helical carbon nanofiber hybrid nanostructures and their application for hydrogen peroxide and glucose detection. *ACS Appl. Mater.Interfaces* **2013,** *5* (22), 12017.

(99) Singh, J.; Roychoudhury, A.; Srivastava, M.; Chaudhary, V.; Prasanna, R.; Lee, D. W.; Lee, S. H.; Malhotra, B. Highly efficient bienzyme functionalized biocompatible nanostructured nickel ferrite–chitosan nanocomposite platform for biomedical application. *J. Phys. Chem. C* **2013,** *117* (16), 8491.

(100) Zhao, Y.; Zhang, W.; Lin, Y.; Du, D. The vital function of Fe 3 O 4@ Au nanocomposites for hydrolase biosensor design and its application in detection of methyl parathion. *Nanoscale* **2013,** *5* (3), 1121.

(101) Grieshaber, D.; MacKenzie, R.; Voeroes, J.; Reimhult, E. Electrochemical biosensors-sensor principles and architectures. *Sensors* **2008,** *8* (3), 1400.

(102) Zhang, X.; Liao, Q.; Chu, M.; Liu, S.; Zhang, Y. Structure effect on graphene-modified enzyme electrode glucose sensors. *Biosens. Bioelectron.* **2014,** *52*, 281.

(103) Liang, B.; Fang, L.; Yang, G.; Hu, Y.; Guo, X.; Ye, X. Direct electron transfer glucose biosensor based on glucose oxidase self-assembled on electrochemically reduced carboxyl graphene. *Biosens. Bioelectron.* **2013,** *43*, 131.

(104) Lang, Q.; Yin, L.; Shi, J.; Li, L.; Xia, L.; Liu, A. Co-immobilization of glucoamylase and glucose oxidase for electrochemical sequential enzyme electrode for starch biosensor and biofuel cell. *Biosens. Bioelectron.* **2014,** *51*, 158.

(105) Vilian, A. E.; Mani, V.; Chen, S.-M.; Dinesh, B.; Huang, S.-T. The Immobilization of Glucose Oxidase at Manganese Dioxide Particles-Decorated Reduced Graphene Oxide Sheets for the Fabrication of a Glucose Biosensor. *Ind. Eng. Chem. Res.* **2014,** *53* (40), 15582.

(106) Wooten, M.; Karra, S.; Zhang, M.; Gorski, W. On the direct electron transfer, sensing, and enzyme activity in the glucose oxidase/carbon nanotubes system. *Anal. Chem.* **2013,** *86* (1), 752.

(107) Bai, Y.-F.; Xu, T.-B.; Luong, J. H.; Cui, H.-F. Direct electron transfer of glucose oxidase-boron doped diamond interface: a new solution for a classical problem. *Anal. Chem.* **2014,** *86* (10), 4910.

(108) Xiong, E.; Zhang, X.; Liu, Y.; Zhou, J.; Yu, P.; Li, X.; Chen, J. Ultrasensitive electrochemical detection of nucleic acids based on the dual-signaling electrochemical ratiometric method and exonuclease III-assisted target recycling amplification strategy. *Anal. Chem.***2015,** *87* (14), 7291.

(109) Chen, J.; Liu, Z.; Peng, H.; Zheng, Y.; Lin, Z.; Liu, A.; Chen, W.; Lin, X. Electrochemical DNA biosensor based on grafting-to mode of terminal deoxynucleoside transferase-mediated extension. *Biosens. Bioelectron.* **2017,** *98*, 345.

(110) Li, Z.; Wang, Y.; Wang, J.; Tang, Z.; Pounds, J. G.; Lin, Y. Rapid and sensitive detection of protein biomarker using a portable fluorescence biosensor based on quantum dots and a lateral flow test strip. *Anal. Chem.* **2010,** *82* (16), 7008.

(111) Zou, Z.; Du, D.; Wang, J.; Smith, J. N.; Timchalk, C.; Li, Y.; Lin, Y. Quantum dot-based immunochromatographic fluorescent biosensor for biomonitoring trichloropyridinol, a biomarker of exposure to chlorpyrifos. *Anal. Chem.* **2010,** *82* (12), 5125.

(112) Kang, J.-H.; Korecka, M.; Toledo, J. B.; Trojanowski, J. Q.; Shaw, L. M. Clinical utility and analytical challenges in measurement of cerebrospinal fluid amyloid-β1–42 and τ proteins as Alzheimer disease biomarkers. *Clinical Chem.* **2013,** *59* (6), 903.

(113) Wang, H.; Wang, J.; Timchalk, C.; Lin, Y. Magnetic electrochemical immunoassays with quantum dot labels for detection of phosphorylated acetylcholinesterase in plasma. *Anal. Chem.* **2008,** *80* (22), 8477.

(114) Wen, W.; Yan, X.; Zhu, C.; Du, D.; Lin, Y. Recent advances in electrochemical immunosensors. *Anal. Chem.* **2017,** *89* (1), 138.

(115) Chikkaveeraiah, B.V.; Bhirde, A. A.; Morgan, N. Y.; Eden, H. S.; Chen, X. Electrochemical immunosensor for detection of cancer protein biomarkers. ACS Nano. 2012, 6 (8), 6546.

(116) Rehm, F. B.; Chen, S.; Rehm, B. H. Bioengineering toward direct production of immobilized enzymes: A paradigm shift in biocatalyst design. *Bioengineered* **2017**, 1.

(117) Liébana, S.; Drago, Guido A. Bioconjugation and stabilisation of biomolecules in biosensors. *Essays in Biochem.* **2016,** *60* (1), 59.

(118) Presentini, R. A new covalent peroxidase conjugation method using bis (sulfosuccinimidyl) suberate as cross-linking reagent in a two-step procedure. *J. Immunoassay Immunochem.* **2017,** *38* (1), 100.

(119) Martín-Fernández, B.; Manzanares-Palenzuela, C. L.; Sánchez-Paniagua López, M.; de-los-Santos-Álvarez, N.; López-Ruiz, B. Electrochemical genosensors in food safety assessment. *Crit. Rev. Food Sci. Nutr.* **2017,** *57* (13), 2758.

(120) Nimse, B. S.; Song, K.; Sonawane, D. M.; Sayyed, R. D.; Kim, T. Immobilization Techniques for Microarray: Challenges and Applications. *Sensors* **2014,** *14* (12).

(121) Vasilescu, A.; Nunes, G.; Hayat, A.; Latif, U.; Marty, J.-L. Electrochemical Affinity Biosensors Based on Disposable Screen-Printed Electrodes for Detection of Food Allergens. *Sensors* **2016,** *16* (11).

(122) Bulaj, G. Formation of disulfide bonds in proteins and peptides. *Biotechnol. Adv.* **2005,** *23* (1), 87.

(123) Steen Redeker, E.; Ta, D. T.; Cortens, D.; Billen, B.; Guedens, W.; Adriaensens, P. Protein engineering for directed immobilization. *Bioconjugate Chem.* **2013,** *24* (11), 1761.

(124) Zheng, M.; Zheng, L.; Zhang, P.; Li, J.; Zhang, Y. Development of bioorthogonal reactions and their applications in bioconjugation. *Molecules* **2015,** *20* (2), 3190.

(125) Patterson, D. M.; Nazarova, L. A.; Prescher, J. A. Finding the right (bioorthogonal) chemistry. *ACS Chem. Biol.* **2014,** *9* (3), 592.

(126) Kristiana, I.; Gallard, H.; Joll, C.; Croué, J.-P. The formation of halogen-specific TOX from chlorination and chloramination of natural organic matter isolates. *Water Res.* **2009,** *43* (17), 4177.

(127) Driedger, A. M.; Rennecker, J. L.; Mariñas, B. J. Sequential inactivation of Cryptosporidium parvum oocysts with ozone and free chlorine. *Water Res.* **2000,** *34* (14), 3591.

(128) Xu, P.; Janex, M.-L.; Savoye, P.; Cockx, A.; Lazarova, V. Wastewater disinfection by ozone: main parameters for process design. *Water Res.* **2002,** *36* (4), 1043.

(129) Venczel, L. V.; Arrowood, M.; Hurd, M.; Sobsey, M. D. Inactivation of Cryptosporidium parvum oocysts and Clostridium perfringens spores by a mixed-oxidant disinfectant and by free chlorine. *App. Environ. Microbiol.* **1997,** *63* (4), 1598.

(130) Larson, M. A.; Mariñas, B. J. Inactivation of Bacillus subtilis spores with ozone and monochloramine. *Water Res.* **2003,** *37* (4), 833.

(131) Dow, S.; Barbeau, B.; Von Gunten, U.; Chandrakanth, M.; Amy, G.; Hernandez, M. The impact of selected water quality parameters on the inactivation of Bacillus subtilis spores by monochloramine and ozone. *Water Res.* **2006,** *40* (2), 373.

(132) Cho, M.; Kim, J.; Kim, J. Y.; Yoon, J.; Kim, J.-H. Mechanisms of Escherichia coli inactivation by several disinfectants. *Water Res.* **2010,** *44* (11), 3410.

(133) Bergmann, M. E.; Koparal, A. Studies on electrochemical disinfectant production using anodes containing RuO 2. *J. Appl. Electrochem.* **2005,** *35* (12), 1321.

(134) Diao, H.; Li, X.; Gu, J.; Shi, H.; Xie, Z. Electron microscopic investigation of the bactericidal action of electrochemical disinfection in comparison with chlorination, ozonation and Fenton reaction. *Process Biochem.* **2004,** *39* (11), 1421.

(135) Li, X.; Diao, H.; Fan, F.; Gu, J.; Ding, F.; Tong, A. Electrochemical wastewater disinfection: Identification of its principal germicidal actions. *J. Environ. Eng.* **2004,** *130* (10), 1217.

(136) Bergmann, H.; Koparal, A. T.; Koparal, A. S.; Ehrig, F. The influence of products and by-products obtained by drinking water electrolysis on microorganisms. *Microchem. J.* **2008,** *89* (2), 98.

(137) Nakajima, N.; Nakano, T.; Harada, F.; Taniguchi, H.; Yokoyama, I.; Hirose, J.; Daikoku, E.; Sano, K. Evaluation of disinfective potential of reactivated free chlorine in pooled tap water by electrolysis. *J. Microbiol. Methods* **2004,** *57* (2), 163.

(138) Delaedt, Y.; Daneels, A.; Declerck, P.; Behets, J.; Ryckeboer, J.; Peters, E.; Ollevier, F. The impact of electrochemical disinfection on Escherichia coli and Legionella pneumophila in tap water. *Microbiol. Res.* **2008,** *163* (2), 192.

(139) Junli, H.; Li, W.; Nanqi, R.; Fang, M. Disinfection effect of chlorine dioxide on bacteria in water. *Water Res.* **1997,** *31* (3), 607.

(140) Tyrrell, S. A.; Rippey, S. R.; Watkins, W. D. Inactivation of bacterial and viral indicators in secondary sewage effluents, using chlorine and ozone. *Water Res.* **1995,** *29* (11), 2483.

(141) Vinodgopal, K.; Stafford, U.; Gray, K. A.; Kamat, P. V. Electrochemically assisted photocatalysis. 2. The role of oxygen and reaction intermediates in the degradation of 4-chlorophenol on immobilized TiO2 particulate films. *J. Phys. Chem.* **1994,** *98* (27), 6797.

(142) Dunlop, P.; Byrne, J.; Manga, N.; Eggins, B. The photocatalytic removal of bacterial pollutants from drinking water. *J. Photochem. Photobiol. A: Chem.* **2002,** *148* (1), 355.

(143) Christensen, P.; Curtis, T.; Egerton, T.; Kosa, S.; Tinlin, J. Photoelectrocatalytic and photocatalytic disinfection of E. coli suspensions by titanium dioxide. *Appl. Catal. B: Environ.* **2003,** *41* (4), 371.

(144) Butterfield, I.; Christensen, P.; Curtis, T.; Gunlazuardi, J. Water disinfection using an immobilised titanium dioxide film in a photochemical reactor with electric field enhancement. *Water Res.* **1997,** *31* (3), 675.

(145) Baram, N.; Starosvetsky, D.; Starosvetsky, J.; Epshtein, M.; Armon, R.; Ein-Eli, Y. Enhanced inactivation of E. coli bacteria using immobilized porous TiO 2 photoelectrocatalysis. *Electrochim. Acta* **2009,** *54* (12), 3381.

(146) Cho, M.; Cates, E. L.; Kim, J.-H. Inactivation and surface interactions of MS-2 bacteriophage in a TiO 2 photoelectrocatalytic reactor. *Water Res.* **2011,** *45* (5), 2104.

(147) Yuan, B.; Wang, Y.; Bian, H.; Shen, T.; Wu, Y.; Chen, Z. Nitrogen doped TiO 2 nanotube arrays with high photoelectrochemical activity for photocatalytic applications. *Appl. Surf. Sci.* **2013,** *280*, 523.

(148) Dale, G.; Hamilton, J.; Dunlop, P.; Byrne, J. Electrochemically assisted photocatalysis on anodic titania nanotubes. *Curr. Top. Electrochem.* **2009,** *14*, 89.

(149) Mazierski, P.; Nischk, M.; Gołkowska, M.; Lisowski, W.; Gazda, M.; Winiarski, M. J.; Klimczuk, T.; Zaleska-Medynska, A. Photocatalytic activity of nitrogen doped TiO 2 nanotubes prepared by anodic oxidation: The effect of applied voltage, anodization time and amount of nitrogen dopant. *Appl. Catal. B: Environ.* **2016,** *196*, 77.

(150) Fan, J.; Zhao, G.; Zhao, H.; Chai, S.; Cao, T. Fabrication and application of mesoporous Sb-doped SnO 2 electrode with high specific surface in electrochemical degradation of ketoprofen. *Electrochim. Acta* **2013,** *94*, 21.

(151) Shao, D.; Liang, J.; Cui, X.; Xu, H.; Yan, W. Electrochemical oxidation of lignin by two typical electrodes: Ti/Sb SnO 2 and Ti/PbO 2. *Chem. Eng. J.* **2014,** *244*, 288.

(152) Zhou, M.; Särkkä, H.; Sillanpää, M. A comparative experimental study on methyl orange degradation by electrochemical oxidation on BDD and MMO electrodes. *Sep. Purif. Technol.* **2011,** *78* (3), 290.

Chapter 3: Materials and Methods

3.1. Introduction

In this chapter, we will discuss a number of electrochemical approaches, primarily based on carbon nanomaterials, for the design of sensors/biosensors for clinically relevant molecules, and bifunctional electrodes for bacterial disinfection. Various techniques and instrumentation employed for the characterization of nanomaterials are also explained in this chapter.

3.2. Experimental

3.2.1. Materials

Valacyclovir, acetaminophen (AP), graphite powder, graphene oxide (GO) 2 mg/mL dispersed in water, SWCNTs (Ø0.7 nm), Poly(2-(trimethylamino)ethyl methacrylate (MADQUAT), *Saccharomyces cerevisiae (EC 1.1.1.1),* β-nicotinamide adenine dinucleotide hydrate (NAD^+), human serum (from human male AB Plasma), ethanol (98%), Trizma base, sodium monobasic phosphate, and sodium dibasic phosphate were purchased from Sigma-Aldrich. Generic valacyclovir (500 mg) and acetaminophen (325 mg) tablets were obtained from the Thunder Bay Regional Health Sciences Centre pharmacy. All valacyclovir and acetaminophen solutions were freshly prepared and used within 24 hours. Titanium plates and RuO_2 for the disinfection project were purchased from Alfa Aesar and Sigma-Aldrich, respectively. *Escherichia coli* ($ATCC^R11775^{TM}$) were purchased from the American Type Culture Collection. Nutrient broth and nutrient agar were purchased from Sigma Aldrich. LIVE/DEAD® *Bac*Light™ bacterial viability kit (Molecular Probes, Invitrogen detection technologies) were used for bacterial staining. All other reagents were of analytical grade and

utilized as supplied. All solutions were prepared with pure water (18.2 MΩ cm), which was generated by a Nanopure® water purification system.

3.2.2. Instruments and electrochemical experiments

A field-emission scanning electron microscope (FE-SEM) (Hitachi SU-70) equipped with an energy-dispersive X-ray spectrometer (EDS) (Oxford Links ISIS) was employed for the characterization of the surface morphologies and compositions of the synthesized samples. Elemental surface compositions based on quantitative EDS analysis were reported as average values of readings that were obtained at five different sites on each sample surface. X-ray diffraction (XRD) was employed to characterize the synthesized graphene oxide (GO). Fourier transform infrared spectroscopy (FTIR, Nicolet) equipped with a liquid N_2-cooled MCT detector was used for the study of the enzyme-MADQUAT interactions. Estimations of secondary structure compositions were carried out via the curve fitting of the amide I bands using the peak fitting software (SeaSlove Software Inc., USA), where the deconvoluted parameters were set with a gamma value of 1.65, with a smoothing length of 55, and the second derivative spectra were calculated over a 13-data-point range (13 cm^{-1}). Qproteome^{TM} Bacterial Protein Preparation Kit (QIAGEN, Hilden, Germany) with some modifications. Protein content was quantified using a Nanodrop instrument (Thermo Fisher Scientific, Massachusetts, USA) at a 280 nm wavelength, and metabolomes were analyzed through ^{1}H NMR (NMR; Bruker AVANCE II 400 MHz, Billerica, MA, USA). Spectra obtained through ^{1}H NMR analysis were processed using Spin Works (version 4) software (University of Manitoba, Winnipeg, Canada).

All electrochemical experiments, including cyclic voltammetry (CV), differential pulse voltammetry (DPV) and amperommetry were conducted using a CHI 660 electrochemical workstation (CH Instruments Inc., USA) with a conventional three-electrode system that

consisted of a platinum wire counter electrode, a 3.0 M KCl saturated Ag/AgCl reference electrode, and a working electrode that was comprised of a modified Ø3 mm glassy carbon electrode (GCE). All measurements were conducted at room temperature (22 ± 2 °C).

3.2.3. Electrode fabrication

3.2.3.1. Sensors/biosensor fabrication

Prior to fabrication, a glassy carbon electrode (GCE) was polished with 0.05 μm alumina powders, subsequently sonicated in pure water, and allowed to dry at room temperature. To produce reduced graphene oxide (rGO), a 2 mg/mL GO solution was added to a 0.067 M pH 7.4 phosphate buffer solution (PBS), via homogenous mixing, to form a 0.3 mg/mL GO colloidal dispersion. The GO suspension in the electrochemical cell was deoxygenated using Ar gas for 15 min Simultaneous electrochemical reduction and deposition of graphene on the GCE were performed in the GO suspension (0.3 mg/mL) with an electrode potential scan of from between -1.5 and 0.5 V at a sweep rate of 10 mV/s. The resulting rGO/GCE was cleaned with pure water, and then dried at room temperature for 1 h.[2,3]

The carbon nanohybrids were formed on GCE by drop-casting and drying 1:1 v/v ratio of the GO and SWCNT suspension (2 μL each), and then reduced by running CV in the potential range of from -0.6 to -1.5 V for five cycles at 20 mVs^{-1} in a 0.1M tris buffer solution. The ADH was immobilized by incubating 2 μL ADH (5.0 mg mL^{-1}) with 2 μL MADQUAT (50 mg ml^{-1}) over the GCE surface, which was modified with the SWCNT-rGO nanohybrid thin film. Incubation was performed in a 4^{o}C refrigerator for 30 min, followed by rinsing with the tris buffer.

3.2.3.2. Bifunctional electrode fabrication

TiO_2 nanoporous structures were grown on a titanium substrate via a three step anodization process. The anodization process was carried out in a cell that was designed with a two electrode system, a Ti plate (1.25 cm x 0.8 cm x 0.5 mm) as the anode, and a Pt coil as the cathode; it contained 0.3 wt% ammonium fluoride; NH_4F (Sigma Aldrich) and 2wt% water in ethylene glycol (Sigma Aldrich) under an applied potential of 50V. Ruthenium (III) chloride hydrate; $RuCl_3.x\ H_2O$ (Sigma Aldrich) was employed as an electrocatalyst, which was painted onto a separate bare Ti substrate. A total of 4-5 coatings of $RuCl_3.x\ H_2O$were painted onto the Ti substrate, followed by calcinations at 450^0C for 2 h in order to obtain robust RuO_2 electrocatalysts. The bifunctional electrode was subsequently fabricated by interfacing the calcinated nanostructured RuO_2 with the nanoporous TiO_2 electrode.

References

1. Chen, A.; Shah, B. Electrochemical sensing and biosensing based on square wave voltammetry. *Anal. Methods* **2013**, *5*, 2158.
2. Adhikari, B.R.; Govindhan, M; Chen, A. Simultaneous and sensitive detection of acetaminophen and valacyclovir based on two dimensional graphene nanosheets. *J. Electroanal. Chem.* **2016**, *780*, 241-248.
3. Adhikari, B.R.; Govindhan, M; Chen, A. Sensitive detection of acetaminophen with graphene-based electrochemical sensor. *Electrochim. Acta* **2015**, *37* (7) 1062-1069.

Chapter 4: Sensitive Detection of Acetaminophen with Graphene-Based Electrochemical Sensor*

4.1. Introduction

Acetaminophen, having the chemical name N-acetyl-p-aminophenol (APAP), is a widely utilized analgesic pain reliever and fever reducer.[1,2] It is considered to be safe when administered at recommended dosages; however, it can cause hepatotoxicity at higher doses.[3] Following oral ingestion, acetaminophen is rapidly absorbed and metabolized, primarily in the liver, to achieve peak plasma levels within 1 h. Plasma concentrations during therapy typically range from 2 to 20 mg/L, whereas levels of 30 – 300 mg/L are often observed in overdosed patients.[4,5] The principle routes of elimination are glucuronidation and sulfation, although oxidation may also occur.[6]

Glucuronidation is the primary route of elimination in human adults, accounting for about 45-55% of an acetaminophen dose.[6,7] This step may be catalyzed by set of *uridine diphosphate glucuronyl transferase enzymes (UGT)* UGT1A1, UGT1A6, UGT1A9, and UGT2B15 in the liver.[7-10] Approximately 30-35% of acetaminophen metabolism occurs via sulfation. In the adult human liver this is catalyzed by SULT1A1, SULT1A3, SULT1A4, SULT1E1 and SULT2A1.[11-13] The bioactivation of acetaminophen in the formation of N-acetyl-p-benzoquinone imine (NAPQI) is carried out via the CYP450 family of enzymes,[6] which are toxic metabolites that are responsible for hepatotoxicity. The toxic metabolite,

---

*This chapter has been published in *Electrochimica Acta*, **2015**, *162*, 198-204.

NAPQI, is initially detoxified by glutathione conjugation within the liver, and subsequently by acetylation in the kidneys, followed by N-acetyl transferase catalyzation, and final excretion in the urine.[8] In cases of overdose the accumulation of NAPQI is high, which causes adverse side effects.

The development of a simple, rapid, sensitive and accurate analytical technique for the determination of acetaminophen in pharmaceuticals and in clinical preparations is indeed warranted. Various methods, such as titrametry,[14,15] spectrophotometry,[16,17] HPLC,[18,19] chemililuminescence,[20] have been developed for the determination of acetaminophen in pharmaceutical tablets and biological fluids. However, titrametric, spectrophotometric and chemiluminescence methods involve tedious extraction processes prior to detection. Additionally, liquid chromatography is time consuming, which makes it unsuitable for the analysis of acetaminophen in practice.[21] On the other hand, electrochemistry provides powerful analytical techniques with advantages of instrumental simplicity, moderate cost and portability .[22] Since most electroanalytic techniques are selective and capable of highly sensitive and rapid measurements over a wide linear range, which require no sample preparation, and given the fact that acetaminophen is electroactive; electrochemical techniques may be considered as viable and improved alternatives for the determination of acetaminophen over other methods.[23]

Since nanomaterials exhibit unique mechanical, electrical, electronic, optical, magnetic, surface and biological properties, which are not found in conventional bulk materials, they have a great potential utility in analytical chemistry for sensor modification.[24,25] Graphene has recently attracted tremendous interest due to its exceptional thermal, mechanical, and electronic properties,[26] thus one of its many promising applications lies in the development of electrochemical sensors.[27,28] Single carbon atom thick graphene sheets provide extremely high

surface areas with readily available access to surface resident atom populations for electron transport, which impart a high sensitivity to adsorbed molecules.[29] Due to the unique properties of graphene, when it is utilized for the modification of bare electrodes, it has great potential for distinguishing a diverse range of organic compounds. To date, the deposition of graphene films on electrodes has typically been achieved via drop-casting solution-based graphene, which is derived from the chemical reduction of graphene oxide (GO) sheets.[30] However, these methodologies have intrinsic limitations such as a lack of control over film thickness and most importantly, toxic chemicals are involved. Most recently, the electrochemical reduction of GO to graphene has garnered considerable attention due to its rapid and green nature.[31-35] The excellent conductivity, high surface area, and oxygen-related defects of ERG films make them a sensitive promoter of electrochemical sensing processes.[36-38]

The objective of this work was to establish a convenient, cost-effective and highly sensitive method for the determination of acetaminophen in pharmaceutical formulations and human bodily fluids based on the ERG/GCE. In the present study, the electrochemical oxidation of acetaminophen on electrochemically reduced graphene (ERG)-modified glassy carbon electrodes (GCEs) was investigated, leading to the development of a high-performance electrochemical sensor for the analysis of acetaminophen, with an extremely low detection limit and a wide linear detection range. In addition, the electrochemical sensor developed in this study was successfully employed for the detection of acetaminophen in human serum and pharmaceutical samples, demonstrating that the proposed electrochemical sensor has strong potential for practical utility in clinical and quality control laboratories, as well for therapeutic drug monitoring and hepatotoxic serum level determination in hospital laboratories.

4.2. Experimental

4.2.1. Apparatus

All electrochemical experiments, including cyclic voltammetry (CV), differential pulse voltammetry (DPV) and amperommetry were performed with a CHI 660 electrochemical workstation (CH Instruments Inc., USA) using a conventional three-electrode system that consisted of a platinum coil counter electrode, a Ag/AgCl (3 M KCl) reference electrode, and a working electrode, which was comprised of 3 mm in diameter (modified and unmodified) glassy carbon electrodes (GCEs). A field-emission scanning electron microscope (FE-SEM) (Hitachi SU-70) was utilized for the characterization of the graphene-modified GCE surface. All experiments were performed at room temperature, 20 ± 2 ˚C, and the electrode potentials quoted are versus an Ag/AgCl electrode.

4.2.2. Chemicals and reagents

Acetaminophen (AP), graphene oxide (GO) dispersed in water (2 mg/mL), and human serum (from human male AB Plasma) were purchased from Sigma-Aldrich. Generic acetaminophen (325 mg tablets) was obtained from the Thunder Bay Regional Health Sciences Center pharmacy. All other reagents were of analytical grade and utilized as supplied. All solutions were prepared with pure water (18.2 MΩ cm), which was generated by a Nanopure® water purification system. All acetaminophen solutions were freshly prepared and used within 24 h.

4.2.3. Electrode fabrication

Prior to modification, a glassy carbon electrode (GCE) was polished with 0.05 μm alumina powders, subsequently sonicated in pure water, and allowed to dry at room temperature.

To produce the ERG, a 2 mg/mL GO solution was added to a 0.067 M pH 7.4 phosphate buffer solution (PBS) via homogenous mixing, to form a 0.3 mg/mL GO colloidal dispersion. The GO suspension in the electrochemical cell was deoxygenated using Ar gas for 15 min Simultaneous electrochemical reduction and deposition of graphene on the GCE were performed in the GO suspension (0.3 mg/mL) with an electrode potential scan of between -1.5 and 0.5 V at a sweep rate of 10 mV/s. The resulting ERG/GCE was cleaned with pure water, and then dried at room temperature for 1 h.

4.2.4 Electrochemical measurements

Electrochemically reduced graphene modified glassy carbon electrodes were used as working electrodes in a three-electrode electrochemical cell. A stock solution of 0.01 M acetaminophen was prepared, where after a calculated amount of stock solution was added to 20 mL of 0.1M phosphate buffer solution (PBS) at pH 7.4 to obtain the desired concentration of acetaminophen. The experiments were carried out by studying the cyclic voltammetric behavior of the acetaminophen at a potential range of from 0.0 to 0.6 V. The DPV was performed at potential range of from 0.0 V to 0.6 V, with a pulse width of 0.2 s, pulse period of 0.5 s and potential increment of 4 mV. All amperommetric measurements were acquired at 0.5 V with continuous magnetic stirring in order to maintain a homogeneous concentration.

4.2.5. Determination of pharmaceutical samples in human serum

The developed sensor was tested for the determination of generic acetaminophen tablets in human serum. Prior to conducting the experiment, the human serum sample had been stored in a freezer. The tablets were weighed, ground into a powder, and then dissolved in 5 mL of human serum samples to obtain a 0.01 M stock solution concentration. The solution was treated with acetonitrile for protein precipitation and then sonicated for 5 min The acetaminophen/human

serum solution was then centrifuged at 4000 rpm for 15 min in order to remove any protein residues. The supernatant was subsequently used as sample for the determination of the acetaminophen concentration using DPV and amperommetry. The calculated volume of acetaminophen concentration from stock solution was added to 20 mL PBS (0.1M) to achieve required concentration of pharmaceutical acetaminophen tablet.

4.3. Result and Discussion

4.3.1. Surface and electrochemical characterization of the ERG/GCE

FE-SEM was employed to study the surface characteristics and morphology of the ERG modified GCE. The SEM image presented in Fig. 4.1A confirmed the existence of uniformly covered ERG on the GCE surface. It is anticipated that the simultaneous electrochemical reduction and deposition of graphene used in this study may be applied to modify any conducting electrode surface (Fig 4.1B). Fig. 4.2 presents the cyclic voltammograms (CVs) of the ERG/GCE recorded in a 0.1 M phosphate buffer solution (PBS) (pH 7.4) at a sweep rate of 20 mV/s in the absence (Curve a), and in the presence of 250 μM acetaminophen (Curve c). For comparison, the CV of a bare GCE measured in a 0.1 M PBS and after addition of 250 μM acetaminophen solution is also included in Fig.4.2 (inset). As expected, no oxidation and reduction peaks appeared for the ERG/GCE, in the PBS at the applied potential range. However, a comparison of Curve obtained from bare GCE and ERG/ GCEin 0.1 M PBS indicates that the surface area/double-layer capacitance of the ERG/GCE was much higher than that of the bare GCE. In the presence of acetaminophen, a broad peak appeared at ~ +0.5 V (inset), which can be attributed to the electrochemical oxidation of acetaminophen, indicating a slow rate of electron transfer at the bare GCE. In contrast, for the ERG/GCE, a pair

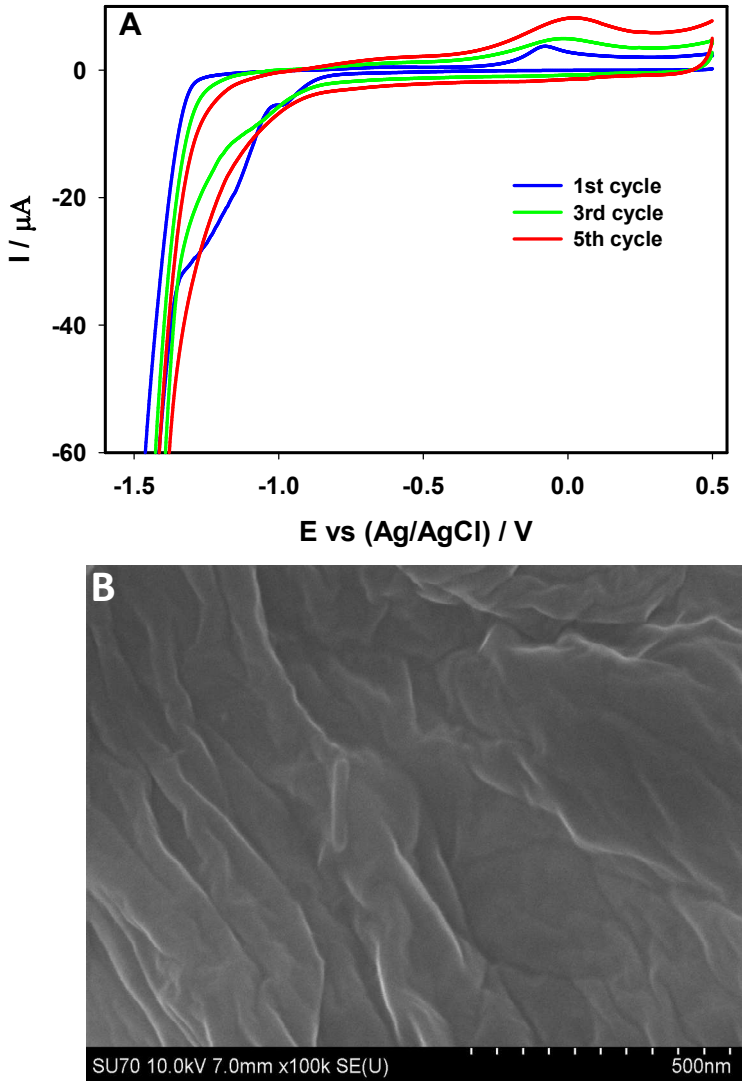

Figure 4. 1. (A) CVs (the 1st, 3rd and 5th cycle) of a glassy carbon electrode (GCE) recorded in 0.1 M PBS (pH 7.4) containing 0.3 mg mL^{-1} GO at a scan rate of 10 m Vs^{-1} . (B) SEM image of the GCE modified with electrochemical reduced graphene (ERG).

of strong and well-defined redox peaks was observed with Epa at 387 mV and Epc at 316 mV, showing that the fabricated ERG/GCE favours the reversible electrochemical reaction, as illustrated in the scheme below:

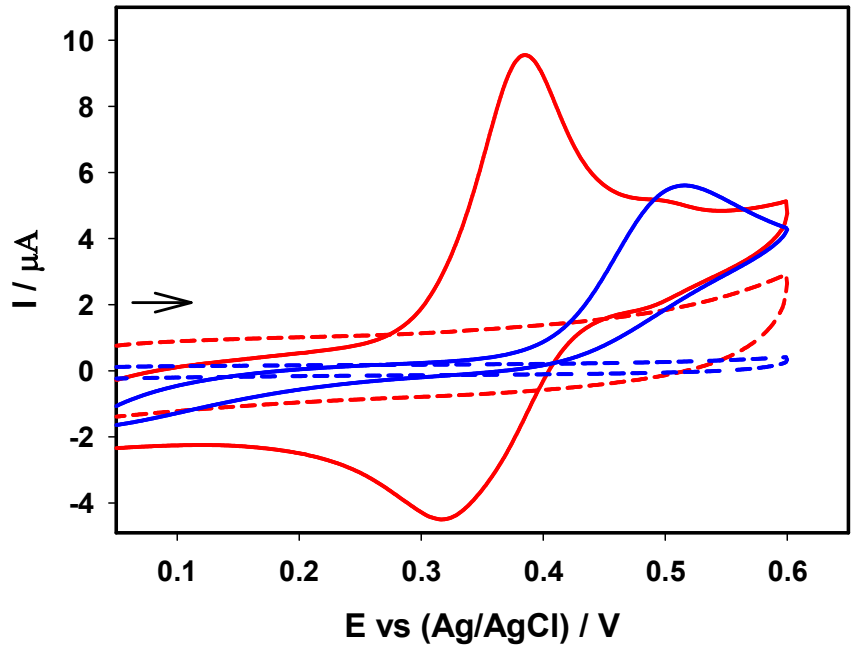

Figure 4. 2. CVs of the bare GCE (blue curves) and the ERG/GCE (red curves) recorded in 0.1 M PBS (pH 7.4) in the absence (dashed lines) and in the presence of 250 µM acetaminophen (solid lines) in 0.1 M PBS at a scan rate of 20 m Vs^{-1}.

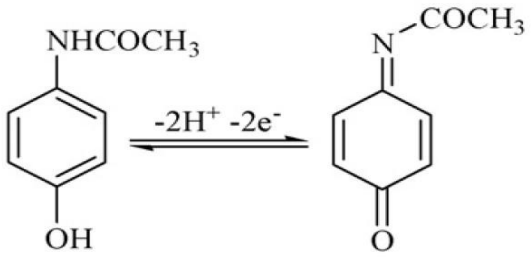

where two electrons and two protons are involved in the oxidation and reduction process. The significant increase in the peak currents and the well-defined redox peaks show that the

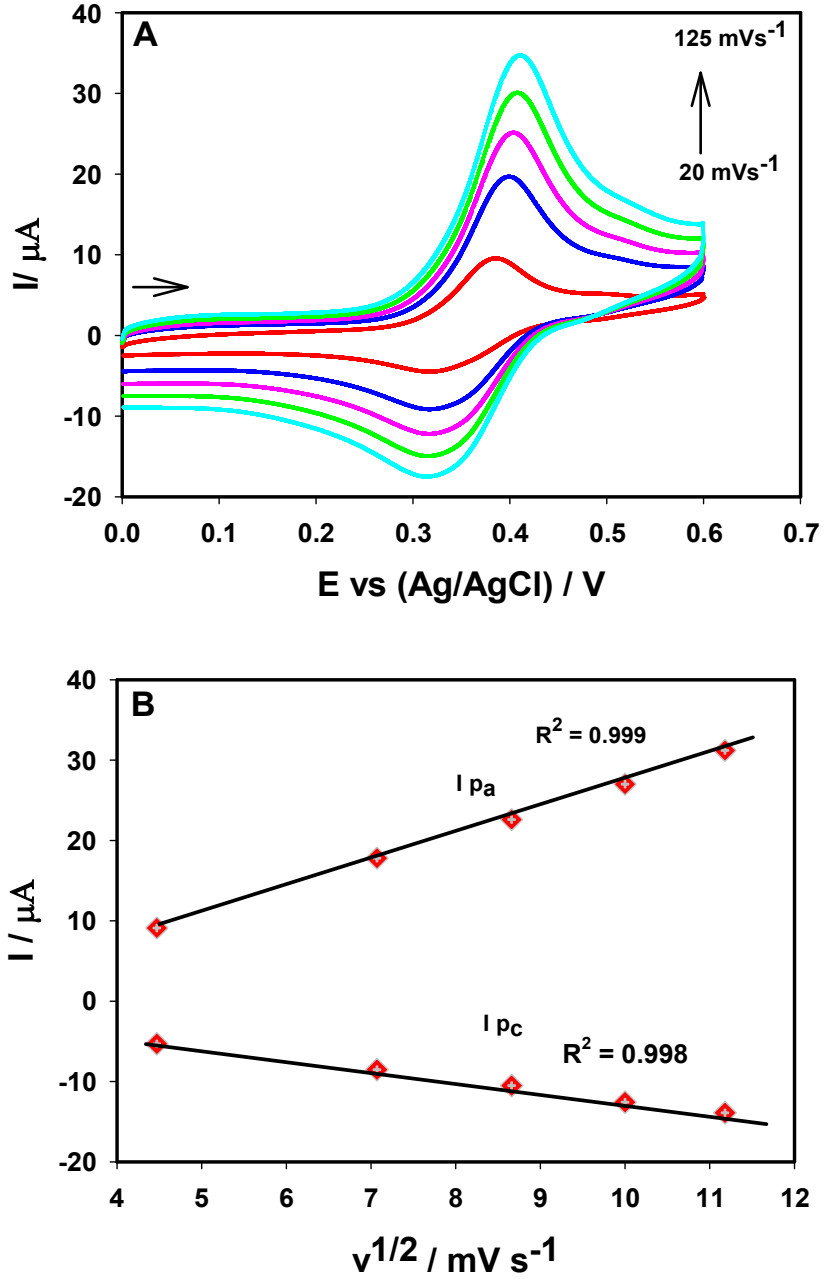

Figure 4. 3. (A) CVs of the ERG/GCE recorded in 0.1 M PBS (pH 7.4) containing 250 µM acetaminophen at different scan rates varied from 20 to 125 mV^{-1} ; (B) Plots of the anodic and cathodic peak currents versus the square root of the scan rates.

ERG/GCE not only had a high electrochemical active surface area, but also possessed excellent electrocatalytic activity, which are desirable attributes for the development of electrochemical biosensors. We also studied the effect of the scan rate on the electrochemical oxidation and

reduction of acetaminophen at the ERG/GCE. Fig. 4.3A displays the CVs recorded in a 0.1 M PBS + 250 µM acetaminophen solution at different scan rates (20, 50, 75, 100 and 125 mV/s).The Epa was only slightly shifted to positive potentials, while the Epc was negatively shifted marginally, further confirming the rapid charge-transfer kinetics of the produced ERG. Fig. 4.3B presents the plots of anodic peak current (I_{Pa}) as well as the cathodic peak current (I_{Pc}) versus the square root of scan rate ($v^{1/2}$); the decent linear relationship indicates that the electrochemical oxidation and reduction was a diffusion-controlled process.[39]

4.3.2. Effect of electrodeposition cycles

The influence of the electrochemical deposition cycles on the behavior of the resulting ERG/GCE was also investigated using DPV. Fig.4.4 presents the DPV curves of three different modified GCEs, which were prepared with two, five and ten electrodeposition cycles, as described in Section 2.3, which was recorded in a 0.1M PBS (pH7.4) containing 250 µM

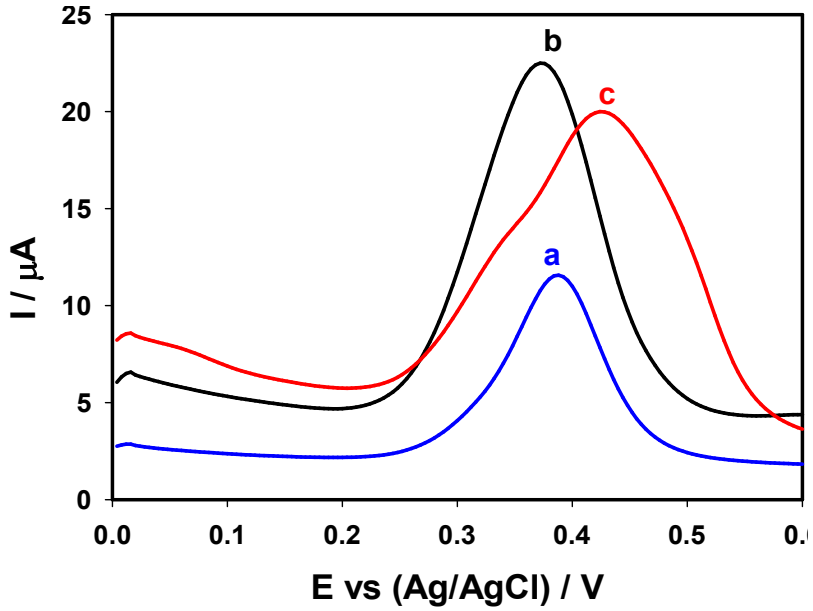

Figure 4. 4. DPVs of the GCE modified with two-cycle (a), five-cycle (b) and ten-cycle (c) electrodeposition of graphene measured in 0.1 M PBS (pH 7.4) containing 250mM acetaminophen.

acetaminophen. When increasing the electrodeposition, from two cycles (Curve a) to five cycles (Curve b), (i) the background current was increased from ~2.5 to 5.0 μA, showing that the electrochemical active surface area/double-layer capacitance was doubled; (ii) the peak potential was negatively shifted from ~385 to ~370 mV, indicating the catalytic activity of the formed ERG was enhanced; and (iii) the current response to acetaminophen was also significantly increased, from ~9.5 to 17.5 μA. However, a further increase of the electrodeposition, from 5 to 10 cycles (Curve c) resulted in a positive shift of the peak potential and a decrease of the current response to acetaminophen, revealing that a thicker ERG coating could inhibit electron transfer and decrease the electrocatalytic activity. Consequently, five electrodeposition cycles were employed to fabricate the ERG/GCEs for the detection of acetaminophen. In addition, a comparison of the CV curve c in Fig. 2 and the DPV curve b in Fig. 4 revealed that the current response to acetaminophen of the ERG/GCE was over twice as high as when measurements were carried out using DPV, indicating that DPV is a superior technique than CV for the detection of acetaminophen.

4.3.3. Acetaminophen detection using DPV

Fig. 4.5A displays a series of the DPV curves of the ERG/GCE recorded in a 0.1M PBS containing n μM acetaminophen, where n was varied from 0.0 to 800. The concentration was increased at 10 and 100-μM intervals when $n \leq 45$ and $n \geq 100$, respectively. For clarification, the DPV curves with the acetaminophen concentration, changing from 0.0 to 45 μM, are enlarged and presented as an insert in Fig. 5A. The current response was observed to be linearly elevated with

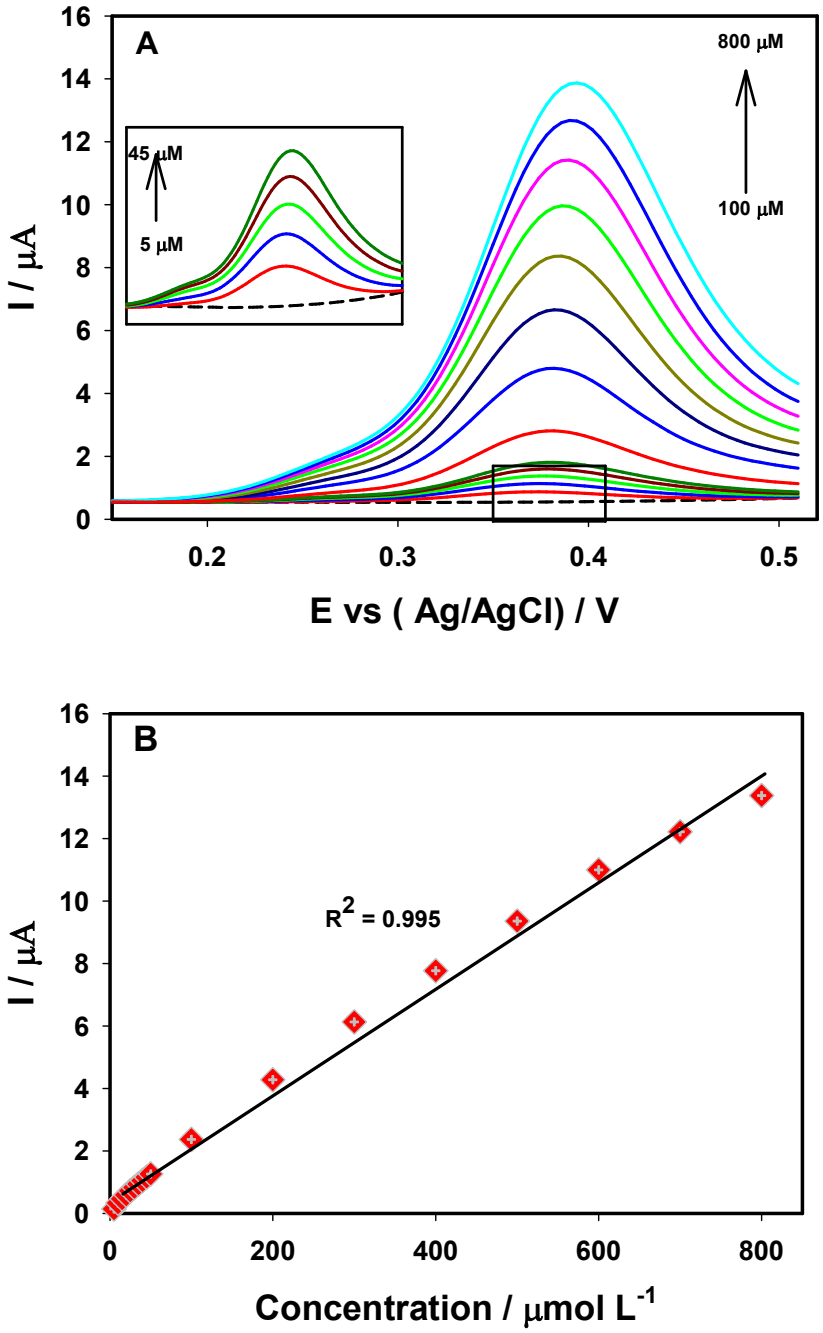

Figure 4. 5. (A) DPVs of the ERG/GCE recorded in 0.1 M PBS (pH 7.4) containing different acetaminophen concentrations (5 to 800mM). For clarification, the inset is the amplified DPV responses to acetaminophen at the low concentrations (5–45mM) marked by the black rectangle; (B) the calibration plot of the current response against acetaminophen concentrations varied from 5 to 800mM.

the increase of acetaminophen concentrations. The calibration plot of the current response of the ERG/GCE versus the acetaminophen concentration is presented in Fig. 4.5B, showing a very good linear relationship, with the correlation coefficient R^2 = 0.996. The limit of detection (LOD) was calculated using 3σ / b, where σ is the standard deviation of the blank, and b is the slope of the calibration curve. The LOD obtained through DPV was 1.2 μM. According to the acetaminophen nomogram (plot of acetaminophen serum concentration against time), a serum plasma concentration of higher than 700 μM at four-hours, or higher than 160 μM at twelve-hours post-ingestion of acetaminophen tablets, is considered as hepatotoxicity.[40,41] Thus, the wide linear detection range (5 – 800 μM) of DPV enabled by the ERG/GCE might be utilized for the detection of acetaminophen serum levels of overdosed patients.

4.3.4. Acetaminophen detection via amperometry

During the pharmaceutical formulation, as well as quality control testing of acetaminophen products, a lower than 5 μM measurable detection limit is required. The analytical performance of the ERG/GCE, challenged with low acetaminophen concentrations (5nM to 4 μM), was evaluated utilizing the amperommetric technique. The effect of the applied electrode potential on the amperommetric response to acetaminophen was investigated at different potentials (0.40, 0.45, 0.50, 0.55 and 0.60 V), showing that the current response was increased when the potential was elevated to 0.5 V. However, the current response remained almost the same with further increases of the electrode potential, to 0.55 and 0.60 V. Thus 0.50 V was selected for the amperommetric detection. Fig. 4.6A depicts the amperommetric response of the ERG/GCE at the applied constant electrode potential of 0.5 V to the addition of acetaminophen in a 0.1 M PBS. A rapid increment of current was observed upon the successive

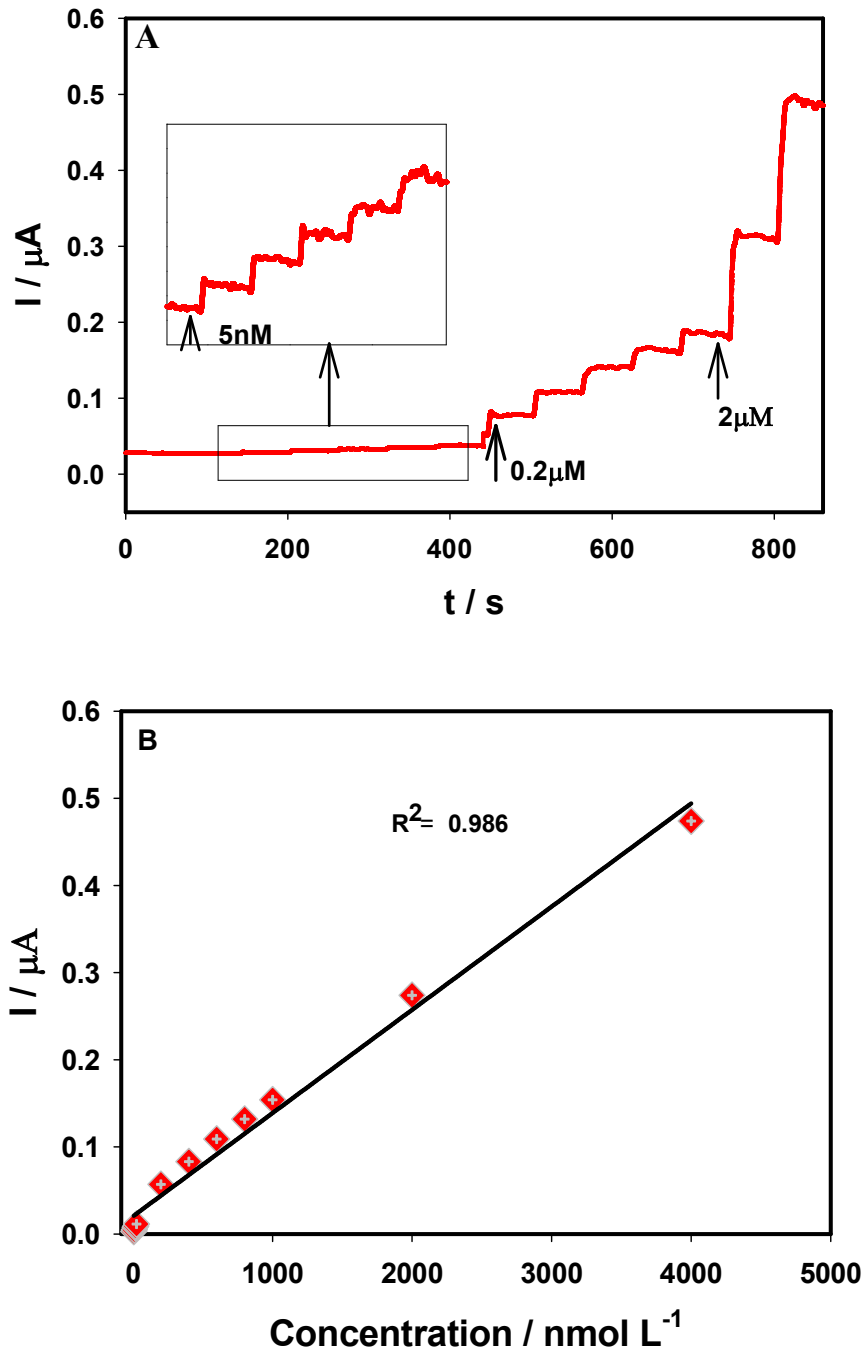

Figure 4. 6. (A) Amperometric current responses of the ERG/GCE as a result of the successive addition of acetaminophen at the increments of 5 nM, 0.2mM and 2mM at the electrode potential of 0.5 V in 0.1 M PBS (pH 7.4). The inset is the amplified amperometric responses to acetaminophen at the low concentrations (5–25 nM) marked by the black rectangle; (B) the calibration plot of the current responses against the acetaminophen concentration varied from 5 to 4000 nM.

addition of 5 nM (first segment), 0.2 µM (second segment) and 2 µM acetaminophen (third segment). For clarification, the initial segment recorded at very low concentrations was enlarged and presented as an insert in Fig. 4.6A. Fig. 4.6B presents the calibration plot of the amperommetric current response versus the acetaminophen concentration, showing a good linear relationship in the tested acetaminophen concentration range, with a correlation coefficient of R^2 = 0.986. The limit of detection (LOD) was calculated as described previous in section 3.3. The LOD obtained through amperometry was 2.13 nM. The performance of different electrochemical sensors for acetaminophen detection reported in the literature is compared in Table 4.1, showing that the ERG/GCE developed in the present study exhibited a much lower LOD, as well as a much wider linear range.

Table 4. 1. Comparison of the recently reported electrochemical sensors for acetaminophen.

Modified electrodes	**pH**	**Analytical methods**	**Detection limit (µM)**	**Linear range (µM)**	**Reference**
SWCNT-GNS/GCE	*7.0*	*DPV*	*0.038*	*0.05-64.5*	*41*
Graphene/GCE	*9.3*	*SWV*	*0.032*	*0.1-20*	*42*
GRPE	*8.5*	*SWV*	*0.60*	*2.5-143*	*43*
Nafion/TiO2-GR/GCE	*7.0*	*DPV*	*0.21*	*1-20*	*44*
Fe3O4-PDDA-G/GCE	*7.0*	*DPV*	*0.037*	*0.1-100*	*45*
ERG/Ni2O3-NiO/GCE	*7.0*	*DPV*	*0.02*	*0.04-100*	*46*
ERG/GCE	***7.4***	***Amperommetry DPV***	***0.0021 1.2***	***0.005-4 5-800***	***This work***

4.3.5. Interference studies

The selective capability of the fabricated ERG/GCE sensor was investigated via the detection of acetaminophen, as well as a number of potential co-existing electroactive species, such as ascorbic acid, uric acid, adenine, glucose andsucrose in a 0.1M PBS (pH 7.4). As shown in Fig. 4.7A, to facilitate the evaluation of the selective detection of acetaminophen, As a DPV response was recorded in seven different measurments keeping 20 μM acetaminophen concentration constant for all the measurments. Initially, 20 μM acetaminophen was injected into a 20 mL 0.1 M PBS; the addition generated a current response of approximately 0.72 μA (a). Thereafter, 40 μM of ascorbic acid(b), uric acid (c), adenine (d), glucose (e), sucrose (f) and their mixture (g) was added in 0.1 M PBS (pH=7.4). Compared to the curves aig, as shown in Fig. 4.7B, considering current response obtained through 20 μM acetaminophen (curve a) as initial current (100%), the current response variation range among curve b, c, d, e, f and g after addition of double amount of interfering biomolecules was within a 3%. The results suggest that the as-prepared sensor showed the good selectivity for acetaminophen detection.

4.3.6. Reproducibility and stability of ERG/GCE sensor

The reproducibility and stability of the ERG/GCE were investigated utilizing the DPV technique. To investigate the reproducibility of the modified electrode, four different electrodes were prepared simultaneously under the same conditions, and DPV was performed in 0.1 M PBS that contained 250 μM acetaminophen. A relative standard deviation (RSD) of 0.78% (n=4) was achieved, which confirmed that the ERG/GCE had excellent reproducibility. In an additional experiment to verify stability, seven different DPVs were conducted each day for up to seven days in a 0.1 M PBS + 250 μM acetaminophen solution. A relative standard deviation (RSD) of

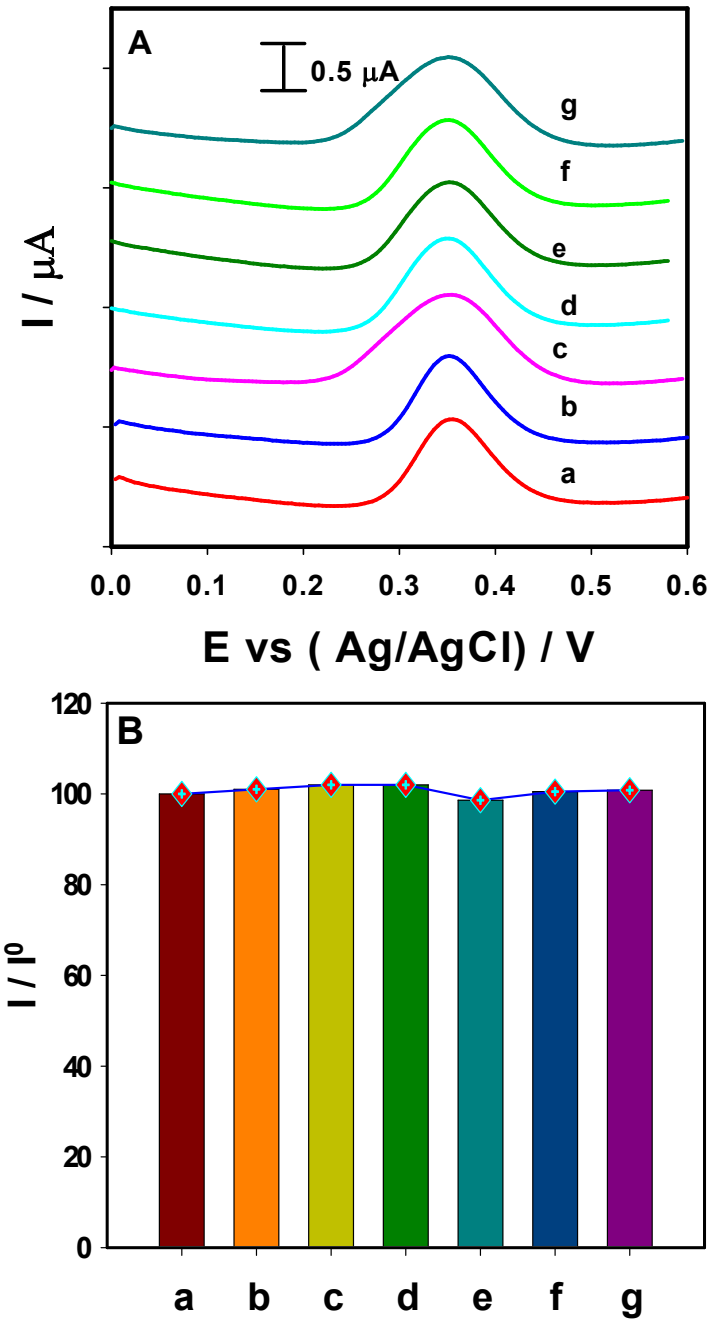

Figure 4. 7. (A) DPVs of the ERG/GCE recorded in 0.1 M PBS (pH 7.4) + 20mM acetaminophen without any interferents (a) and in the presence of 40mM ascorbic acid (b), 40mM uric acid (c), 40mM adenine (d), 40mM glucose (e), 40mM sucrose (f) and the mixture of all these biomolecules with 40mM each (g). (B) Relative anodic peak current response derived from Fig. 4.7A.

7.07% (n=7) was found, which revealed strong performance stability of the ERG/GCE in the detection of acetaminophen.

4.3.7. Detection of acetaminophen in actual samples

To validate the practical application of the proposed sensor, the fabricated electrode was tested to determine the concentration of acetaminophen within an actual sample of acetaminophen tablets in human serum plasma. The recovery tests of acetaminophen were carried out using DPV. Recovery studies were carried out subsequently to the addition of a known volume of acetaminophen tablets (325 mg) to the human serum plasma. As depicted in Table 4.2, the proposed sensor exhibited an excellent recovery, of from 96.08% to 103.2%.

Table 4.2. Recovery tests of acetaminophen in human serum plasma.

Concentration spiked/μM	Concentration detected/μM	% Recovery
10.00	10.32	103.2
20.00	19.80	98.89
25.00	24.02	96.08

4.4. Conclusions

In summary, an electrochemical sensor based on electrochemically reduced graphene was successfully fabricated for the detection of acetaminophen. The developed ERG/GCE sensor demonstrated excellent electrocatalytic activity toward the oxidation and reduction of acetaminophen. The sensor exhibited high stability, good reproducibility and exclusive selectivity for the detection of acetaminophen in the presence of other biomolecules. The newly fabricated sensor was also studied with generic acetaminophen tablet concentrations in human serum plasma, further demonstrating its capabilities in practical medical applications. The

proposed ERG/GCE sensor exhibited a much lower detection limit and a far wider linear detection range in contrast to other electrochemical sensors reported in the literature. It demonstrated strong potential for applications in the quality control testing of pharmaceutical products, as well as hepatotoxicity monitoring in hospitals and clinical laboratories.

References

1. Aghababian, R.V. Essentials of emergency medicine. *Jones and Bartlett Publishers*, Massachusetts, **2010**.
2. Ahmad, J. Hepatology and transplant hepatology: a case based approach. *Springer*, **2010**.
3. James, L.P.; Mayeux, P.R.; Hinson, J.A. Acetaminophen-induced hepatotoxicity. *Drug Metab. Dispos.* **2003**, *31*, 1499–1506.
4. Shihana, F.; Dissanayake, D.; Dargan, P.; Dawson, A. A modified low-cost colorimetric method for paracetamol (acetaminophen) measurement in plasma. *Clin. Toxicol.* **2010**, *48*, 42–46.
5. Baselt, R. Disposition of toxic drugs and chemicals in Man, *Biomedical Publications*, California, **2011**.
6. Bessems, J.G.; Vermeulen, N.P. Paracetamol (acetaminophen)-induced toxicity: molecular and biochemical mechanisms, analogues and protective approaches. *Crit. Rev. Toxicol*. **2001**, *31*, 55–138.
7. Araba, A.A.; Andrea, G.; Stephen, S.D.; Weinshilboum, R.M.; Leeder, J.S. Interindividual variability in acetaminophen sulfation by human fetal liver: Implications for pharmacogenetic investigations of drug-induced birth defects. *Clin. Mol. Teratol*. **2008**, *82*, 155–165.

8. Bock, K.W.; Forster, A.; Gschaidmeier, H.; Brück, M.; Münzel, P.; Schareck, W.; Fournel, S.G.; Burchell, B. Paracetamol glucuronidation by recombinant rat and human phenol UDP-glucuronosyltransferases. *Biochem. Pharmacol*. **1993**, *45*, 1809–1814.
9. Court, M.H.; Duan, S.X.; Von Moltke, L.L.; Greenblatt, D.J.; Patten, C.J.; Miners, J.O.; Mackenzie, P. I. Interindividual variability in acetaminophen glucuronidation by human liver microsomes: identification of relevant acetaminophen UDP glucuronosyltransferase isoforms. *J. Phar. Exp. Ther.* **2001**, *299*, 998–1006.
10. Navarro, S.L.; Chen, Y.; Li, L.; Li, S.S.; Chang, J.L.; Schwarz, Y.; King, I.B.; Potter, J.D.; Bigler, J.; Lampe, J.W. UGT1A6 and UGT2B15 polymorphisms and acetaminophen conjugation in response to a randomized, controlled diet of select fruits and vegetables. *Drug Metab. Dispos*. **2011**, *39*, 1650–1657.
11. Nagar, S.; Walther, S.; Blanchard, R.L. Sulfotransferase (SULT) 1A1 polymorphic variants *1, *2, and *3 are associated with altered enzymatic activity, cellular phenotype and protein degradation, *Mol. Pharmacol.* **2006**, *69*, 2084–2092.
12. Coughtrie, M.W. Sulfation through the looking glass-recent advances in sulfotransferase research for the curious. *Pharmacogen. J.* **2002**, *2*, 297–308.
13. Bonham Carter, S.M.; Rein, G.; Glover, V.; Sandler, M.; Caldwell, J. Human platelet phenolsulphotransferase M and P: substrate specificities and correlation with in vivo sulphoconjugation of paracetamol and salicylamide. *Br. J. Clin. Pharmacol.* **1983**, *15*, 323–330.
14. Kumar, K.G.; Latha, R. Determination of paracetamol in pure form and in dosage forms using N,N-dibromo dimethylhydantoin. *J. Pharm. Biomed. Anal.* **1997**, *15*, 1725–1728.

15. Burgot, G.; Auffret, F.; Burgot, J.L. Determination of acetaminophen by thermometric titrimetry. *Anal. Chem. Acta* **1997**, *343*, 125–128.
16. Moreira, A.B.; Oliveira, H.P.M.; Atvars, T.D.Z.; Dias, L.L.T.; Neto, G.O.; Zagatto, E.A.G.; Kubota, L.T. Direct determination of paracetamol in powered pharmaceutical samples by fluorescence spectroscopy, *Anal. Chem. Acta* 2005, 539, 257–261.
17. Nagaraja, P.; Murthy, K.C.S.; Rangappa, K.S. Spectrophotometric method for the determination of paracetamol and phenacetin, *J. Pharm. Biomed. Anal.* 1998, 17, 501–506.
18. Ravisankar, S.; Vasudevan, M.; Ganhimathi, M.; Suresh, B. Reversed-phase HPLC method for the estimation of acetaminophen, ibuprofen and chlorzoxazone in formulations. *Talanta* **1998**, *46*, 1577–1581.
19. Fujino, H.; Yoshida, H.; Nohta, H.; Yamaguchi, M. HPLC determination of acetaminophen in saliva based on precolumn fluorescence derivatization with 12-(3,5-dichloro-2,4,6-triazinyl) benzo[d]benzo[1',2'-6,5]isoindolo[1, 2-b][1,3]thiazolidine, *Anal Sci.* **2005**, *21*, 1121–1124.
20. Easwaramoorthy, D.; Yu, Y.C.; Huang, H.J. Chemiluminescence detection of paracetamol by a luminol-permanganate based reaction, *Anal. Chim. Acta* **2001**, *439*, 95–100.
21. Kang, X.; Wang, J.; Wu, H.; Liu, J.; Aksay, I.A.; Lin, Y. A graphene-based electrochemical sensor for sensitive detection of paracetamol, *Talanta* **2010**, *81*, 754–759.
22. Chen, A.; Chatterjee, S. Nanomaterials based electrochemical sensors for biomedical applications. *Chem. Soc. Rev.* **2013**, *42*, 5425–5438.
23. Manjunathaa, R.; Nagarajub, D.H.; Suresha, G.S.; Meloc, J.S.; D'souzac, S.F.; Venkateshad, T.V. Electrochemical detection of acetaminophen on the functionalized

MWCNTs modified electrode using layer-by-layer technique. *Electrochim. Acta* **2011**, *56*, 6619–6627.

24. Yang, X.; Feng, B.; He, X.; Li, F.; Ding, Y.; Fei, J. Carbon nanomaterial based electrochemical sensors for biogenic amines, *Microchim. Acta* **2013**, *80*, 935–956.
25. Chen, A. Electrocatalysis and photoelectrocehmistry based on functional nanomaterials, *Can. J. Chem.* **2014**, *92*, 581–597.
26. Novoselov, K.S.; Geim, A.K.; Morozov, S.V.; Jiang, D.; Zhang, Y.; Dubonos, S.V.; Grigorieva, I.V.; Firsov, A.A. Electric field effect in atomically thin carbon films, *Science* **2004**, *306* , 666–669.
27. Zhou, M.; Zhai, Y.M.; Dong, S.J. Electrochemical sensing and biosensing platform based on chemically reduced graphene oxide, *Anal. Chem.* **2009**, *81*, 5603–5613.
28. Shan, C.S.; Yang, H.F.; Song, J.F.; Han, D.X.; Ivaska, A.; Niu, L. Direct electrochemistry of glucose oxidase and biosensing for glucose based on graphene, *Anal. Chem.* **2009**, *81*, 2378–2382.
29. Rochefort, J.D. Interaction of substituted aromatic compounds with graphene, *Langmuir* **2009**, *25*, 210–215.
30. Pumera, M.; Ambrosi, A.; Chng, E.L.K.; Poh, H.L. Graphene for electrochemical sensing and biosensing, *Trends. Anal. Chem.* **2010,** *29*, 954–965.
31. Guo, H.L.; Wang, X.F.; Qian, Q.Y.; Wang, F.B.; Xia, X.H. A Green approach to the synthesis of graphene nanosheets, *ACS Nano* **2009**, *3*, 2653–2659.
32. Shao, Y.; Wang, J.; Engelhard, M.; Wang, C.; Lin, Y. Facile and controllable electrochemical reduction of graphene oxide and its applications. *J. Mater. Chem.* **2010**, *20*, 743–748.

33. Zhou, M.; Wang, Y.L.; Zhai, Y.M.; Zhai, J.F.; Ren, W.; Wang, F.; Dong, S.J. Controlled synthesis of large area and patterned electrochemically reduced graphene oxide films, *Chem. Eur. J.* **2009**, *15*, 6116–6120.

34. Pu, Z.; Liu, Q.; Asiri, A.M.; Obaid, Y.Y.; Sun, X. One-step electrodeposition fabrication of graphene film-confined WS2 nanoparticles with enhanced electrochemical catalytic activity for hydrogen evolution, *Electrochim. Acta* 2014, 134, 8–12.

35. Chen, L.; Tang, Y.; Wang, K.; Liu, C.; Luo, S. Direct electrodeposition of reduced graphene oxide on glassy carbon rlectrode and its rlectrochemical application. *Electrochem. Commun.* 2011, 13, 133–137.

36. Pumera, M. Graphene-based nanomaterials and their electrochemistry, *Chem. Soc. Rev.* 2010, 39, 4146–4157.

37. Pumera, M. Electrochemistry of graphene: new horizons for sensing and energy storage, *Chem. Rec.* **2009**, *9*, 211–223.

38. Randviir, E.D.; Brownson, D.A.C.; Metters, J.P.; Kadara, R.O.; Banks, C.E. The fabrication, characterisation and electrochemical investigation of screen printed graphene electrodes. *Phys.Chem.Chem.Phys.* **2014**, *6*, 4598–4611.

39. Liu, G.T.; Chen, H.F.; Lin, G.M.; Ye, P.P.; Wang, X.P.; Jiao, Y.Z.; Guo, X.Y.; Wen, Y.; Yang, H.F. One-step electrodeposition of graphene loaded nickel oxides nanoparticles for acetaminophen detection. *Biosens.Bioelectron*. **2014**, *56*, 26–32.

40. Rothrock, S.G. Acetaminophen: tarascon adult emergency pocketbook, *Jones and Bartlett publishers*, Massachusetts. **2008**.

41. Rumack, B.H. Acetaminophen hepatotoxicity: the first 35 years, *J. Toxicol. Clin. Toxicol.* **2002,** *40*, 3–20.

42. Chen, X.; Zhu, J.; Xi, Q.; Yang, W. A high performance electrochemical sensor for acetaminophen based on single-walled carbon nanotube graphene nanosheet hybrid films, *Sens. Actuat. B: Chem.* **2012**, *161*, 648–654.

43. Kang, X.; Wang, J.; Wu, H.; Liu, J.; Aksay, I.A.; Lin, Y. A graphene-based electrochemical sensor for sensitive detection of paracetamol. *Talanta* **2010**, *81*, 754–759.

44. Hossein, B.; Fahimeh, J. Sensitive determinationof paracetamol using a graphene modified carbon- paste electrode. *Afr. J. Pharm. Pharmacol*. **2012,** *6*, 1298–1305.

45. Fan, Y.; Liu, J.H.; Lu, H.T.; Zhang, Q. Electrochemical behavior and voltammetric determination of paracetamol on nafion/TiO_2-graphene modified glassy carbon electrode. *Colloid Surf. B Biointerface* **2011**, *85,* 289–292.

46. Lu, D.; Zhang, Y.; Wang, L.; Lin, S.; Wang, C.; Chen, X. Sensitive detection of acetaminophen based on Fe_3O_4 nanoparticles-coated poly(diallyldimethylammonium chloride)-functionalized graphene nanocomposite film, *Talanta* **2012**, *88,* 181–186.

Chapter 5: Simultaneous and Sensitive Detection of Acetaminophen and Valacyclovir Based on Two Dimensional Graphene Nanosheets*

5.1. Introduction

Acetaminophen (paracetamol, N-acetyl-p-aminophenol) is an extensively used analgesic anti-pyretic drug. It is primarily metabolized in liver and is safe when used at prescribed dosages; despite that all non-prescribed high dosages may cause hepatotoxicity.[1,2] Valacylovir (L-valine 2-[(2-amino-1, 6- dihydro-6-oxo-9h-purin-9-yl) methoxyl]ethyl ester) is a prodrug of the antiviral drug acyclovir, which is used for the treatment of the herpes simplex viruses and the varicella zoster virus. This compound is converted rapidly and extensively to acyclovir (the active antiviral component of valacyclovir) and L-valine, most likely in the liver and the intestine, via hydrolysis, subsequent to oral administration. Acyclovir, a prototype antiviral drug, is a DNA polymerase inhibitor with variable oral bioavailability. By contrast, valacyclovir has an oral bioavailability that is three to five times higher than that of acyclovir.[3,4] Acyclovir and its prodrug valacyclovir comprise guanine analogue antiviral drugs. They are activated by the phosphorylation of virus-specific thymidine kinase. Acyclovir uptake has been shown to be enhanced in herpes virus-infected cells, with a 10 to 30 fold greater affinity for infected cells than uninfected cells.[5]

Several traditional methods, for instance, spectrophotometry,[6,7] LC-MS[8,3] and HPLC,[4,9] have been generally utilized for the determination of valacyclovir compounds. Spectrophotometric and chromatographic methods involve time consuming analytical processes for the determination of these drugs. In recent years, electroanalytical techniques have garnered

*This chapter has been published in *Journal of Electroanalytical Chemistry*, **2016**, *162*, 198-204.

considerable attention for the detection of drugs and environmental pollutants due to their high sensitivity, excellent selectivity, low cost, rapid response, as well as expedited and straightforward operation.[10,11] A review of the literature has revealed very few publications that describe electrochemical studies on valacyclovir, and a practically nil number of publications as relates to the simultaneous detection of acetaminophen and valacyclovir compounds. Thus, there is an urgent need to explore the quantitative determination of these drugs through electrochemical techniques.

Nanomaterials with high surface areas and electrocatalytic activity have strong potential to be employed in sensor/biosensor fabrication to facilitate electrochemical measurements.[12,13] Graphene comprises a one-atom thick planar sheet of sp^2-bonded carbon atoms, which is attracting tremendous attention in terms of fundamental research and potential applications.[14,15] This nanomaterial holds tremendous promise for prospective applications in many technological fields, such as nanoelectronics[15,16] and sensors.[17,18] Graphene and its nanocomposite materials have been utilized for the electrochemical detection of various drug molecules. Cuprous oxide nanoparticles-graphene, graphene/poly(brilliant cresyl blue) nanocomposite, and single walled carbon nanotube/reduced graphene oxide nanohybrids have been utilized for the determination of acetaminophen, epinephrine, valacyclovir.[19-22] Graphene sheet provide an extremely sensitive and remarkable electrical conductor for adsorbed molecules to enable excellent electrocatalytic performance.[23-25] Chemical methods are an efficient approach for the bulk production of graphene-based sheets at low cost.[26,27] However, the excessive use of reducing agents in these techniques raises the risk of contamination in the resulting materials.

Additionally, oxygenated species that cannot be fully removed via chemical treatment may degrade the electronic properties of the product to further limit applications. [28]

Electrochemical techniques comprise an effective green method for the modification of electronic states through the adjustment of an external power source, to alter the Fermi energy level of surfaces of electrode materials. During electrochemical reduction, the aggregation of GO takes place due to increased π - π interactions between graphene layers.[29] It has been indicated through FTIR spectra that a variety of oxygen-containing functional groups are completely removed from the graphene oxide planes of electrochemically reduced graphene nanosheets. Chemically reduced graphene is not conducive to preserving its typical electronic properties due to residual defects.[30]

Market Research and Global Industry Analysts, Inc. has released recent research on the global market for acetaminophen, which is to reach $999.4 million USD by 2020 with an annual 3.8% growth, whereas valacyclovir is to attain $4.8 billion USD by 2017. According to Center for Disease Control (CDC) guideline for prevention and treatment of varicella zoster virus, analgesic (acetaminophen) drugs are usually prescribed along with valacyclovir as treatment regime to relieve from the pain**.** So simultaneous monitoring of these two drugs is highly recommended during the suspicious acetaminophen overdose cases**.** Herein, we have demonstrated a promising graphene based electrochemical sensing platform for the exclusive detection of valacyclovir, as well as for the simultaneous detection of acetaminophen and valacyclovir. The aim of the present work was to design a graphene sheet modified GCE via a facile electrochemical method for the electrochemical quantification of both emerging drugs toward practical applications in pharmacology and in biological fluids.

5.2. Experimental

5.2.1. Apparatus

For all electrochemical analysis, a three-electrode system electrochemical cell comprised of platinum wire as counter electrode, 3M KCl saturated Ag/AgCl as reference electrode, and a 3 mm glassy carbon electrode (GCE) as working electrode were utilized through CHI 660 electrochemical workstation (CH Instruments Inc., USA). Electrochemical techniques including e.g. cyclic voltammetry (CV) and differential pulse voltammetry (DPV) were employed for the electroanalysis of the drug compounds. The as-prepared rGO/GCE surface during sensor fabrication was characterized through the field-emission scanning electron microscope (FE-SEM) (Hitachi SU-70) equipped with an energy dispersive X-ray (EDX) spectrometer (Oxford AZtec operated at 20 kV). Raman spectra were recorded with a confocal micro-Raman spectrometer system built in-house.. In brief, the system consists of a Nikon eclipse E400 upright microscope coupled to a Chromex 250is spectrograph with intermediate coupling lenses and Rayleigh reject filters. The detector was a Santa Barbara Instruments (SBIG) low noise ST-10 cooled CCD camera cooled to -10°C. An Ar+ ion laser with 514.5 nm line was used for excitation and focused to ~2 μm diameter spot at a power of 5 mW. Catalina Scientific Kestrelspec software was used to control the spectrometer and collect the spectra.

5.2.2. Chemicals and reagents

All the chemicals including valacyclovir, acetaminophen (AP), and 2 mg/mL graphene oxide (GO) dispersed in water and human serum (from human male AB plasma) were purchased through Sigma-Aldrich. Generic tablets valacyclovir (500 mg) and acetaminophen (325 mg) were purchased from local pharmacy in Thunder Bay. All chemicals were used as received without further purification. Pure water was supplied through Nanopure® water purification

system for all solutions preparation. All working solutions were freshly prepared to overcome possible drug hydrolysis problem.

5.2.3. Sensor fabrication

For the sensor fabrication, GCE was polished using alumina slurry (0.05 μm) followed by sonication in pure water. 0.3 mg/mL of GO suspension was prepared in 0.1 M (pH 9.0) phosphate buffer solution (PBS) followed by 30 min of sonication. The prepared GO suspension was de-aerated with Ar gas to completely remove oxygen from the solution. Cyclic voltammetric reduction was performed in the GO suspension (0.3 mg/mL) with applied potential between 0.5 and -1.5 V, using a three-electrode system, with a bare GCE serving as the working electrode.[31] Five reduction cycles were employed in this study to deposit electrochemically reduced graphene oxide (rGO) onto the GCE surface. The sensor was ready to use for electrochemical measurements after rinsing with pure water followed by air dry.

5.2.4. Determination of pharmaceutical tablets in biological fluids (human plasma)

The fabricated sensor was utilized for the detection of generic tablets (acetaminophen and valacyclovir) spiked in human serum. For the working solution, both tablets (acetaminophen and valacyclovir) were crushed and spiked in human serum to obtain a final concentration of 0.01 M as a stock solution. The spiked plasma was then treated with acetonitrile for protein precipitation and sonicated for 6 min. This spiked human serum solution was then centrifuged at 12200g for 15 min in order to remove any residual proteins.[32,33] The supernatant was employed as a sample for the determination of acetaminophen and valacyclovir concentrations through DPV.

5.3. Result and Discussion

5.3.1. Characterization of electrochemically reduced graphene oxide (rGO) on the GCE

Figure 5.1A presents the FE-SEM image of the rGO/GCE surface prepared with 0.3 mg mL^{-1} GO dispersed in 0.1M PBS (pH 9) by continuous five-cycle electrodeposition scanned in the potential range between 0.5 and -1.5 V. Energy dispersive X-ray spectroscopy (EDS) was employed to study the degree of oxygen removal from GO, subsequent to electrochemical reduction. As shown in Figure 5.1B, a dramatic change in the carbon : oxygen (C:O) ratio was found in exfoliated GO and rGO. Through EDS, it was observed that a C:O ratio of 1:3 existed in exfoliated GO on the GCE surface, whereas a 6:1 ratio of total C:O was revealed in the rGO on the GCE surface, which indicated the successful removal of a large quantity of oxygen from the graphene oxide during electrochemical reduction. Aside from the primary carbon and oxygen peaks, additional small peaks were also observed. The prominent Na and P peaks found in the EDS measurement might have been obtained through PBS during sample preparation.

Raman spectroscopy was employed to further distinguish between exfoliated GO and rGO. The G band is typically assigned to the E_{2g} phonon of C sp2 atoms, while the D band is a breathing mode of _κ-point phonons of A_{1g} symmetry.[34] Figure 5.1C depicts the Raman spectra of rGO (a), and exfoliated GO (b) on a glassy carbon electrode. In the figure, exfoliated GO and rGO both had D bands at 1350 cm^{-1}; however, the intensity of the D band was significantly increased to electrochemical reduced graphene oxide (rGO), indicating the decreased size of the sp2 domains, which was possibly due to extensive oxidation. This may be owing to defects that were introduced into the rGO during preparation.[35,36]

5.3.2. Electrocatalytic activity of rGO/GCE

To investigate the electrocatalytic properties of rGO/GCE, the CV responses of a 50 μM acetaminophen, valacyclovir, and acetaminophen-valacyclovir mixture were studied. CVs of the

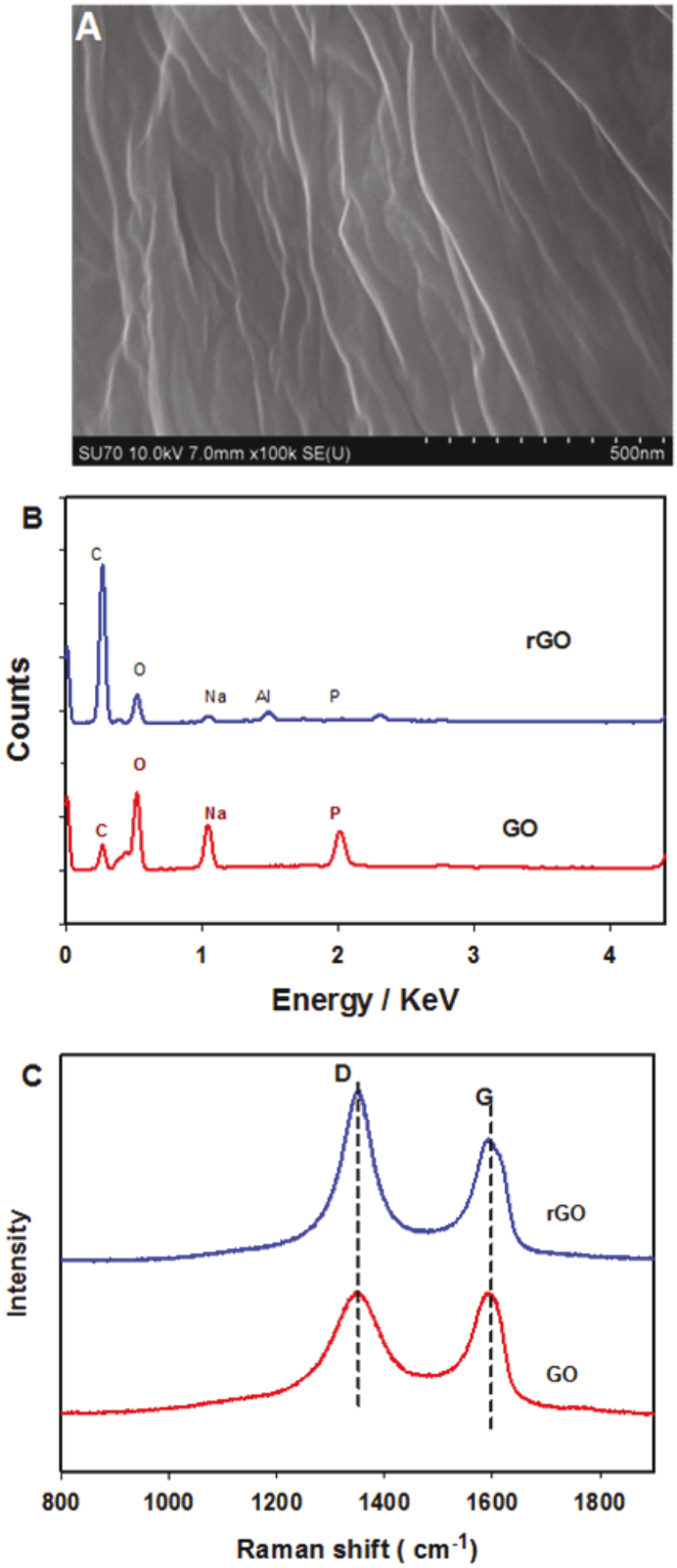

Figure 5. 1. (A) SEM image of GCE following modification with electrochemically reduced graphene oxide (rGO). (B) EDX spectrum of rGO and GO film on the electrode surface. (C) Raman spectra of rGO and GO film on the electrode surface.

rGO/GCEs recorded in a 0.1 M PBS (pH 7.2) at a scan rate of 20 mV/s in the absence (blue), and in the presence of acetaminophen (red) are shown in Figure 5.2A. CVs of bare GCE captured in a 0.1M PBS (blue) followed by addition of 50 µM acetaminophen (red) are presented in the inset Fig.2A. As seen in Figure 5.2A, the rGO/GCE produced a pair of typical redox peaks, with an Epa at 391 mV and Epc at 309 mV, revealing a reversible electrochemical process as shown in the following two-electron reaction:

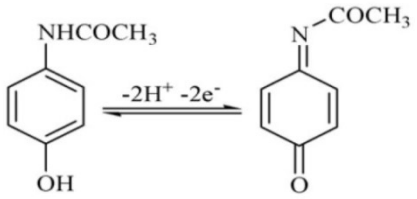

Electrochemical oxidation behaviour of valacyclovir at rGO/GCE was studied and presented in Figure 5.2B. After addition of 50 µM valacyclovir in a 0.1 M PBS (pH 7.2) at a scan rate of 20 mV/s, a distinct oxidation peak (red) was observed at ~0.98 V. However, no reduction peak was seen during the cathodic scan from 1.2 to 0.0 V. An irreversible electrochemical behavior was obtained for valacyclovir oxidation at the electrode surface. The CVs of a bare GCE recorded under identical experimental conditions are shown as an inset in the same figure. The broad oxidation peak obtained from the bare GCE at a higher potential (1.1 V) and with a lower current response demonstrated the higher electroanalytical properties of the rGO/GCE. The electrochemical oxidation of valacyclovir involved a two-electron/two-proton transfer process through the formation of an intermediate (8-oxovalacyclovir), as depicted below:

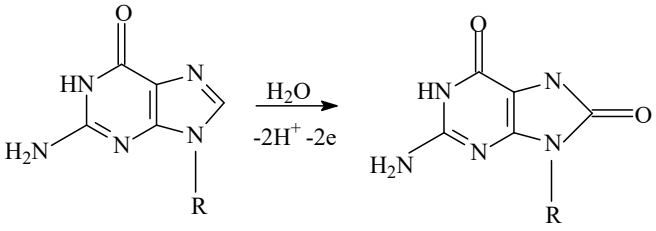

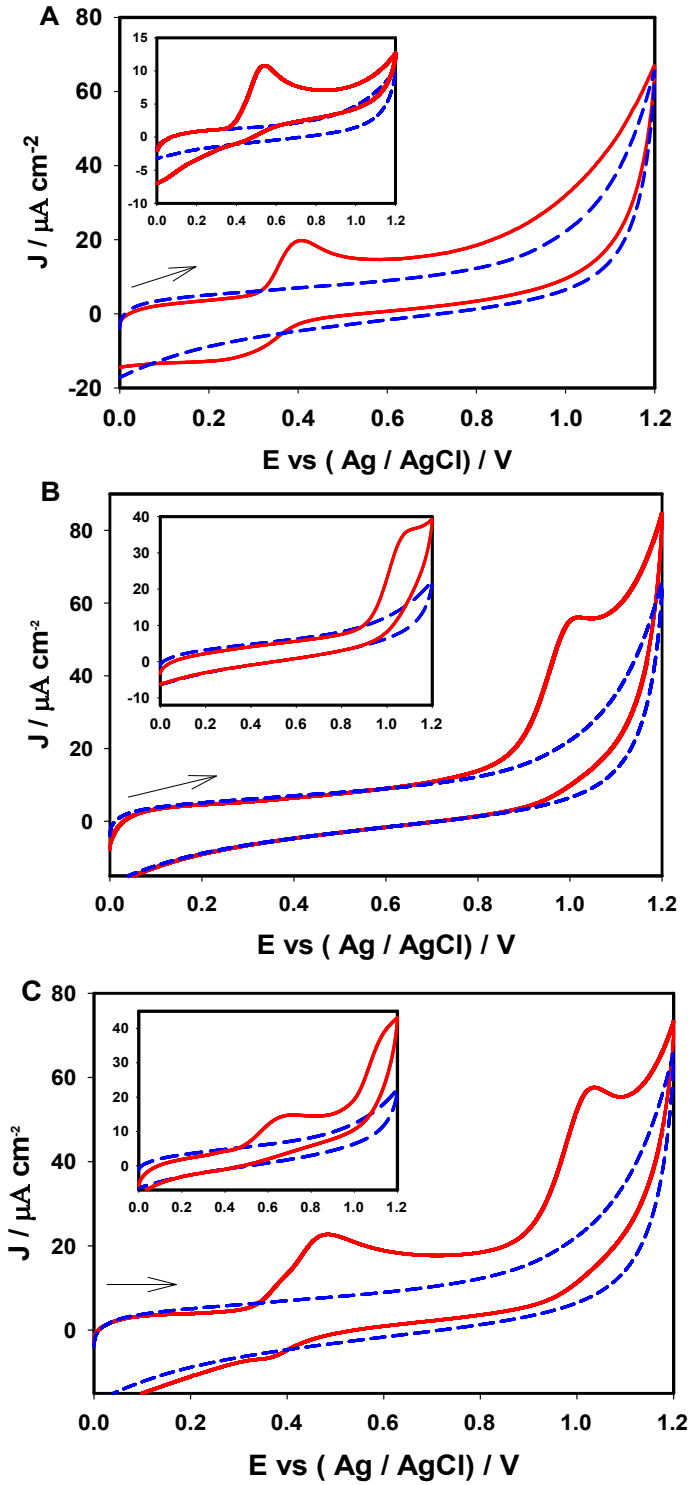

Figure 5. 2. CVs recorded at rGO/GCE (5 cycle electrodeposition) for absence (blue line) and the presence (redline) in 0.1 M PBS (pH 7.2), scan rate 20 mVs^{-1}; Inset: CVs response at bare GCE for absence (blue line) and the presence (redline) in 0.1 M PBS (pH 7.2) (A) 50 µM acetaminophen (B) 50 µM valacyclovir and (C) 50 µM mixture of acetaminophen and valacyclovir.

which is analogous to the initial oxidation product of guanine.[37,38] The electrocatalytic behaviour of rGO/GCE for concurrent detection was also studied through CV in a 50 μM acetaminophen and valacyclovir mixture in 0.1 M PBS (pH 7.2) at a scan rate of 20 mV/s. As shown in Figure 5.2C, two distinct peaks were observed; the first oxidation peak appeared at the potential of 0.43 V, which was associated with the oxidation of acetaminophen, whereas the valacyclovir oxidation peak occurred at ~1.05V. The small positive peak potential shift was observed for both acetaminophen and valacyclovir during simultaneous detection. No distinct oxidation peaks were observed for acetaminophen and valacyclovir with the bare GCE. Rather, a single broad peak at 0.7 V, with a small anodic current was observed (Figure 5.2C - inset). These results indicated that the rGO/GCE significantly enhanced the electrochemical oxidation of acetaminophen and valacyclovir separately, as well as for a mixture thereof, with well-defined anodic peaks. The excellent conductivity, high surface area, and oxygen-related defects of the rGO film made it a sensitive promoter of electrochemical sensing processes, in comparison to a bare untreated GCE .[39-41]

The Figure 5.3A depicts an effect of the different scan rate on the electrochemical oxidation of a 50 μM acetaminophen and valacyclovir mixture at the rGO/GCE. The oxidation peak currents of acetaminophen and valacyclovir were elevated with increasing scan rates, where the anodic peaks gradually shifted toward a more positive potential. Plots (Figure 5.3B) of the anodic peak currents versus the square root of the scan rate varied from 10 to 100 mVs^{-1} showed a linear relationship (R^2 =0.995) for the acetaminophen peak (a) and a linear relationship of R^2 =0.995 for the valacyclovir peak (b), indicating the diffusion-controlled electrode processes.

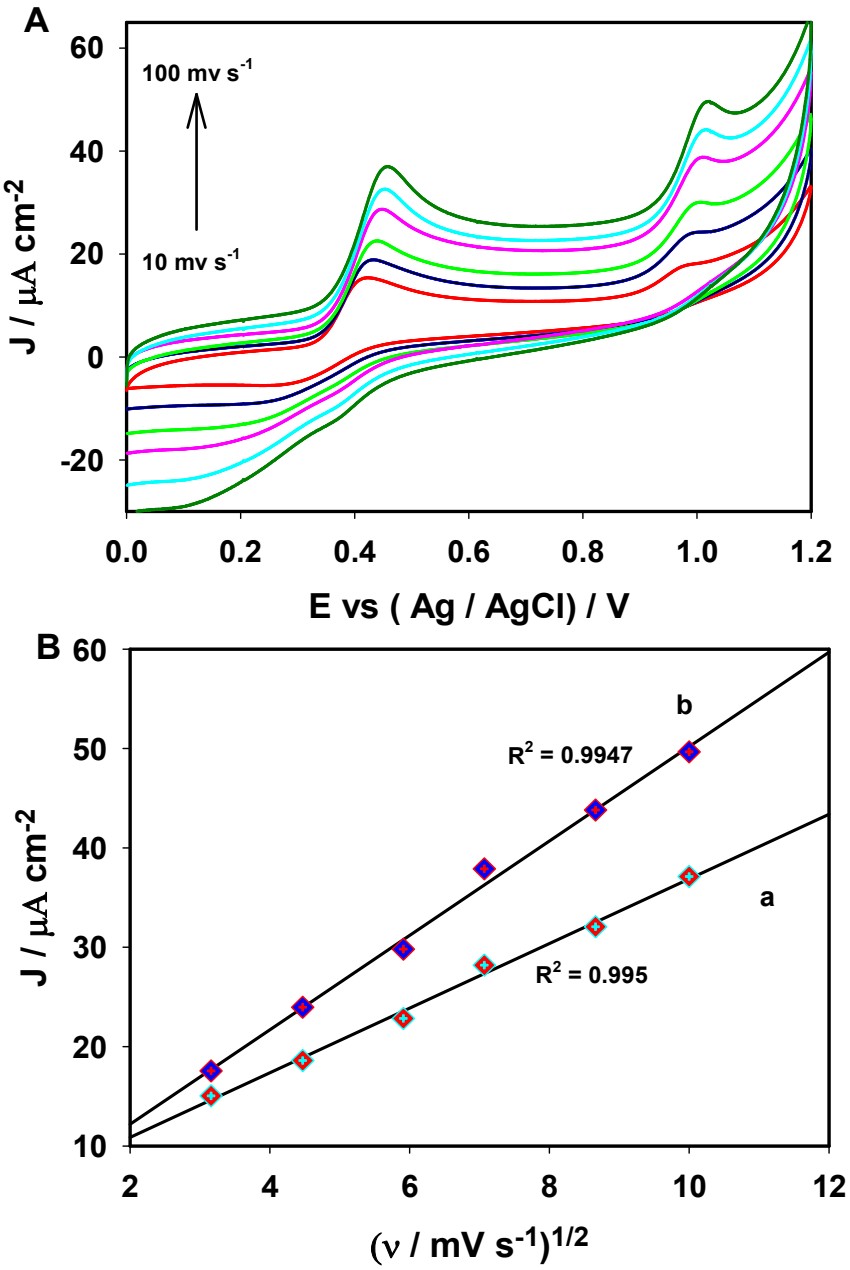

Figure 5. 3. (A) CVs of the rGO/GCE recorded in 0.1 M PBS (pH 7.2) containing a mixture of 50 µM acetaminophen and valacyclovir, each at different scan rates, varied from 10 to 100 mVs^{-1} ; (B)) a. Plots of the anodic peak currents versus the square root of the scan rates obtained through the acetaminophen peak b. Plots of the anodic peak currents versus the square root of the scan rates obtained through the valacyclovir peak.

5.3.3. Optimization of graphene deposition

To achieve highly sensitive, stable, and effective electrocatalytic activity, the electrochemical deposition conditions were optimized with various graphene oxide (GO)

concentrations and deposition cycles. To determine the optimum deposition cycle, four different rGO/GCEs were prepared in a 0.3 mg mL^{-1} graphene oxide colloidal solution in 0.1M PBS (pH 7.2) at a scan rate

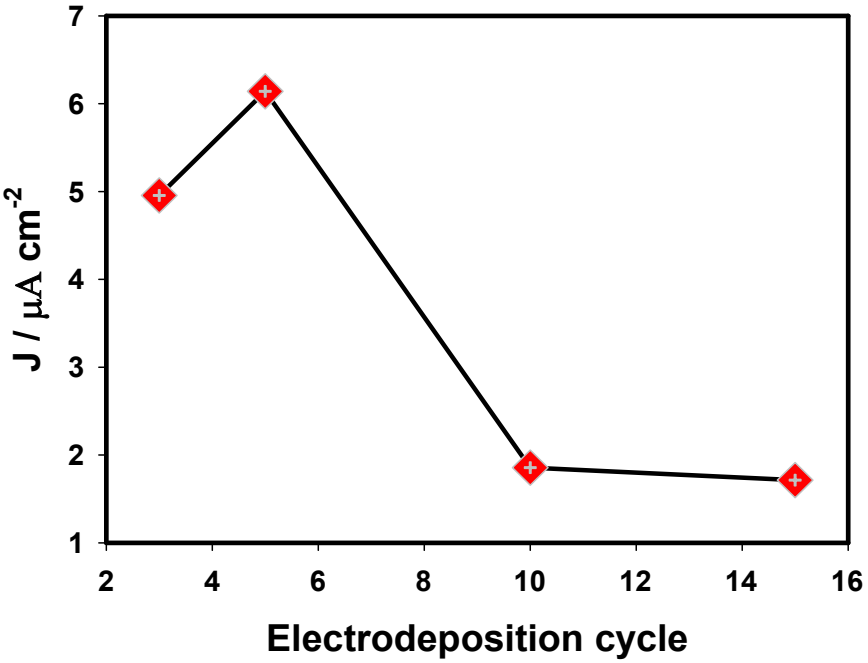

Figure 5. 4. Plot of anodic peak current of 20 µM valacyclovir in 0.1 M PBS (pH 7.2) recorded at rGO/GCE (0.3 mg mL^{-1}) along with different deposition cycles (3, 5, 10 and 15).

of 20 mVs^{-1} with four different electrodeposition cycles (3, 5, 10, and 15), as shown in Figure 5.4. The electrocatalytic performance of the as prepared electrodes was compared in a 0.1M PBS + 20 µM valacylovir suspension. The plot of the anodic peak currents (Figure 5.4), obtained through four different electrodes, clearly indicated that the electrode prepared through the five-cycle electrodeposition imparted higher current responses than the other electrodes. The anodic peak current increased remarkably with additional deposition cycles (from 3 to 5). It was expected that as the total volume of the deposited graphene on GCE surface was increased, it would lead to enhanced electrochemical responses.[42] With a further increase of the deposition

cycles, from 5 to 15, the oxidation peak current of valacyclovir was found to gradually decrease. This may have been due to excessive deposition, and hence, thickness of the graphene film on the GCE surface, which may have constrained electron transfer in the oxidation of valacyclovir.

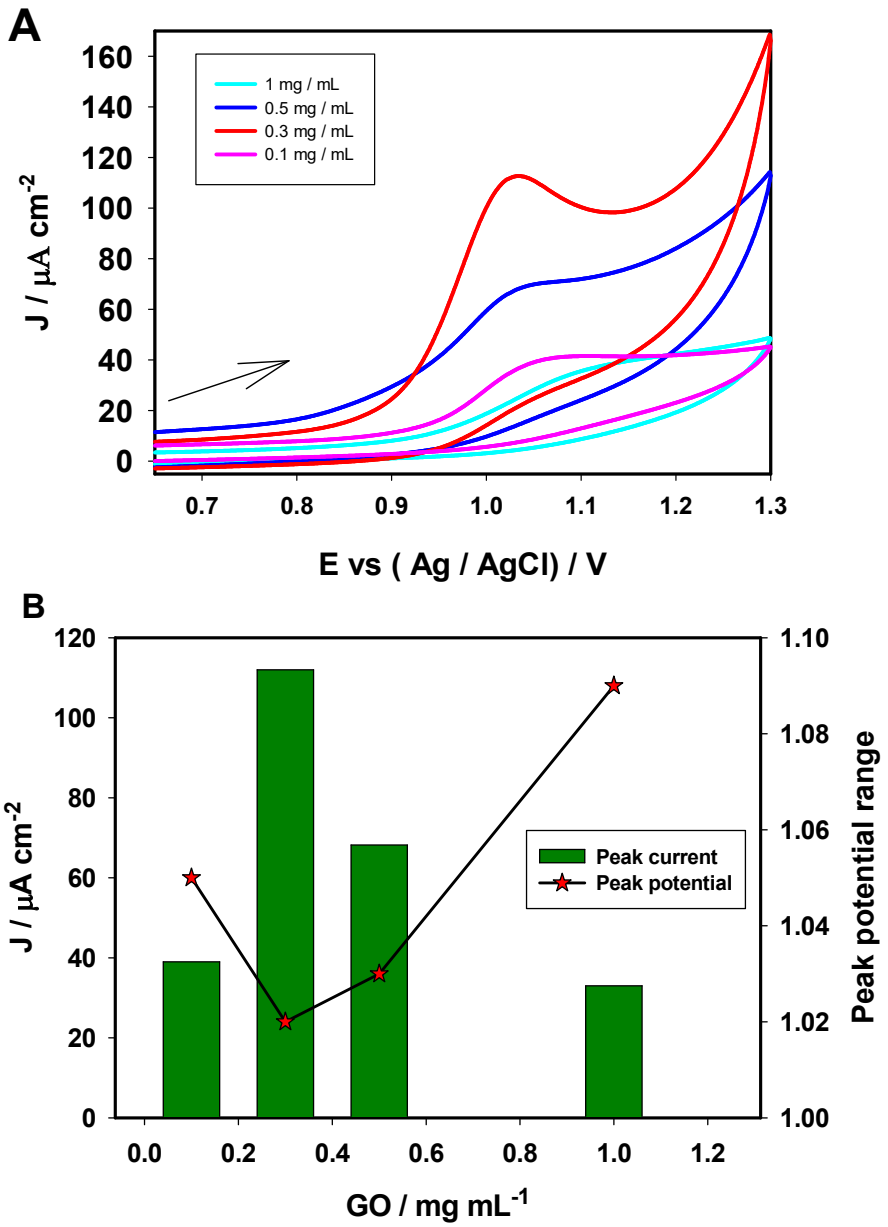

Figure 5. 5. (A) CV responses of 100 µM valacyclovir at rGO/GCE (5 cycles of electrodeposition) prepared with different concentrations of graphene oxide (0.1, 0.3, 0.5 and 1 mg mL^{-1}) in 0.1 M PBS (pH7.2), scan rate 20 mVs^{-1} (B) Anodic peak current responses and peak potentials derived through Fig. 5.5A.

For a further investigation toward the quantification of the optimal graphene oxide (GO) concentration, four different rGO/GCEs were prepared at four different concentrations (0.1, 0.3, 0.5, and 1 mg mL^{-1}) of the graphene oxide colloidal solution in 0.1M PBS (pH 7.2) using CV at a constant 5 cycle electrodeposition. The electrocatalytic performance was studied through CV in a 0.1M PBS mixture with 100 µM valacyclovir (Figure 5.5A). The rGO/GCE prepared using 0.3 mg mL^{-1} GO exhibited a higher anodic current response for valacyclovir oxidation over 0.1, 0.5, and 1 mg mL^{-1} GO. An increased anodic peak current was observed with the increasing concentration of the GO suspension, from 0.1 to 0.3 mg mL^{-1}(Figure 5.5B). However, further increasing the concentration of GO, from 0.5 to 1 mg mL^{-1}, led to a large diminution of the peak current. This might have been due to the excessive aggregation of graphene material on the GCE surface, which ultimately blocked electron transfer for oxidation.

5.3.4 Electrochemical detection of valacyclovir

Analytical measurements of valacyclovir at the rGO/GCE were carried out through DPV in the potential range of from 0.0 V to 1.2 V. Figure 5.6A shows the current response of the rGO/GCE to the successive addition of valacyclovir in the range of from 10 nM to 45.1 µM. Through the successive addition of valacyclovir concentrations in 0.1M PBS, pH 7.2, two linear regression lines were obtained corresponding to concentration ranges. One line from 10 nM to 1.35 µM (R^2 = 0.987) with sensitivity of 8.77 $AM^{-1}cm^{-2}$, and another from 5.1 µM to 45.1 µM (R^2 = 0.992) with a sensitivity of 0.489 $AM^{-1}cm^{-2}$ (Figure 5.6B) were obtained. The two concentration range calibration plots acquired in this study were comparable to other studies that involved the measurement of NADH, ascorbic acid, dopamine, and uric acid.[43-45] This might be explained through the mechanism behind the inner-sphere electrode reaction.[46] The oxidation

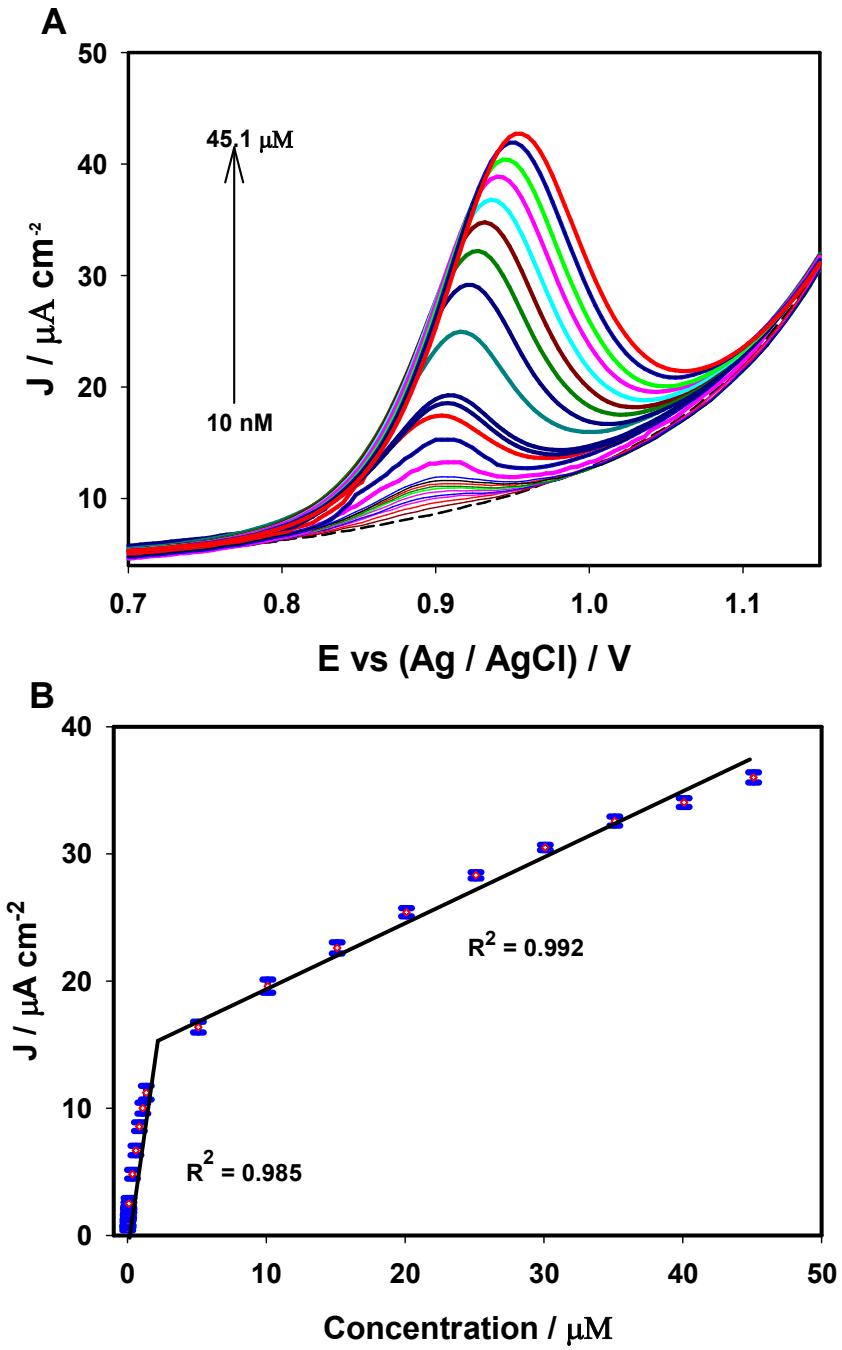

Figure 5. 6. (A) DPV responses of the rGO/GCE to the successive addition of 10 nM, 250 nM and 5.1 µM valacyclovir in 0.1 M PBS (pH 7.2). (B) Calibration plot of current response against valacyclovir concentration.

of valacyclovir is an irreversible reaction; hence, following the addition of high concentrations of valacyclovir, there may be an accumulation of intermediate and oxidized molecules at the

modified electrode surface. The strong interaction of the reactant, intermediates, and products on the electrode surface may impact the electron transfer rate. The limit of detection (LOD) for valacyclovir concentrations was estimated at a signal-to-noise ratio of 3, to be 1.34 nM. The LOD obtained in this study was an improvement over previous work, as presented in Table 1. The detection range obtained in this study might be utilized for the bioavailability evaluation of orally administered valacyclovir. The average ± SD peak level in serum 2 h after the administration of a 1000 mg valacyclovir dose was 23.5 ± 5.7 μM (range, 18.1 to 36.0 μM).[47] This range was fully addressed in the present study (analytical range from 10 nM to 45.1 μM).

5.3.5 Simultaneous detection of acetaminophen and valacyclovir

Due to the increasing pharmaceutical production of generic acetaminophen and valacyclovir tablets, a robust sensor that is simple to operate is required for quality control and bioavailability testing. The detection range obtained through this work might be employed for the simultaneous bioavailability evaluation of both acetaminophen and valacyclovir. The average plasma concentration of acetaminophen (500 mg) and valacyclovir (1000 mg) through oral administration after 2 h was 15.6 μM and 18.1 μM, respectively.[48,47] Figure 5.7A shows the DPV recorded at the rGO/GCE under various concentrations of acetaminophen and valacyclovir in mixtures. Two well-defined oxidation peaks corresponding to acetaminophen and valacyclovir were observed at 0.381 V and 0.953 V, respectively. Two linear regression equations were achieved for both acetaminophen and valacyclovir following the successive addition of different concentrations (Figure 5.7B). For acetaminophen (AP), two linear regression equations were

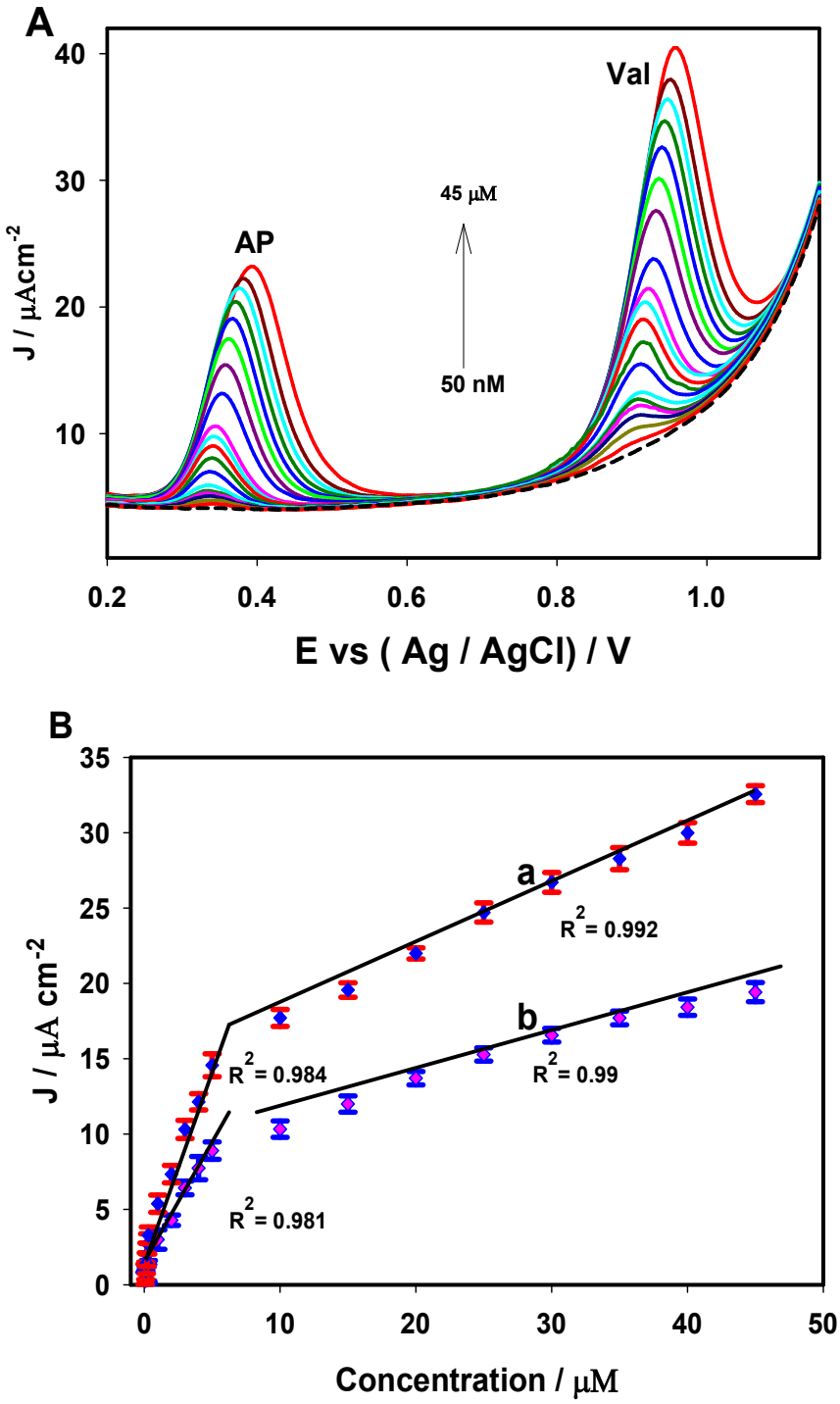

Figure 5. 7. (A) DPV responses of rGO/GCE to the successive addition of 50 nM, 1µM, and 5 µM acetaminophen (AP) and valacyclovir (Val mixtures in 0.1 M PBS (pH 7.2). (B) Calibration plot obtained through the simultaneous detection of (a) valacyclovir and (b) acetaminophen concentrations.

obtained, as j_{AP} (μA cm^{-2}) = 0.419 + 1.82[AP] ([AP]: 50 nM to 5 μM, R^2 = 0.987), and j_{AP} (μA cm^{-2}) = 7.55 + 0.298[AP] ([AP]: 10 μM to 45 μM, R^2 = 0.993). Similarly, two linear regression equations were obtained for valacyclovir (Val): j_{Val} (μA cm^{-2}) = 1.93 + 2.67[Val] ([Val]: 50 nM to 5 μM, R^2 = 0.982), and j_{Val} (μA cm^{-2}) = 13.6 + 0.421[Val] ([Val]: 10 μM to 45 μM, R^2 = 0.995). The two regression lines obtained in this study for simultaneous detection were comparable with previous studies for the simultaneous detection of ascorbic acid (AA), dopamine (DA), and uric acid (UA).[43] The LOD of acetaminophen and valacyclovir were found to be 4.65 nM and 3.1 nM, respectively. The LOD obtained for acetaminophen and valacyclovir through simultaneous measurement was comparable, and even improved, over previous studies, as presented in Table 5.1.[4,49-55] It is worthy to mention that there was no demonstration of the simultaneous detection and determination of acetaminophen and valacyclovir mixtures using any analytical method in the literature.

5.3.6. Interference studies

The selective performance of newly designed rGO/GCE sensor was studied through the simultaneous measurements of acetaminophen and valacyclovir in presence of representative potential interfering biomolecules, such as ascorbic acid, dopamine, uric acid and glutathione in 0.1 M PBS (pH 7.2). Figure 5.8A shows the DPV responses to 25 μM acetaminophen and valacyclovir (a), following the addition of 25 μM ascorbic acid (b), dopamine (c), uric acid (d), glutathione (e), and their mixture (f). Two defined anodic peaks were obtained in the presence of acetaminophen and valacyclovir, as seen in Figure 5.8A. The oxidation peak potentials for acetaminophen and valacyclovir were comparable with the previous publications].[52,53] Subsequent to the addition of the interferents (curve b–e), no obvious changes of the peak

Table 5. 1. Comparison of different methods for the detection of valacyclovir and acetaminophen.

Methods	Compounds	Linear Range (µM)	Limit of Detection (µM)	Ref.
HPLC	Valacyclovir	2.49 -16.62	0.831	[4]
Micellar electrokinetic chromatography	Valacyclovir	0.28-330	0.088	[49]
RP-HPLC	Valacyclovir	13.8-83.1	0.69	[50]
DPV	Valacyclovir	4-200	0.1	[51]
SWV	Valacyclovir	4-200	0.046	[51]
DPV	Valacyclovir	0.005-0.055	0.0018	[52]
DPV	Acetaminophen	0.04-100	0.02	[53]
SWV	Acetaminophen	0.1-20	0.032	[54]
DPV	Acetaminophen	1-100	0.21	[55]
DPV	**Valacyclovir/ Acetaminophen + Valacyclovir mix**	**0.01-45.1/ 0.05-45**	**0.0013/ 0.0046+0.0031**	**This work**

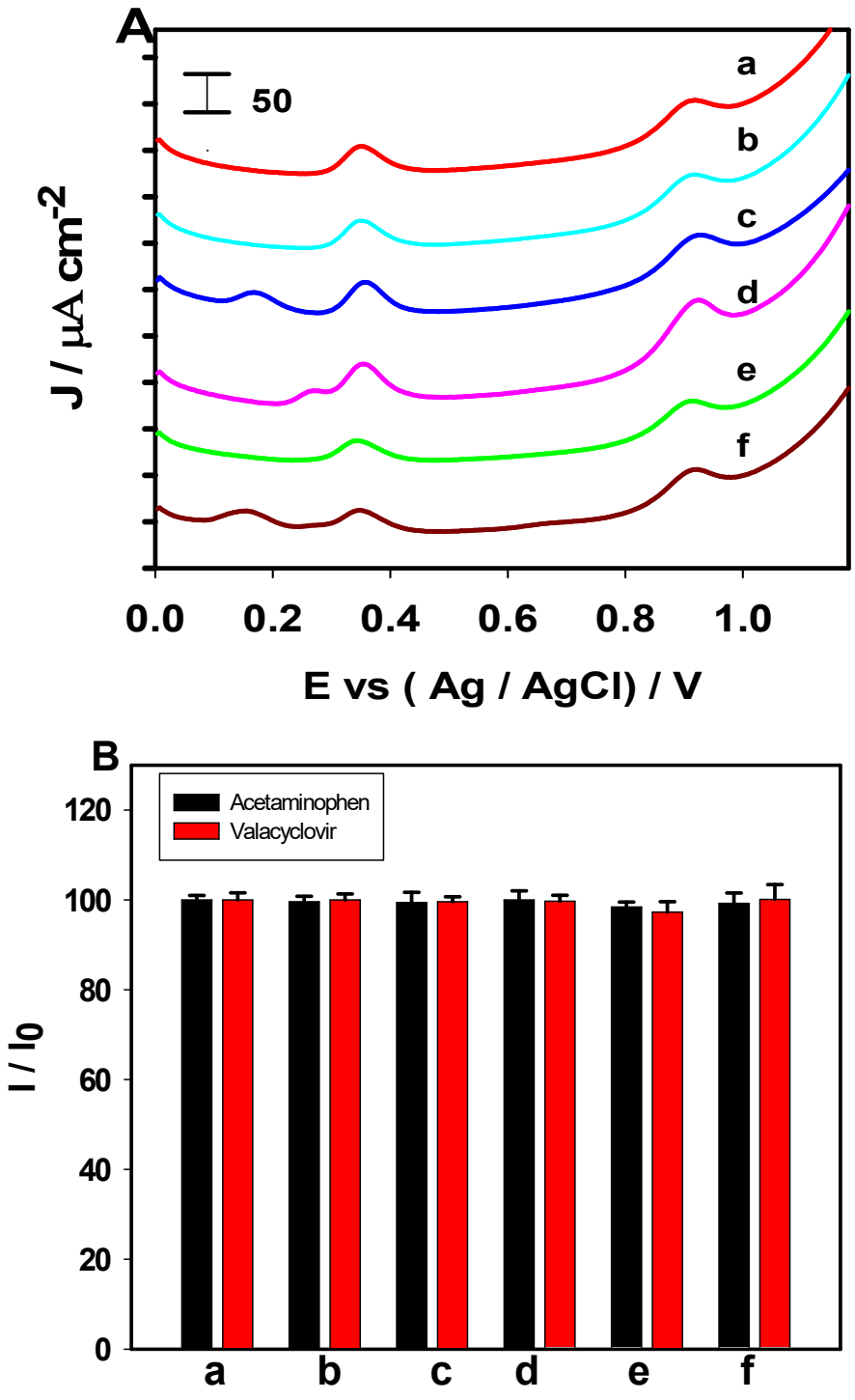

Figure 5. 8. (A) DPVs of the rGO/GCE recorded in 0.1 M PBS (pH 7.2) + 25 µM mixture of acetaminophen and valacyclovir without interferents (a) and in the presence of 25 µM ascorbic acid (b), 25 µM dopamine (c), 25 µM uric acid (d), and 25 µM glutathione (e) and mixture (f). (B) Relative anodic peak current response derived from Fig. 5A for both acetaminophen and valacyclovir.

potential and peak current for acetaminophen and valacyclovir were observed. As shown in Fig. 5A, no oxidation peak (curve b) for ascorbic acid and glutathione (curve e) was observed in the selected potential range, which is consistent with the study by Liu et al.,[53] where authors demonstrated an ascorbic acid oxidation peak at -0.3 V. Compared with the individual results (c-f) in Fig. 5A, distinct peaks at 0.170 V, 0.267V, 0.356V, and 0.91V were observed for dopamine, uric acid, acetaminophen and valacyclovir, respectively. The neighboring peak to peak separation between these analytes was 97, 89, and 554 mV, respectively. These large peak to peak separations were sufficient for the selective measurements of acetaminophen and valacyclovir in the presence of these co-existing molecules. Figure 5.8B, presents the relative anodic peak current responses to acetaminophen and valacyclovir in the absence and presence of interferents calculated from Figure 5.8A. The average peak current difference of~2.5% was noticed for acetaminophen oxidation where as nearly 3.0% of the peak current variation was observed for the oxidation of valacyclovir, which confirmed that the fabricated sensor was highly selective in presence of potential interfering molecules.

5.3.7. Reproducibility and stability of the rGO/GCE sensor

The fabricated rGO/GCEs were tested for reproducibility and stability through DPV. Four parallel rGO/GCEs fabricated under identical experimental conditions were analysed for electrocatalytic activity of valacyclovir in 0.1M PBS (pH 7.2) (Figure 5.9A). A very low relative standard deviation (RSD) of 1.08% (n=4) was observed among the peak currents obtained through four electrodes. This observation confirmed that the preparation of the rGO/GCE had excellent reproducibility. To verify the stability of the as prepared rGO/GCE sensor, DPV measurements were recorded in 0.1 M PBS (pH 7.2) + 5 μM valacyclovir (Figure 5.9B). The

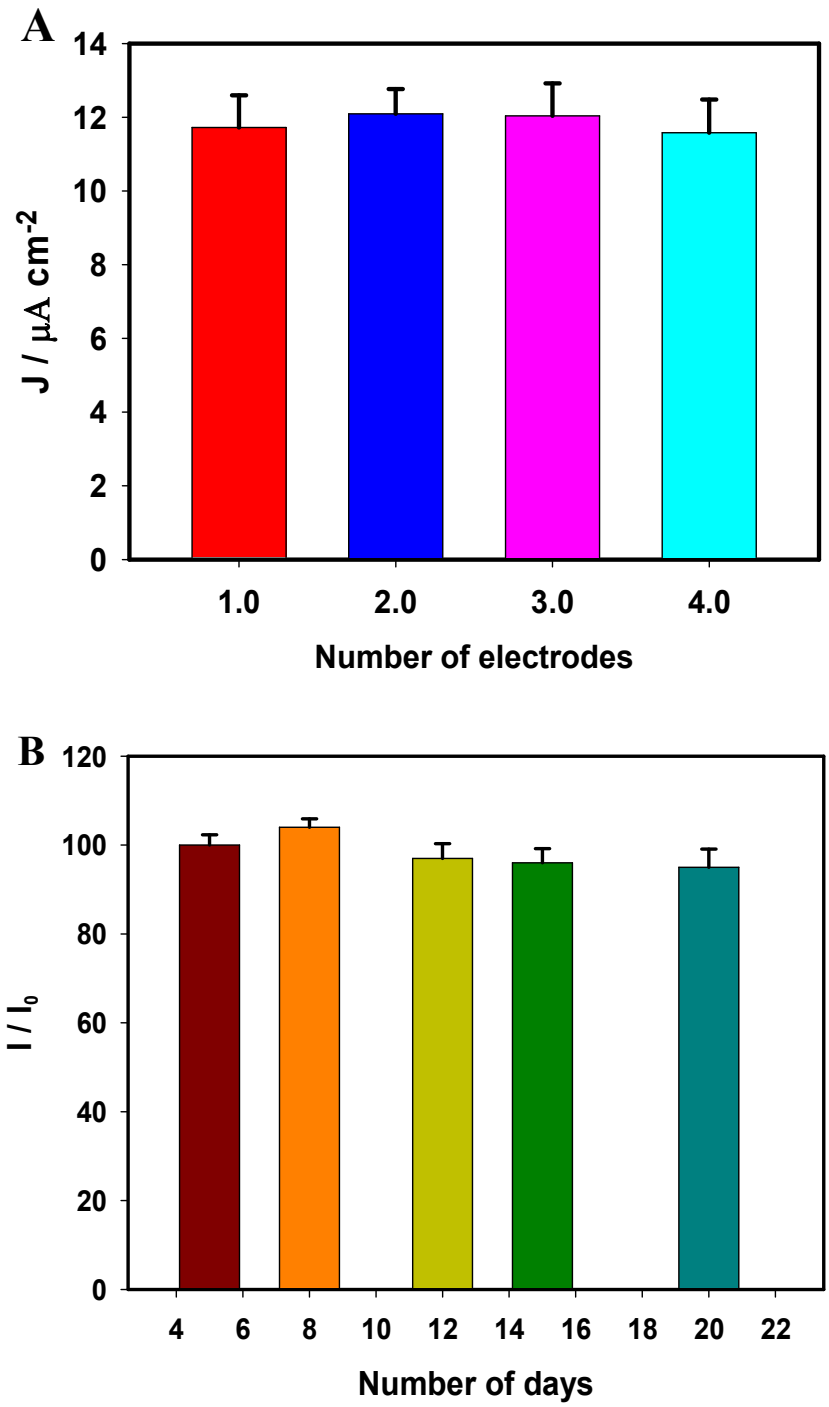

Figure 5. 9. (A) Current response of rGO/GCE for the detection of 5 μM valacyclovir with four identically prepared GCEs. (B) Current response of the rGO/GCE to 5 μM valacyclovir over 20 days versus the initial current response (I^0)

electrochemical performance of rGO/GCE was observed once a day over 20 days. At the end of 20th day, approximately 5.26% current loss was observed when compared with the initial peak current, showing the highly stable performance of the as prepared rGO/GCE.

5.3.8. Detection of acetaminophen and valacyclovir mixture in actual sample

The performance of the optimized electrochemical sensor for real sample analysis was studied through the spiked concentration of generic acetaminophen and valacylovir tablets in human serum using DPV. The recovery obtained for acetaminophen and valacyclovir in mixture is presented in Table 5.2., the rGO/GCE exhibited an excellent recovery for acetaminophen, ranging from 95% to 106 % with RSD 1.75% to 5.5%, and 94.3% to 99.3 % with RSD 0.99% to 5.3% for valacyclovir. The recovery rates and the RSDs for the two samples were found to be highly acceptable.

Table 5.2. Actual sample analysis in human plasma: simultaneous detection of acetaminophen (325 mg) and valacyclovir (500 mg) generic tablets.

Added (μM)	Found (μM)		Recovery (%)		RSD (%)	
	Acetaminophen	*Valacyclovir*	*Acetaminophen*	*Valacyclovir*	*Acetaminophen*	*Valacyclovir*
5	*5.3*	*4.96*	*106*	*99.33*	*2.17*	*5.3*
10	*10.1*	*9.43*	*101*	*94.33*	*5.5*	*0.99*
15	*14.25*	*14.55*	*95*	*97*	*1.75*	*2.75*

5.4. Conclusions

We have successfully developed a highly sensitive, stable and reproducible electrochemical sensor based on reduced graphene oxide for the exclusive detection of valacyclovir, as well as for the simultaneous detection of acetaminophen and valacyclovir in

mixtures. The optimized rGO/GCE sensor exhibited very high electrocatalytic activity for the simultaneous oxidation of acetaminophen and valacyclovir. The proposed rGO/GCE sensor displayed an extremely low detection limit with excellent selectivity for valacyclovir in isolation, as well as acetaminophen and valacyclovir mixtures, in contrast to other electrochemical sensors reported in the literature. The sensor proposed in this study has a great potential to be used in pharmaceutical quality control, clinical drug monitoring, and bioavailability testing for therapeutic purposes.

References

1. James, L.P.; Mayeux, P.R.; Hinson, J.A. Acetaminophen-induced hepatotoxicity. *Drug Metab. Dispos.* **2003**, *31*, 1499-1506.
2. Shihana, F.; Dissanayake, D.; Dargan, P.; Dawson, A. A modified low-cost colorimetric method for paracetamol (acetaminophen) measurement in plasma. *Clin. Toxicol.* **2010**, *48*, 42-46.
3. Yadav, M.; Upadhyay, V.; Singhal, P.; Goswami, S.; Shrivastav, P.S. Stability evaluation and sensitive determination of antiviral drug, valacyclovir and its metabolite acyclovir in human plasma by a rapid liquid chromatography-tandem mass spectrometry method. *J. Chromatogr. B* **2009**, *877*, 680-688.
4. Jadhav, A.S.; Pathare, D.B.; Shingare, M.S. Development and validation of enantioselective high performance liquid chromatographic method for Valacyclovir, an antiviral drug in drug substance. *J. Pharm. Biomed. Anal.* 2007, 43, 1568-1572.
5. Beutner, K.R. Valacyclovir: a review of its antiviral activity, pharmacokinetic properties and clinical efficacy. *Antivir. Res.* **1995**, *28*, 281-290.

6. Ganesh, M.; Narasimharao, C.V.; Kumar, A.S.; Kamalakannan, K.; Vinoba, M.; Mahajan, H.S.; Sivakumar, T. UV spectrophotometric method for the estimation of valacyclovir hcl in tablet dosage form. *J. Chem.* **2009,** *6*, 814-818.

7. Bhaskar, V.V.; Gurupadayya, B.M.; Manohara, Y.N.; Reddy, D.V. HPLC and UV spectrophotometric determination of amrinone lactate. *Asian J. Chem.* **2007**, *19* , 5049-5056.

8. Kanneti, R.; Rajesh, R.; Raj, J.A.; Bhatt, P.A. An LC–MS–MS method for the simultaneous quantitation of acyclovir and valacyclovir in human plasma, *Chromatogr.* **2009**, *70*, 407-414.

9. Maes, A.; Garre, B.; Desmet, N.I.; Van Der Meulen, K.; Nauwynck, H.; De Backer, P.; Croubels, S. Determination of acyclovir in horse plasma and body fluids by high-performance liquid chromatography combined with fluorescence detection and heated electrospray ionization tandem mass spectrometry, *Biomed. Chromatogr.* **2009**, *23,* 132-140.

10. Li, J.; Liu, J.; Tan, G.; Jiang, J.; Peng, S.; Deng, M.; Qian, D.; Feng, Y.; Liu, Y. High-sensitivity paracetamol sensor based on Pd/graphene oxide nanocomposite as an enhanced electrochemical sensing platform. *Biosens. Bioelectron.* **2014**, *54*, 468-475.

11. Zhang, A.; Guo, Y.; Dong, C. Electrochemical sensor for ultrasensitive determination of isoquercitrin and baicalin based on DM-β-cyclodextrin functionalized graphene nanosheets. *Biosens. Bioelectron.* **2014**, *58*, 242-248.

12. Chen, A.; Chatterjee, S. Nanomaterials based electrochemical sensors for biomedical applications, *Chem. Soc. Rev.* **2013**, *42*, 5425-5438.

13. Yang, X.; Feng, B.; He, X.; Li, F.; Ding, Y.; Fei, J. Carbon nanomaterial based electrochemical sensors for biogenic amines. *Microchim. Acta* **2013**, *180* , 935-956.

14. Lui, C.H.; Liu, L.; Mak, K.F.; Flynn, G.W.; Heinz, T.F. Ultraflat Graphene, *Nature* 2009, 462, 339-341.

15. Katsnelson, M.I. Graphene: carbon in two dimensions. *Mater. Today* **2007**, *10*, 20-27.

16. Avouris, P.; Chen, Z.; Perebeinos, V. Carbon-based electronics. *Nat. Nanotechnol.* **2007**, *2*, 605-615.

17. Son, Y.W.; Cohen, M.L.; Louie, S.G. Half-metallic graphene nanoribbons, *Nature* **2006**, *444*, 347-349.

18. Schedin, F.; Geim, A.K.; Morozov, S.V.; Hill, E.W.; Blake, P.; Katsnelson, M.I.; Novoselov, K.S. Detection of individual gas molecules adsorbed on graphene. *Nat. Mater.* **2007**, *6*, 652-655.

19. Chang, J.; Zhou, G.; Christensen, E.R.; Heideman, R.; Chen, J. Graphene-based sensors for detection of heavy metals in water: a review. *Anal. Bioanal. Chem.* **2014**, *406* , 3957-3975.

20. Yang, H.; Liu, B.; Ding, Y.; Li, L.; Ouyang, X. Fabrication of cuprous oxide nanoparticles-graphene nanocomposite for determination of acetaminophen, *J. Electroanal. chem.* **2015**, *757*, 88-93.

21. Ding, M.; Zhou, Y.; Liang, X.; Zou, H.; Wang, Z.; Wang, M.; Ma, J. An electrochemical sensor based on graphene/poly(brilliant cresyl blue) nanocomposite for determination of epinephrine. *J. Electroanal. chem.* **2016**, *763*, 25-31.

22. Adhikari, B.-R.; Govindhan, M.; Chen, A. Carbon nanomaterials based electrochemical sensors/biosensors for the sensitive detection of pharmaceutical and biological compounds. *Sensors* **2015**, *15,* 22490-22508.

23. Rochefort, A.; Wuest, J.D. Interaction of substituted aromatic compounds with graphene, *Langmuir* **2008**, *25*, 210-215.

24. Bai, H.; Wang, C.; Chen, J.; Peng, J.; Cao, Q. A novel sensitive electrochemical sensor based on in-situ polymerized molecularly imprinted membranes at graphene modified electrode for artemisinin determination. *Biosens. Bioelectrons.* **2015**, *64*, 352-258.

25. Adhikari, B.-R.; Govindhan, M.; Chen, A. Sensitive detection of acetaminophen with graphene-based electrochemical sensor. *Electrochem. Acta* **2015**, *165*, 198-204.

26. Stankovich, S.; Piner, R.D.; Chen, X.; Wu, N.; Nguyen, S.T.; Ruoff, R.S. Stable aqueous dispersions of graphitic nanoplatelets via the reduction of exfoliated graphite oxide in the presence of poly (sodium 4-styrenesulfonate). *J. Mater. Chem.* **2006**, *16*, 155-158.

27. Stankovich, S.; Dikin, D.A.; Piner, R.D.; Kohlhaas, K.A.; Kleinhammes, A.; Jia, Y.; Wu, Y.; Nguyen, S.T.; Ruoff, R.S. Synthesis of graphene-based nanosheets via chemical reduction of exfoliated graphite oxide. *Carbon* **2007,** 45, 1558-1565.

28. Hernandez, Y.; Nicolosi, V.; Lotya, M.; Blighe, F.M.; Sun, Z.; De, S.; McGovern, I.T.; Holland, B.; Byrne, M.; GunKo, Y.K. High-yield production of graphene by liquid-phase exfoliation of graphite. *Nat. Nanotechnol.* **2008**, *3*, 563-568.

29. Raj, A.M.; John, A.S. Graphene layer modified glassy carbon electrode for the determination of norepinephrine and theophylline in pharmaceutical formulations. *Anal. Methods* **2014,** *6*, 2181-2188.

30. Guo, H.L.; Wang, X.F.; Qian, Q.Y.; Wang, F.B.; Xia, X.H. A green approach to the synthesis of graphene nanosheets. *ACS Nano* **2009**, *3*, 2653-2659.

31. Chen, L.; Tang, Y.; Wang, K.; Liu, C.; Luo, S. Direct electrodeposition of reduced graphene oxide on glassy carbon electrode and its electrochemical application, *Electrochem. Commun.* **2011**, *13*, 133-137.

32. Boon, V.; Glass, B.; Nimmo, A. High-performance liquid chromatographic assay of indomethacin in porcine plasma with applicability to human levels. *J. Chromatogr. Sci.* **2006**, *44*, 41-44.

33. Taylor, R.R.; Hoffman, K.L.; Schniedewind, B.; Clavijo, C.; Galinkin, J.L.; Christians, U. Comparison of the quantification of acetaminophen in plasma, cerebrospinal fluid and dried blood spots using high-performance liquid chromatography–tandem mass spectrometry. *J. Pharm. Biomed. Anal.* **2013**, *83*, 1-9.

34. Tulnstra, F.; Koenlg, J.L. Raman spectrum of graphite. *J. Chem. Phys.* **1970**, *53*, 1126-1130.

35. Ni, Z.H.; Wang, H.M.; Ma, Y.; Kasim, J.; Wu, Y.H.; Shen, Z.X. Tunable stress and controlled thickness modification in graphene by annealing. *ACS Nano* **2008**, *2*, 1033-1039.

36. Gupta, A.; Chen, P. Joshi, S. Tadigadapa, P.C. Eklund, Raman scattering from high-frequency phonons in supported n-graphene layer films, *Nano lett.* **2006,** *6,* 2667-2673.

37. Goyal, R.N.; Dryhurst, G. Redox chemistry of guanine and 8-oxyguanine and a comparison of the peroxidase catalyzed and electrochemical oxidation of 8-oxyguanine, *J. Electroanal. Chem.* **1982,** *135*, 75-91.

38. Oliveira-Brett, A.M.; Diculescu, V.; Piedade, J.A.P. Electrochemical oxidation mechanism of guanine and adenine using a glassy carbon microelectrode, *Bioelectrochem*. **2002**, *55*, 61-62.

39. Pumera, M. Electrochemistry of graphene: new horizons for sensing and energy storage, T*he Chem. Rec.* **2009**, *9*, 211-223.

40. Pumera, M. Graphene-based nanomaterials and their electrochemistry, *Chem. Soc. Rev.* **2010**, *39* , 4146-4157.

41. Brownson, D.A.C.; Varey, A.S.; Hussain, F.; Haigh, J.S.; Banks, E.C. Electrochemical properties of CVD grown pristine graphene: monolayer-vs. quasi-graphene, *Nanoscale* **2014,** *6*, 1607-1621.

42. Teymourian, H.; Salimi, A.; Khezrian, S. Fe_3O_4 magnetic nanoparticles/reduced graphene oxide nanosheets as a novel electrochemical and bioeletrochemical sensing platform. *Biosens. Bioelectron.* **2013**, *49*, 1-8.

43. Li, L.; Lu, H.; Deng, L. A sensitive NADH and ethanol biosensor based on graphene–Au nanorods nanocomposites. *Talanta* **2013**, *113*, 1-6.

44. Shalini, J.; Sankaran, K.J.; Chen, H.C.; Lee, C.Y.; Tai, N.H.; Lin, I.N. Mediatorless N_2 incorporated diamond nanowire electrode for selective detection of NADH at stable low oxidation potential, *Analyst* **2014**, *139*, 778-785.

45. Maduraiveeran, G.; Amiri, M.; Chen, A. Au nanoparticle/graphene nanocomposite as a platform for the sensitive detection of NADH in human urine. *Biosens. Bioelectron.* **2015**, *66*, 474-480.

46. Bard, J.A.; Faulkner, R.L. Electrochemical Methods. Second ed. New Jersey: *John Wiley and Sons.* **2001**. PP.247.

47. Lycke, J.; Malmeström, C.; Ståhle, L. Acyclovir levels in serum and cerebrospinal fluid after oral administration of valacyclovir. *Antimicrob. Agents Chemother.* **2003**, 47, 2438-2441.

48. Rawlins, M.D.; Henderson, D.B.; Hijab, A.R. Pharmacokinetics of paracetamol (acetaminophen) after intravenous and oral administration. *Eur. J. clin. pharmacol.* **1977**, *11*, 11:283-286.

49. Al Azzam, K.M.; Saad, B.; Makahleah, A. Assay and stability-indicating micellar electrokinetic chromatography method for the simultaneous determination of valacyclovir, acyclovir and their major impurity guanine in pharmaceutical formulations, *Biomed. Chromatogr.* **2010**, *24*, 535-543.

50. Sugumaran, M.; Bharathi, V.; Hemachander, R.; Lakshmi, M. RP–HPLC method for the determination of valacyclovir in bulk and pharmaceutical formulation. *Der Pharma Chemica* **2011**, *3*, 190-194.

51. Uslu, B.; Uzkan, S.A.; Senturk, Z. Electrooxidation of the antiviral drug valacyclovir and its square-wave and differential pulse voltammetric determination in pharmaceuticals and human biological fluids, *Anal. Chim. Acta* **2006**, *555*, 341-347.

52. Shah, B.; Lafleur, T.; Chen, A. Carbon nanotube based electrochemical sensor for the sensitive detection of valacyclovir, *Faraday Discuss.* **2013**, *164*, 135-146.

53. Liu, G.T.; Chen, H.F.; Lin, G.M.; Ye, P.P.; Wang, X.P.; Jiao, Y.Z.; Guo, X.Y.; Wen, Y.; Yang, H.F. One-step electrodeposition of graphene loaded nickel oxides nanoparticles for acetaminophen detection. *Biosens. Bioelectron.* **2014**, *56*, 26–32.

54. Kang, X.; Wang, J.; Wu, H.; Liu, J.; Aksay, I.A.; Lin, Y. A graphene-based electrochemical sensor for sensitive detection of paracetamol, *Talanta* **2010**, *81*, 754–759.

55. Fan, Y.; Liu, J.H.; Lu, H.T.; Zhang, Q. Electrochemical behavior and voltammetric determination of paracetamol on Nafion/TiO_2–graphene modified glassy carbon electrode, *Colloids Surf., B* **2011**, *85*, 289–292.

Chapter 6: A High-performance Enzyme Entrapment Platform Facilitated by a Cationic Polymer for the Efficient Electrochemical Sensing of Ethanol*

6.1. Introduction

Cationic polymers such as poly(amidoamine) (PAMAM), protamine sulfate, poly(L-lysine) (PLL), chitosan derivates, poly(ethylenimine) (PEI), and MADQUAT have been explored as non-viral carriers for gene delivery.[1] These cationic polymers have strong electrostatic interaction with different negatively charged molecules, particularly in blood components like red blood cells (RBCs) or plasma proteins.[2] There is a great interest in developing high-performance electrochemical biosensors for medical and environmental applications. Entrapment is one of facile methods for enzyme immobilization; however, enzyme leakage and sluggish substrate-enzyme active site mass transfer are the two major issues with the existing entrapment based electrochemical biosensors.[3,4] Although MADQUAT is a cationic polymer and has strong electrostatic affinity with various negatively charged biomolecules, to the best of our knowledge, there is no report on its utilization in entrapment of enzyme for biosensor fabrication.

Blood alcohol determination plays an important role in forensic and laboratory medicine; drunk driving is a serious problem in the modern world, which results in many fatal accidents each year. In addition, it is necessary in clinical laboratories for the detection of acute alcoholism and syndromes that are related to alcohol abuse. Presently, many methods have been employed for

*This chapter has been published in *Analyst*, **2017**, *142*, 2595-2602

the quantification of alcohol levels, including spectrometric, chromatographic and colorimetric analysis. However, these methods are time consuming and complex to perform due to laborious sample pre-treatment and expensive analytical instrumentation. Thus, there is an increasing requirement for rapid, accurate, and inexpensive methods for the determination of alcohol.[5] Electrochemical biosensors are attractive alternatives for biomolecules monitoring as they may provide specific, rapid, and repetitive assays through the use of low-cost miniaturized transducers.[6,7]

Ethanol biosensors are typically based on NAD-dependent alcohol dehydrogenase.[8-11] NAD-dependent oxidoreductases exist in virtually all organisms and catalyze the reversible oxidation of primary and secondary alcohols into aldehydes and ketones, respectively. Medium-chain alcohol dehydrogenases (ADHs, EC 1.1.1.1) contain 327−376 amino acid residues per chain and are generally zinc-dependent.[9] Yeast alcohol dehydrogenase (ADH1) is a tetramer of four identical subunits that contain 347 amino acid residues each, with an estimated mass of 147396 Da.[12,13] Electrochemical enzyme-based biosensors combine the high specificity of enzymes with the sensitivity of electrochemical transducers. Enzyme electrodes are electrochemical probes that incorporate a thin layer of immobilized enzymes on the surface of the working electrode.[14] Alcohol dehydrogenase (ADH) based biosensors have been extensively employed for the determination of ethanol for many years due to their cost effectiveness, rapidity, reliability, and specificity. In these types of biosensors, ADH catalyzes the oxidation of ethanol to acetaldehyde in the presence of NAD^+. The generated NADH in the reaction can be detected amperometrically following the application of a suitable potential to the electrode.[15-18]

Nanocomposites/hybrids can often combine the advantages of their constituent components to exhibit enhanced properties.[19-21] SWCNTs, which consist of single graphene

sheets that are seamlessly wrapped into cylindrical tubes with diameters of between 0.4 and 2.5 nm, offer excellent physical and chemical properties that enable a wide range of biomedical applications.[22,23] Graphene nanosheets are one-atom thick planar sheets of sp^2-bonded carbon atoms that are attracting tremendous attention in terms of fundamental research and potential applications.[24-26] The high surface to volume ratio of nanomaterials along with layered structure contributed to the highly sensitive chemical/biospecies interaction; atomically thick graphene sheets provide extremely high surface areas and abundant surface-resident atoms for electron transport, which make them highly sensitive to detect target molecules.[27-29] CNTs and GO share many similar properties, while being structurally dissimilar, rGO/CNT non-covalent composites provides significantly higher heterogeneous electron transfer (HET) rate with great potential to be utilized in high-performance biosensor fabrication.[30]

In the present study, we have proposed a new enzyme entrapment platform based on the SWCNT–rGO nanohybrid with the assistance of the MADQUAT polymer. The entrapped ADH was assessed for any conformational changes through secondary structure analysis, revealing no structural changes. A significant synergistic enhancement of the SWCNT-rGO nanohybrid was confirmed, and the ADH entrapped by MADQUAT showed high sensitivity, selectivity and stability for the detection of ethanol.

6.2. Experimental Section

6.2.1. Chemicals and reagents

Graphite powder, SWCNTs (Ø0.7 nm), Poly(2-(dimethylamino)ethyl methacrylate (MADQUAT), ADH from *Saccharomyces cerevisiae (EC 1.1.1.1),* β-nicotinamide adenine dinucleotide hydrate (NAD^+), human serum (from human male AB Plasma), ethanol (98%) and Trizma base were purchased from Sigma-Aldrich. All chemicals used were of analytical grade,

and all solutions and buffers were prepared with double deionized (DI) water (Nanopure® water purification systems).

6.2.2. Apparatus

All electrochemical experiments, including cyclic voltammetry (CV) and amperommetry were performed using a CHI 660 electrochemical workstation (CH Instruments Inc., USA) using a conventional three-electrode system that consisted of a platinum wire counter electrode, a 3.0 M KCl saturated Ag/AgCl reference electrode, and a working electrode comprised of a modified Ø3 mm glassy carbon electrode (GCE). X-ray diffraction (XRD) was used to characterize the synthesized graphene oxide (GO). Fourier transform infrared spectroscopy (FTIR, Nicolet) equipped with a liquid N_2-cooled MCT detector was employed for the study of the enzyme-MADQUAT interaction. The estimation of the secondary structure composition was carried out by the curve fitting of the amide I bands using the peak fitting software (SeaSlove Software Inc., USA), where the deconvoluted parameters were set with a gamma value of 1.65 with a smoothing length of 55 and the second derivative spectra were calculated over a 13-data-point range (13 cm^{-1}).[31] A field-emission scanning electron microscope (FE-SEM) (Hitachi SU-70) was employed for the surface characterization of the SWCNT-rGO nanohybrid. All experiments were performed at room temperature and all of the potentials quoted are versus the Ag/AgCl reference electrode.

6.2.3. Fabrication of biosensor

The graphite oxide was synthesized using the simplified Hummer's method [32] and the GO suspension was prepared by ultrasonicating 5.0 mg of the graphite oxide powder in 1.0 ml DI water for 30 min. The SWCNT suspension was prepared by ultrasonicating 5.0 mg mL^{-1} of SWCNTs in dimethylformamide (DMF) for 30 min. Tris buffer solutions (0.1 M) for the

electrochemical studies was prepared using a Trizma base and adjusted the pH to 8.2 using 1 M HCl. The carbon nanohybrids were formed on GCE by drop-casting and drying 1:1 v/v ratio of the GO and SWCNT suspension (2 µL each), and then reduced by running CV in the potential range of -0.6 to -1.5 V for five cycles at 20 mVs^{-1} in 0.1M tris buffer solution after purging with Argon gas for 10 min. The ADH was immobilized by incubating 2.0 µL ADH (5.0 mg mL^{-1}) with 2.0 µL MADQUAT (50 mg ml^{-1}) over the GCE surface that was modified with the SWCNT-rGO nanohybrid thin film. Incubation was performed in a 4^{o}C refrigerator for 30 min, followed by rinsing with the tris buffer.

6.3. Result and Discussion

6.3.1. Characterization of SWCNT-rGO nanohybrid on the GCE surface

The morphologies of the individual rGO and SWCNT films and the SWCNT–rGO nanohybrid were characterized via FE-SEM. Figure 6.1A displays the SEM image of the rGO formed on the GCE surface, revealing a rippled-like surface structure, which is a typical feature of pristine graphene. Figure 6.1B depicts a FE-SEM image of SWCNTs, showing the GCE surface was homogeneously covered by the carbon nanotubes. Figure 6.1C shows the nanohybrid film, in which rGO sheets were uniformly dispersed throughout the SWCNTs. The typical aggregation and distinctive formation between individual rGO layers were inhibited in the SWCNT–rGO nanohybrid film due to the presence of the SWCNTs, leading to the enhancement of the specific surface areas and porosity**.** Figure 6.1D presents the energy dispersive X-ray (EDX) spectra of the SWCNT-rGO nanohybrid (red), as well as isolated SWCNTs (blue), and rGO (green). Their oxygen: carbon ratio was decreased in the following order: rGO > SWCNT-rGO > SWCNTs, Indicating the oxygen functional groups of the GO was partially removed during the electrochemical reduction treatment.[33]

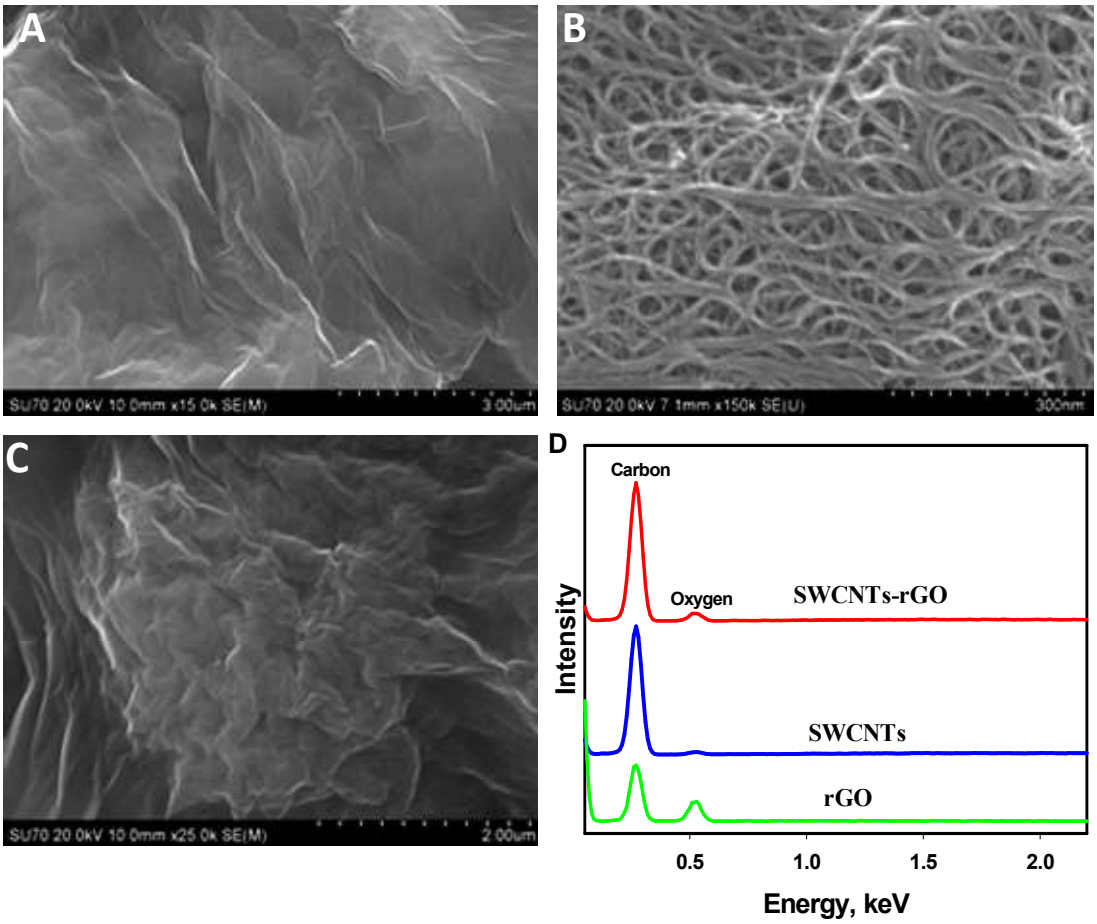

Figure 6. 1. SEM images of (A) rGO, (B) SWCNTs and (C) SWCNT-rGO nanohybrids; (D) EDX spectra of rGO (green), SWCNTs (blue) and SWCNT-rGO nanobybrid (red).

In order to investigate the electrochemical behaviors of the SWCNT-rGO nanohybrid thin film, CV (Figure 6.2) was performed with the $[Fe(CN)_6]^{3-/4-}$couple as the redox probe. The CVs of the GC electrode (blue), as well as those modified with SWCNT-rGO nanohybrid (pink), SWCNTs (sky blue), and rGO (red), were recorded in 2.5 mM $K_3Fe(CN)_6$ + 0.1 M KCl. The peak potential

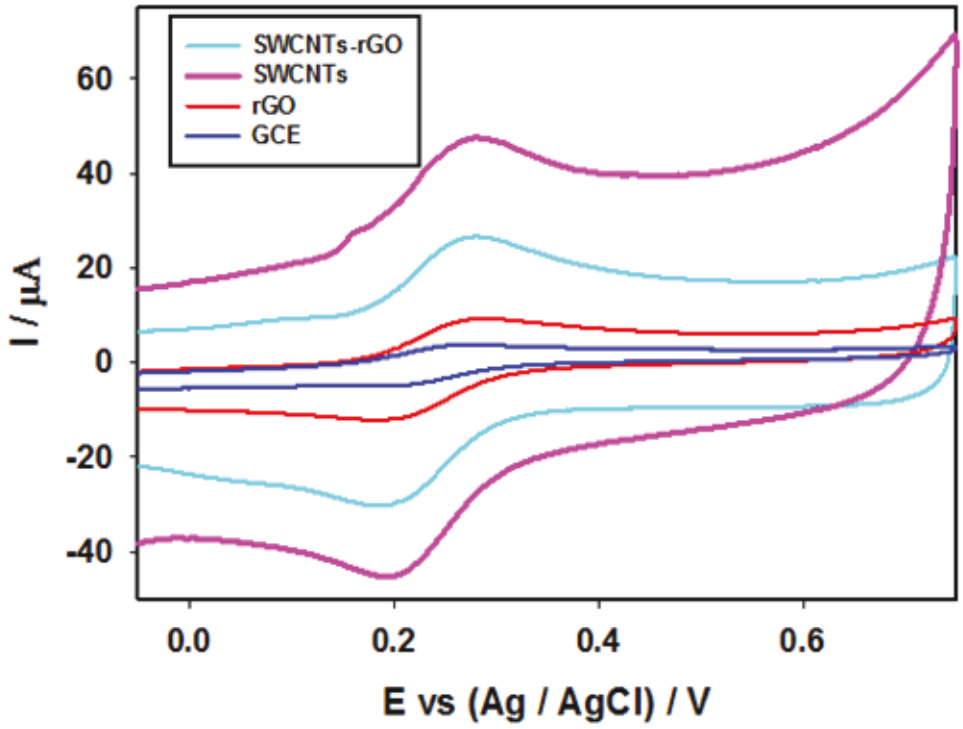

Figure 6. 2. CV responses of a bare GC electrode (blue), a GC electrode modified with rGO (red), SWCNTs (sky blue) and SWCNTs-rGO nanohybrid (pink) recorded in a 0.1 M KCl solution containing 2.5 mM $K_3Fe(CN)_6$ at the scan rate of 20 mVs^{-1}.

separation (ΔE_p) between the anodic (Epa) and cathodic (Epc) peak among the nanohybrid, SWCNTs and rGO remained ~55 mV but with significantly increased current response at the SWCNT-rGO nanohybrid as compared to the GCE that was modified with SWCNTs or rGO nanosheets alone. In contrast, a low current response with a large peak separation was observed at the bare GCE. The significant increase of the current response and the decrease of the peak separation show that the SWCNT-rGO nanohybrid provide a desirable platform with high conductivity and a large surface area for enzyme immobilization

6.3.2. Structural studies of the immobilized ADH

The immobilization method is an important factor, which determines the electron transfer rates between electrodes and the enzymes.[34] Among various immobilization techniques, the entrapment of enzymes within the polymer matrix yielded higher electron

transfer compared to physisorbed enzymes.[35] The polymer backbone supporting the methacrylate in MADQUAT were attached with non-covalent polar π interactions.[36] The nanohybrid structure provides a unique π-π hydrophobic interaction to communicate with polymer and enzyme. MADQUAT is a cationic polymer, composed of cationic functional groups. These cationic functional groups interact with negatively charged amino acid chains of ADH in tris buffer, whose pH was higher than the isoelectric point of ADH (pI 5.4-5.8). The strong electrostatic self-assembly of MADQUAT with ADH makes it possible to design an advanced platform for ethanol detection. The conformational changes of the enzymes upon immobilization were investigated, in comparison to their native structures in aqueous media. Figure 6.3A shows the FTIR spectra of the pure ADH enzyme in aqueous media (a) (pH 8.2, tris buffer 0.1M) and the immobilized ADH (b). The analysis of the amide I band in the range of 1600–1700 cm^{-1} (due to the C=O stretching vibration) makes it possible to study the effect of immobilization on the secondary structure of the protein.[37] The amide I band consisted of several overlapping components that were assigned to different secondary structural elements. These individual components were identified from the second-derivative spectra. The bands at 1610–1640 cm^{-1} and 1685–1695 cm^{-1} were assigned to β-sheets, at 1640–1650 cm^{-1} to random coils, at 1650–1660 cm^{-1} to α-helix, and at 1660–1685 cm^{-1} to β–turns.[38] In order to estimate the

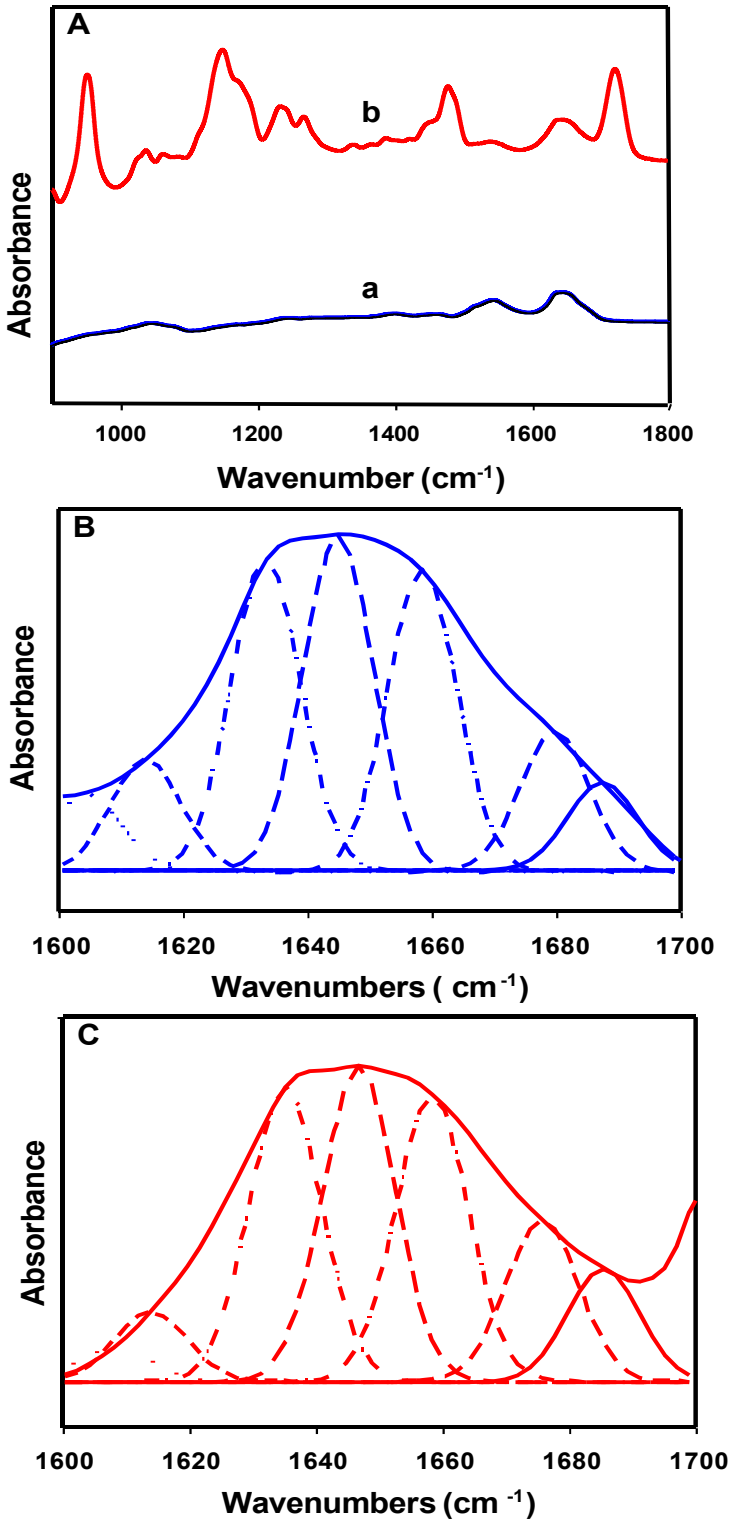

Figure 6. 3. (A) FTIR spectra of ADH: free (a), and after being entrapped on the SWCNT-rGO nanobybrid film by MADQUAT (b). Deconvoluted FTIR spectra in the amide I region together with the respective best-fitted individual band components of the free (B) and entrapped (C) ADH

secondary structural composition of the enzyme, a curve fitting of the deconvoluted amide I region was performed through the software aforementioned in experimental section for ADH in the aqueous solution (Figure 6.3B) and the immobilized ADH (Figure 6.3C). The secondary structural information following the deconvolution of the amide I region obtained from Figures 6.3B and 6.3C are presented in supplementary Table 6.1. As shown in Table 6.1, the free ADH in the aqueous solution had a high β-sheet (29%) content, in comparison to α-helix (22%), followed by 25% randomly coiled structures, and 11% β-turns. The components derived from α-helix structures were an excellent indicator of the desirable folding of the enzyme; the loss of this secondary structure typically leads to enzyme inactivation. As seen in Table 6.1, α-helix content present in the aqueous ADH (22%) and the immobilized ADH (21%) was almost identical, revealing the desirable folding of the enzyme after being entrapped on the SWCNT-rGO nanohybrid film with the assistance of the new polymer MADQUAT. Only a minor decrease of β-sheet from 25% to 23% and a small increase of β-turn content from 11% to 14% were observed following the immobilization. The slight variances in secondary structural changes observed were likely related to transesterification activity expressed by the enzyme subsequent to its immobilization.[39] To verify the positive association between both secondary structural panels, we further calculated the

Table 6.1. Secondary structure composition of alcohol dehydrogenase (ADH) as calculated by fitting the amide I region for the pure ADH in the aqueous solution (Figure 6.3B) and the immobilized ADH (Figure 6.3C).

Band assignment	Band position		Area %	
	ADH (cm^{-1})	*ADH+ Poly-methyl chloride (cm^{-1})*	*ADH*	*ADH+ Poly-methyl chloride*
Amino acid absorption	1604,1614	1608,1614	13	10
ß-sheet	1633, 1689	1635	29	23
Random coils	1645	1646	25	23
α-helix	1658	1658	22	21
ß-turns	1677	1675, 1686	11	14

correlation coefficient (r) value; and the high r value (0.92) indicated that the structure of the immobilized enzyme was not significantly altered.

6.3.3. Electrocatalytic behaviour of ADH onto SWCNT-rGO nanohybrid for ethanol detection

Figure 6.4 presents the CVs of the GCE modified with MADQUAT entrapped ADH onto rGO (A), SWCNTs (B), SWCNT-rGO nanohybrid (C) recorded in 10 mM NAD^++ 0.1 M trish buffer in the presence of 50 mM ethanol (red solid line) and in the absence of ethanol (blue dashed line) at a scan rate of 20 mVs^{-1}. The ADH immobilized on the SWCNT-rGO nanohybrid showed a distinct and much stronger NADH oxidation peak at ~0.41V in the presence of ethanol (Figure 6.4C), in comparison to the ADH entrapped on SWCNTs (Figure 6.4B), whereas almost no oxidation peak was observed for the ADH entrapped on the rGO (Figure 6.4A). The performance of physisorbed ADH on the SWCNT-rGO nanohybrid (green dashed line) has also been compared with the MADQUAT entrapped ADH on the SWCNT-rGO nanohybrid (red solid line) in Figure 6.4C, revealing that the MADQUAT entrapped ADH on the SWCNT-rGO

nanohybrid exhibited a significant improvement in performance over the physisorbed ADH. Figure 6.4D displays the direct NADH oxidation on the MADQUAT-SWCNT-rGO nanohybrid thin film without the enzyme in presence of 10.0 mM NADH in 0.1M tris buffer (pH 8.2),

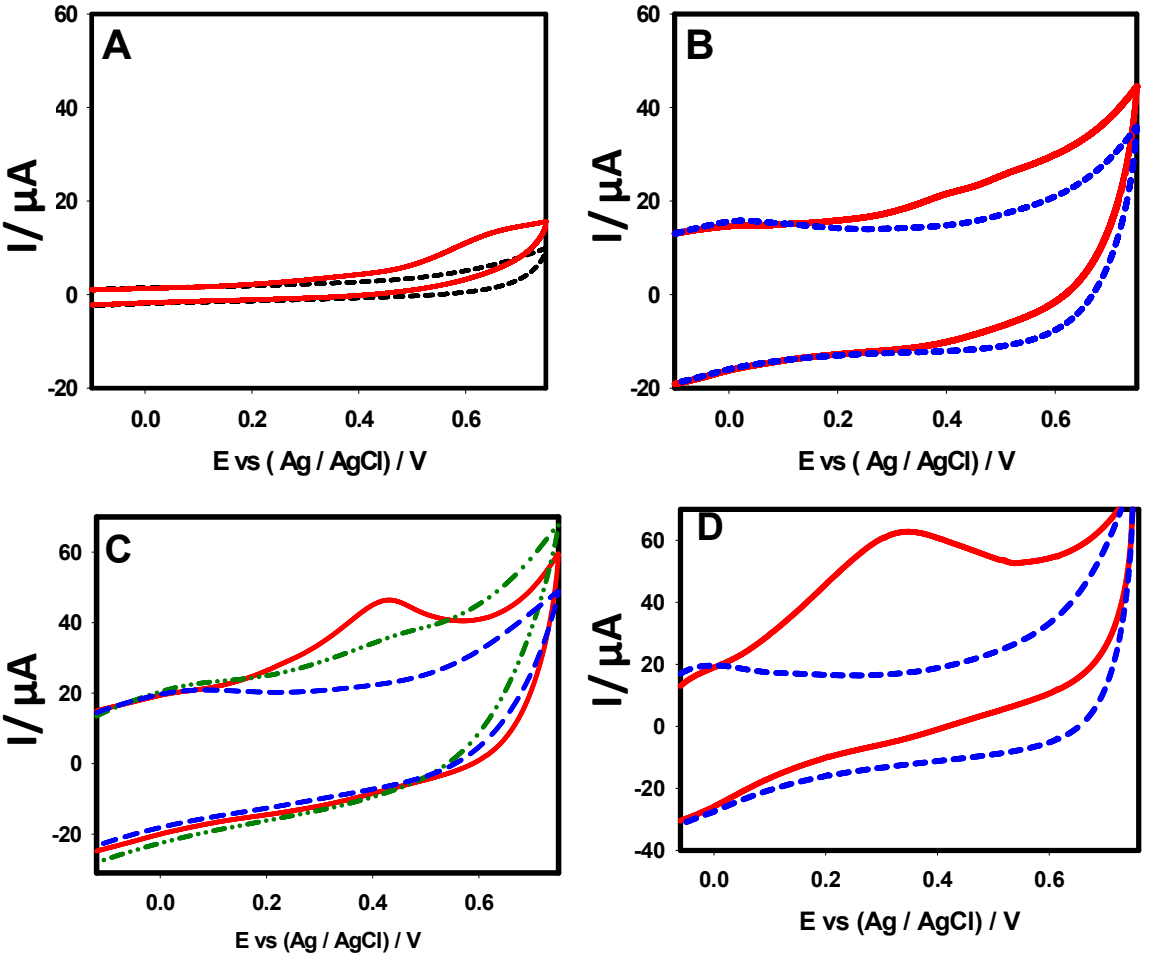

Figure 6. 4. CV responses at scan rate of 20 mVs^{-1} of the GC electrodes modified with (A) ADH-rGO, (B) ADH-SWCNT and (C) ADH-SWCNT-rGO nanohybrid (entrapped ADH-red solid line); physisorbed ADH (green dashed line) in a 0.1M tris buffer containing 50 mM ethanol + 10 mM NAD+ and only 10 mM NAD+(blue dashed line). (D) CV responses of the SWCNT-rGO without ADH in a 0.1M tris buffer in the absence of NADH (blue dashed line) and in the presence of 10 mM NADH (red solid line).

further confirming that the large well-defined peak appeared in Fig. 3C was due to the oxidation of NADH generated by the immobilized ADH during the ethanol oxidation. The mechanisms of ethanol oxidation catalyzed by ADH, which contains four different subunits that are arranged as two dimers albeit structurally similar (Scheme 1). Each subunit within the dimers encompasses a coenzyme (NAD^+) binding domain, which is typical of the Rossmann fold (six-stranded parallel β-pleated sheets with two helices on both sides of the sheets) to which the coenzyme is bound at the terminal ends of the carboxyl. Each subunit also possesses a catalytic domain that contains zinc to which alcohol binds, and the substrates bind within the clefts

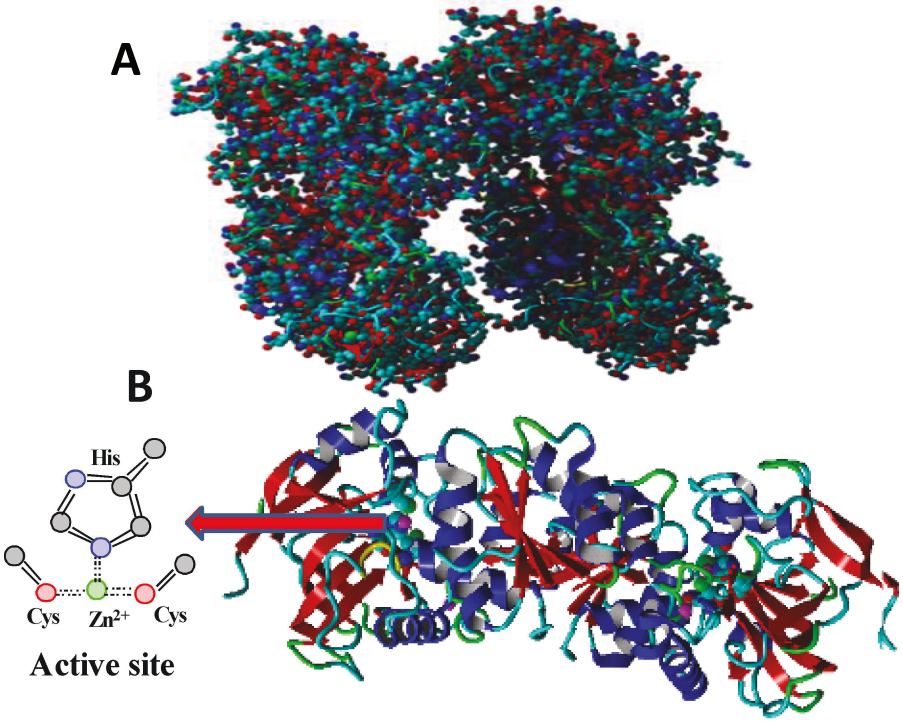

Scheme 6. 1. (A) Tetramer structure of ADH; and (B) Active sites of the ADH enzyme.

between the domains.[40] Ethanol oxidation proceeds through the deprotonation of nicotinamide ribose by His-51, Ser-48 by nicotinamide ribose, and alcohol by Ser-48, in sequential order.[41]

The hydride transferring from the alkoxide ion to NAD^+ leads to the formation of NADH and aldehyde or ketone being bound to NAD^+ leads to the formation of NADH and aldehyde or ketone being bound to the zinc active site. ADH typically catalyzes ethanol oxidation via the following bi-bi mechanism:[42]

$$E + A + B \rightleftharpoons EA + B \rightleftharpoons EAB \rightleftharpoons EPQ \rightleftharpoons EQ + P \rightleftharpoons E + P + Q$$

where E is the enzyme; A represents β-NAD^+; B denotes the alcohol; whereas P and Q are the products of acetaldehyde and NADH. In our case, the overall reactions at the electrode/electrolyte interface may be described as follows:

$$CH_3CH_2OH + NAD^+ \xrightarrow{ADH} CH_3CHO + NADH + H^+$$

$$NADH \longrightarrow NAD^+ + H^+ + 2e^-$$

The ADH immobilized on the SWCNT-rGO nanohybrid film effectively catalyzed the oxidation of ethanol to acetaldehyde and the conversion of NAD^+ to NADH. The NAD^+ was regenerated via the electrochemical oxidation of the formed NADH, where a two-electron transfer was involved.

To understand the effect of the amount of MADQUAT used for the entrapment of ADH on the SWCNT-rGO nanohybrid, five different concentrations (5.0, 20.0, 30.0, 50.0, and 60.0 mg mL^{-1}) of MADQUAT were used, while the ADH concentration was kept constant (5.0 mg mL^{-1}). Figure 6.5A presents the amperometric responses of the modified electrodes measured in a 20 μM ethanol + 10 mM NAD^+ solution. The peak current was increased with the increase of the concentration of MADQUAT from 5.0 to 50.0 mg mL^{-1}, which may be attributed to the increase of the electrostatic force of the polymeric cations and the enzymatic anions, thus lowering the zeta potential between ADH and MADQUAT. However, the current response was

slightly decreased when the MADQUAT concentration was increased from 50.0 to 60.0 mg mL^{-1}, which might result in imbalance of the cationic/anionic ratio between polymer and enzyme, thus lowering their electrostatic force and increasing the zeta potential.[43] Hence, 50.0 mg mL^{-1}

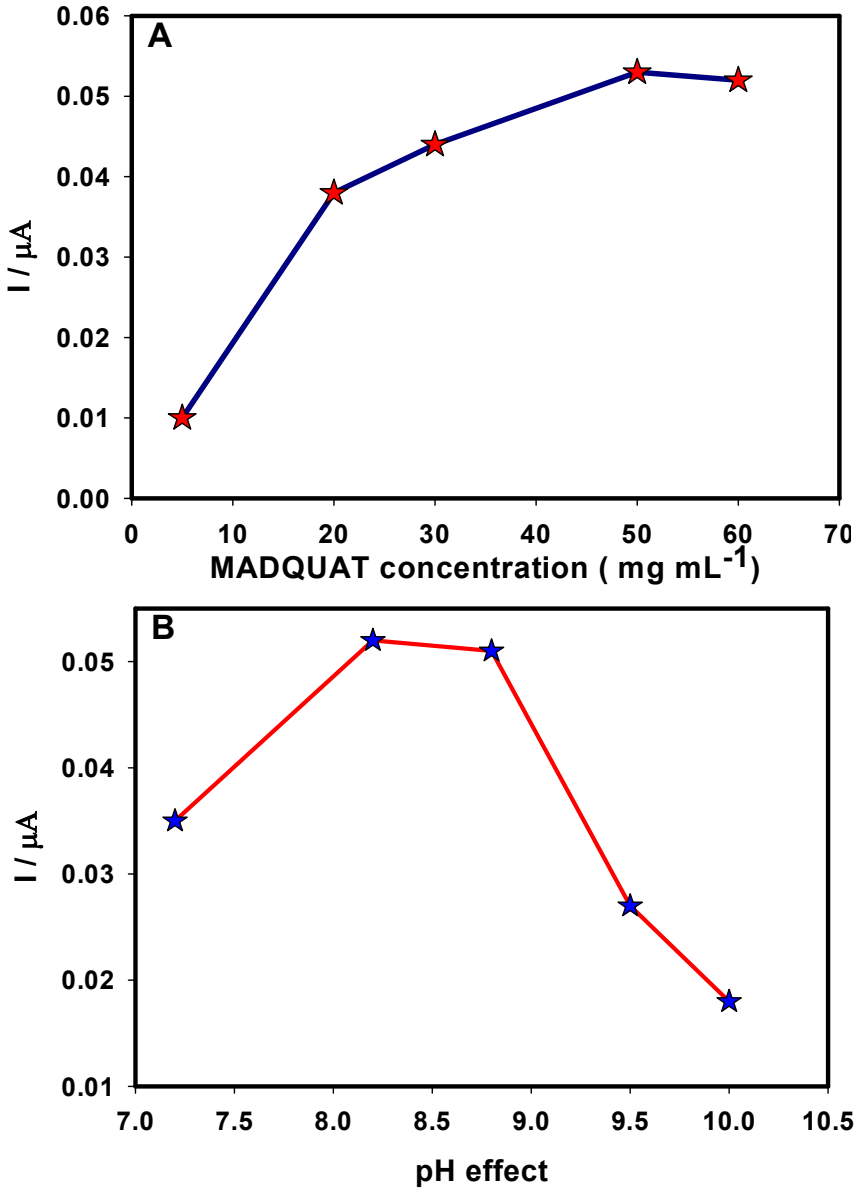

Figure 6. 5. (A) Effect of the concentration of MADQUAT used for entrapping ADH on the SWCNT-rGO/GCE on the peak current measured in a 0.1M tris buffer containing 20 µM ethanol and 10 mM NAD^+. (B) Effect of pH (7.2, 8.2, 8.8, 9.5 and 10) on ADH-SWCNT-rGO/GCE in a 0.1M tris buffer containing 20 µM ethanol and 10 mM NAD^+; E_{app} 0.5 V.

MADQUAT was chosen as the optimum concentration for the entrapment of the enzyme ADH. The effect of pH on the biosensor was investigated in 20 µM ethanol + 10 mM NAD^+ solution. As shown in Figure 6.5B, the response was increased with the increase of the pH from 7.2 to **8.2;** but it was decreased with the further increase of the pH from 8.8 to 10.0., indicating that 8.2 was the optimized pH.

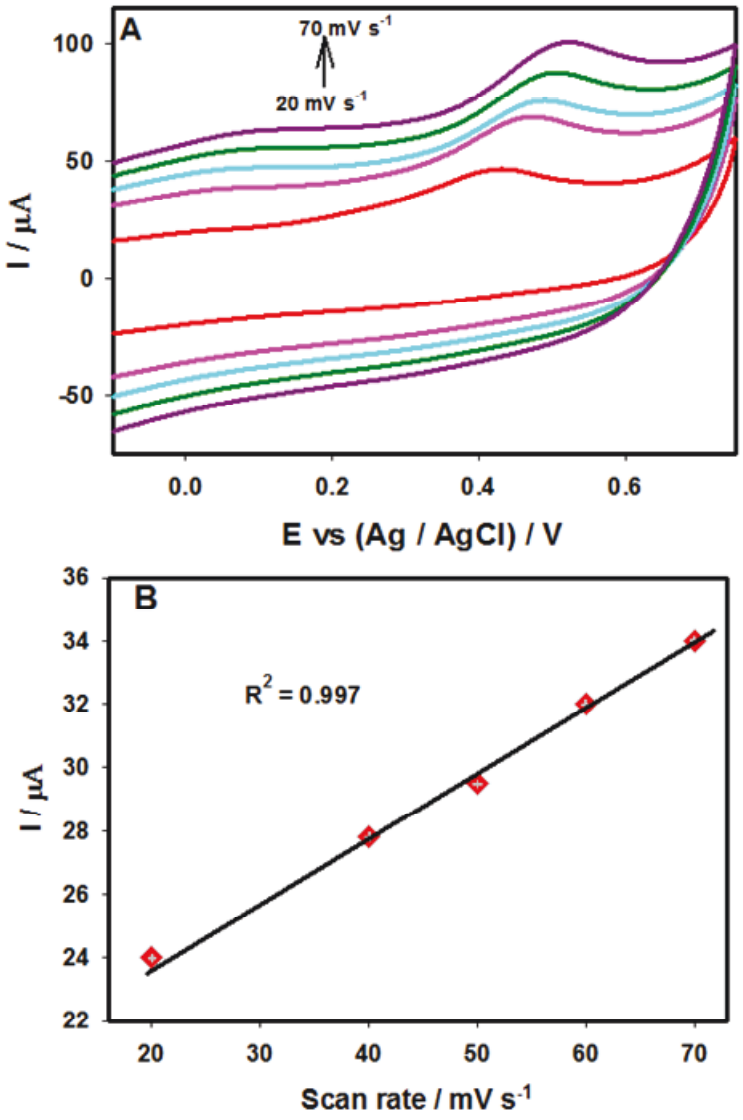

Figure 6. 6. (A) CVs of the ADH-SWCNTs-rGO/GCE recorded in 0.1 M tris buffer (pH 8.2) containing 50 mM ethanol and 10 mM NAD+ at different scan rates of 20, 40, 50, 60 and 70 mVs^{-1}. (B) Plot of anodic peak currents versus the scan rates obtained from Fig. 6.6A.

The effect of the scan rate on the electrochemical behavior of the MADQUAT entrapped ADH on the SWCNT-rGO nanohybrid was investigated in a 0.1 M tris buffer (pH 8.2) containing 50mM ethanol and 10mM NAD^+.As shown in Figure 6.6A, the peak current due to the anodic oxidation of NADH was in elevated with the increase of the scan rate from 20 to 70 mVs^{-1}, whereas the peak potential gradually shifted toward more positive. The plot of anodic peak current versus the scan rate (Figure 6.6B) exhibited a linear relationship (R^2 = 0.997), showing that the electrochemical oxidation was a surface-controlled process.

6.3.4. Performance of the ethanol biosensor

The analytical performance of the prepared ethanol biosensor was assessed using CV and amperometry. Figure 6.7A displays the CV responses to the successive addition of ethanol (1mM to 30 mM) into a 0.1M tris buffer (pH 8.2) containing 10 mM NAD^+. The analytical performance of the prepared ethanol biosensor was assessed using CV and amperometry. Figure 6.7Adisplays the CV responses to the successive addition of ethanol (1mM to 30 mM) into a 0.1M tris buffer (pH 8.2) containing 10 mM NAD^+. For clarification, the oxidation peak range of the CV was enlarged and is presented as an inset of Figure 6.7A, showing that the current was increased with the increase of the ethanol concentration. A linear increment of the current response with R^2= 0.986 was attained with the sensitivity of 0.26 μA mM^{-1}as seen in Figure 6.7B. The limit of detection (LOD) was estimated to be 110 μM based on a signal-to-noise ratio of 3σ/b, where σ is standard deviation of blank and b is slope value obtained through calibration curve. The wide

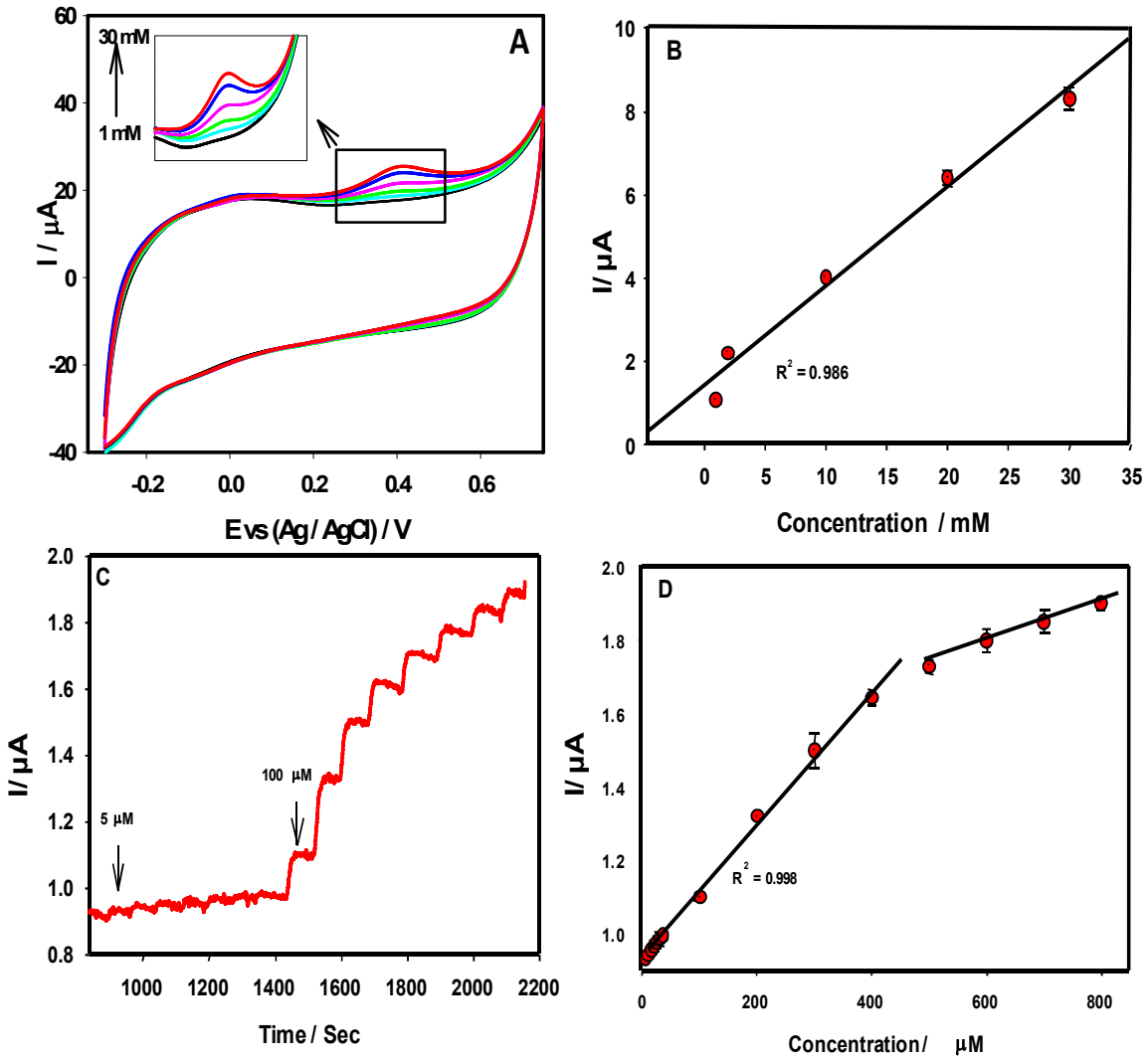

Figure 6. 7. (A) CV responses at 20 mVs^{-1} scan rate of the ADH-SWCNT-rGO/GCE in 0.1M tris buffer (pH 8.2) containing different concentrations of ethanol (1 – 30 mM) + 10 mM NAD^+. (B) Calibration plot of the current responses derived from Figure 6.7A. (C) Amperometric responses of the optimized ADH-SWCNT-rGO/GCE to the successive addition of ethanol varied from 5 - 800 µM into a 0.1M tris buffer (pH 8.2) + 10 mM NAD^+(E_{app}= 0.5V). (D) Calibration plot of the current responses derived from Figure 6.7C.

detection range obtained through CV might be utilized for the serum level detection of ethanol, especially for road safety and medical purposes. According to the International Center for Alcohol Policies (ICAP), an average serum level of >17.4 mM is considered as unsafe for

driving in Canada and USA. Amperometric technique was employed to detect the comparatively low concentration range of ethanol. To optimize the applied electrode potential, four different electrode potentials including 0.40, 0.45, 0.50 and 0.55 V were evaluated for the amperometric detection of 50 µM ethanol in 0.1M tris buffer (pH 8.2) containing 10mM NAD^+. The amperometric current response was increased with the increase of the potential from 0.40 to 0.50V; however, the current response remained almost constant when the potential was further increased from 0.50 to 0.55 V. Therefore, 0.5V was chosen as the optimum potential for all the amperometric measurements as displayed in Figure 6.7C, where rapid response was observed after the addition of ethanol. The corresponding calibration plot is presented in Figure 6.7D, showing two linear regression ranges. The LOD value of 0.16µM with a sensitivity of 1.84 µA mM^{-1} was achieved in the concentration from 5 - 400 µM with R^2= 0.998.

The LOD, sensitivity and linear detection range obtained with this study was superior to those reported in the literature,[15,44-49] as listed in supplementary Table 6.2. The amperometric response of ethanol at the concentration 400 µM gave a characteristic plateau current, showing the pattern of Michaelis−Menten kinetics as seen in Fig. 5D. The Michaelis-Menten constant (K_m) of the enzymatic reaction was calculated using the Lineweaver−Burk equation:[50]

$$\frac{1}{I_{ss}} = \frac{K_m}{I_{max}} \times \frac{1}{C} + \frac{1}{I_{max}}$$

where K_m is the Michaelis-Menten constant, I_{ss} is the steady state current, I_{max} is the maximum current obtained and c is the concentration of the substrate (ethanol). The K_m value calculated in this study for immobilized ADH on SWCNT-rGO nanohybrid was 0.088 mM. This value was much lower than those typically reported in the literature.[34,48,51] All of the parameters obtained

Table 6.2. Comparison of the performance of various electrodes for the electrochemical sensing of ethanol reported in the literature.

Electrode	*LOD (μM)*	*Sensitivity (μA/mM cm²)*	*Linear range (mM)*	*References*
ADH-CNF/GCE	3	-	0.01-0.425	44
ADH-PNB-	50	-	0.1-3	45
NiONPs-ADH-Nafion/GCE	6.4	0.0036	0.0064-6	46
Nafion-ADH-Graphene/GCE	25	-	0.2-21	47
ADH-Aucoll-MWCNTs-Teflon/GCE	32	2.27	0.02-1	48
ADH-IL-Graphene-Chitosan/GCE	5	-	0.025-0.3	49
SWCNTs-Polytyr(oxidized)/ADH/Naf	0.67	5.8	0.01-0.15	15
ADH-SWCNT-rGO nanohybrids	**0.16**	**26.27**	**0.005 - 0.8 (Amperommetry) 1 – 30 (CV)**	**This work**

through different techniques indicated that the ADH-SWCNT-rGO biosensor exhibited a high enzymatic activity toward the ethanol detection over a wide range of concentrations, which makes it useful for various ethanol sensing applications.

The ADH-SWCNT-rGO biosensor was further investigated for stability, interference with co-existing molecules, and real sample applications. The stability of the biosensor was tested through amperometric measurements in a 0.1M tris buffer (pH 8.2) containing 20 μM ethanol

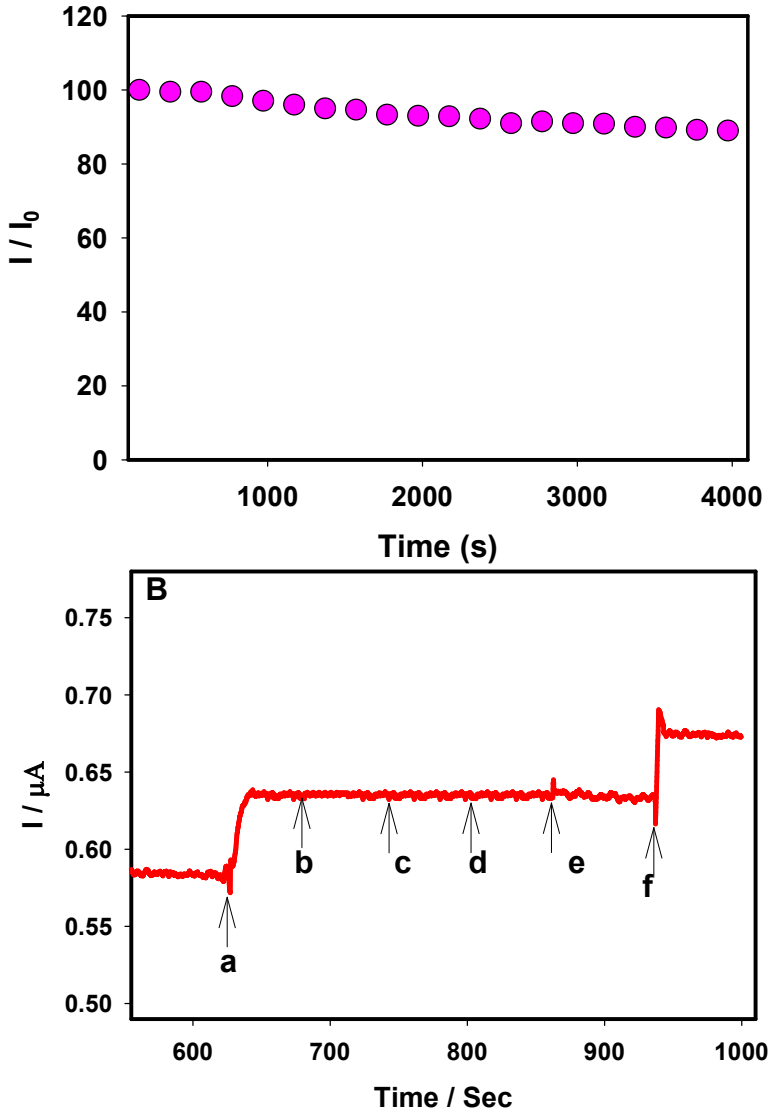

Figure 6. 8. (A) Stability test: relative amperometric current responses of the ADH-SWCNT-rGO/GCE in 0.1M tris buffer containing 20 µM ethanol + 10 mM NAD^+ (E_{app}: 0.5V). (B) Interference tests: amperometric injection of 20 µM ethanol (a), 1mM of each ascorbic acid (b), glutathione (c), glucose (d), uric acid (e) and 20 µM ethanol (f) at E_{app}: 0.5 V in presence of 10 mM NAD^+ in 0.1 M tris buffer.

and 10 mM NAD^+ at a constant applied potential of 0.50 V over 4000 s. As seen in Figure 6.8A, the relative current was decreased by ~8% throughout the experiment, showing that the fabricated biosensor possessed high stability toward the detection of ethanol. The selectivity of the biosensor with possible coexisting molecules such as ascorbic acid, glutathione, uric acid

and glucose was investigated with 20 µM ethanol+ 10 mM NAD^+ in presence of 1mM of each of these potential interfering molecules; app 0.50V (Figure 6.8B). As shown in Figure 6.8B, there were no significant changes in the current response, prior to and following the addition of interfering molecules, which confirmed that the proposed ADH-SWCNT-rGO biosensor possessed a highly selective response to ethanol. We also further examined the proposed biosensor to demonstrate its capacity for practical applications. The determination of ethanol in serum, wine and beer using the standard addition method is presented in Table 6.3. High recoveries in the range of between 93% - 105% were achieved through the actual sample

Table 6.3. Determination of ethanol in real samples by the optimized ADH-SWCNT-rGO/GCE biosensor.

Sample	Concentration added (mM)	Concentration detected (mM)	Recovery (%)	RSD (%)
	10.00	9.30	93.0	3.3
Wine	20.00	19.80	98.9	2.4
	30.00	29.91	99.7	4.1
	10.00	9.82	98.2	1.9
Beer	20.00	20.06	100.3	3.6
	30.00	29.55	98.5	2.1
	10.00	10.40	104.0	4.3
Blood alcohol	20.00	20.30	102.0	4.7
	30.00	31.00	105.0	1.6

analysis, confirming that the developed biosensor is applicable for practical ethanol detection across a wide variety of samples.

6.4. Conclusion

In this study, a novel biosensor platform has been designed based on the SWCNT–rGO nanohybrid with the assistance of the MADQUAT polymer for enzyme entrapment. The entrapped ADH was assessed for any conformational changes through secondary structure analysis, revealing that no structural change occurred in comparison to the free ADH. A significant synergistic enhancement of the SWCNT-rGO nanohybrid was confirmed, and the ADH entrapped by MADQUAT showed high activity for the detection of ethanol. The developed ADH-SWCNT-rGO biosensor exhibited high sensitivity with a remarkable low detection limit of 163 nM. The wide linear detection range, high stability and selectivity with a low K_m value make this biosensor a promising candidate for ethanol sensing in both clinical and environmental settings. The SWCNT-rGO nanohybrid and MADQUAT used in this study not only provide an excellent platform for the ethanol detection, but will also have significant impacts in the field of the development of high-performance enzymatic biosensors for food, clinical and environmental applications.

References

1. Zhang, S.; Xu, Y.; Wang, B.; Qiao, W.; Liu, D.; Li, Z. Cationic compounds used in lipoplexes and polyplexes for gene delivery. *J. Control. Release* **2004,** *100* (2), 165.
2. Moreau, É.; Ferrari, I.; Drochon, A.; Chapon, P.; Vert, M.; Domurado, D. Interactions between red blood cells and a lethal, partly quaternized tertiary polyamine. *J. Control. Release* **2000,** *64* (1), 115.
3. Górecka, E.; Jastrzębska, M. Immobilization techniques and biopolymer carriers. *Biotechnol. Food Sci.* **2011,** *75* (1), 65.

4. Ormategui, N.; Veloso, A.; Leal, G. P.; Rodriguez-Couto, S.; Tomovska, R. Design of stable and powerful nanobiocatalysts, based on enzyme laccase immobilized on self-assembled 3D graphene/polymer composite hydrogels. *ACS App. Mater. Interfaces* **2015,** *7* (25), 14104.
5. C.A. Weatherly, R.M. Woods and D.W. Armstrong, J. Agric. Food Chem., 2014, **62**, 1832-1838.
6. Jia, X.; Dong, S.; Wang, E. Engineering the bioelectrochemical interface using functional nanomaterials and microchip technique toward sensitive and portable electrochemical biosensors. *Biosens. Bioelectron.* **2016,** *76*, 80.
7. Cao, T.; Zhang, F.-T.; Cai, L.-Y.; Zhou, Y.-L.; Buurma, N. J.; Zhang, X.-X. Investigation of the interactions between methylene blue and intramolecular G-quadruplexes: an explicit distinction in electrochemical behavior. *Analyst* **2017,** *142* (6), 987.
8. Azevedo, A. M.; Prazeres, D. M. F.; Cabral, J. M.; Fonseca, L. P. Ethanol biosensors based on alcohol oxidase. *Biosens. Bioelectron.* **2005,** *21* (2), 235.
9. Jörnvall, H.; Hedlund, J.; Bergman, T.; Kallberg, Y.; Cederlund, E.; Persson, B. Origin and evolution of medium chain alcohol dehydrogenases. *Chem.Biol. Interactions* **2013,** *202* (1), 91.
10. Zhang, M.; Gorski, W. Amperometric Ethanol Biosensors Based on Chitosan-NAD+-Alcohol Dehydrogenase Films. *Electroanal.* **2011,** *23* (8), 1856.
11. Zhang, M.; Mullens, C.; Gorski, W. Coimmobilization of dehydrogenases and their cofactors in electrochemical biosensors. *Anal. Chem.* **2007,** *79* (6), 2446.
12. Jörnvall, H. The primary structure of yeast alcohol dehydrogenase. *The FEBS J.* **1977,** *72* (3), 425.

13. Bennetzen, J.; Hall, B. The primary structure of the Saccharomyces cerevisiae gene for alcohol dehydrogenase. *J. Biol. Chem.* **1982,** *257* (6), 3018.
14. Zhu, C.; Yang, G.; Li, H.; Du, D.; Lin, Y. Electrochemical sensors and biosensors based on nanomaterials and nanostructures. *Anal. Chem.* **2014,** *87* (1), 230.
15. Eguílaz, M.; Gutierrez, F.; González-Domínguez, J. M.; Martínez, M. T.; Rivas, G. Single-walled carbon nanotubes covalently functionalized with polytyrosine: A new material for the development of NADH-based biosensors. *Biosens. Bioelectron.* **2016,** *86*, 308.
16. Govindhan, M.; Amiri, M.; Chen, A. Au nanoparticle/graphene nanocomposite as a platform for the sensitive detection of NADH in human urine. *Biosens. Bioelectron.* **2015,** *66*, 474.
17. Zhang, M.; Smith, A.; Gorski, W. Carbon nanotube− chitosan system for electrochemical sensing based on dehydrogenase enzymes. *Anal. Chem.* **2004,** *76* (17), 5045.
18. Wooten, M.; Gorski, W. Facilitation of NADH electro-oxidation at treated carbon nanotubes. *Anal. Chem.* **2010,** *82* (4), 1299.
19. Zhang, R.; Wang, X. One step synthesis of multiwalled carbon nanotube/gold nanocomposites for enhancing electrochemical response. *Chem. Mater.* **2007,** *19* (5), 976.
20. Yang, T.; Zhou, N.; Zhang, Y.; Zhang, W.; Jiao, K.; Li, G. Synergistically improved sensitivity for the detection of specific DNA sequences using polyaniline nanofibers and multi-walled carbon nanotubes composites. *Biosens. Bioelectron.* **2009,** *24* (7), 2165.
21. Adhikari, B.-R.; Govindhan, M.; Chen, A. Carbon nanomaterials based electrochemical sensors/biosensors for the sensitive detection of pharmaceutical and biological compounds. *Sensors* **2015,** *15* (9), 22490.
22. Chen, A.; Chatterjee, S. Nanomaterials based electrochemical sensors for biomedical applications. *Chem. Soc. Rev.* **2013,** *42* (12), 5425.

23. Gao, C.; Guo, Z.; Liu, J.-H.; Huang, X.-J. The new age of carbon nanotubes: An updated review of functionalized carbon nanotubes in electrochemical sensors. *Nanoscale* **2012,** *4* (6), 1948.

24. Brownson, D. A.; Banks, C. E. Graphene electrochemistry : an overview of potential applications. *Analyst* **2010,** *135* (11), 2768.

25. Brownson, D. A.; Kampouris, D. K.; Banks, C. E. Graphene electrochemistry: fundamental concepts through to prominent applications. *Chem. Soc. Rev.* **2012,** *41* (21), 6944.

26. Ayazi, Z. Application of nanocomposite-based sorbents in microextraction techniques: a review. *Analyst* **2017,** *142* (5), 721.

27. Kalantar-zadeh, K.; Ou, J. Z. Biosensors based on two-dimensional MoS2. *ACS Sens.* **2016**, *1*, 5-16.

28. Meng, F.-L.; Guo, Z.; Huang, X.-J. Graphene-based hybrids for chemiresistive gas sensors. *TrAC Trends in Anal. Chem.* **2015,** *68*, 37.

29. Adhikari, B.-R.; Govindhan, M.; Schraft, H.; Chen, A. Simultaneous and sensitive detection of acetaminophen and valacyclovir based on two dimensional graphene nanosheets. *J. Electroanal. Chem.* **2016,** *780*, 241.

30. Mao, X.; Simeon, F.; Rutledge, G. C.; Hatton, T. A. Electrospun carbon nanofiber webs with controlled density of states for sensor applications. *Adv. Mater.* **2013,** *25* (9), 1309.

31. Baldassarre, M.; Scirè, A.; Fiume, I.; Tanfani, F. Insights into the structural properties of D-serine dehydratase from Saccharomyces cerevisiae: an FT-IR spectroscopic and in silico approach. *Biochimie* **2011,** *93* (3), 542.

32. Huang, N.; Lim, H.; Chia, C. H.; Yarmo, M. A.; Muhamad, M. Simple room-temperature preparation of high-yield large-area graphene oxide. *Int. J. Nanomed.* **2011,** *6*, 3443.

33. Adhikari, B.-R.; Govindhan, M.; Chen, A. Sensitive detection of acetaminophen with graphene-based electrochemical sensor. *Electrochim. Acta* **2015,** *162*, 198.
34. Putzbach, W.; Ronkainen, N. J. Immobilization techniques in the fabrication of nanomaterial-based electrochemical biosensors: A review. *Sensors* **2013,** *13* (4), 4811.
35. Umasankar, Y.; Ramasamy, R. P. Enhanced Electron Transfer in Enzymatic Bioelectrodes by a Poly (vinyl alcohol) N-Methyl-4 (4′-formylstyryl) Pyridinium Methosulfate Acetal Cationic Polymer. *ChemElectroChem* **2014,** *1* (11), 1834.
36. Murphy, R.; Coleman, J. N.; Cadek, M.; McCarthy, B.; Bent, M.; Drury, A.; Barklie, R. C.; Blau, W. J. High-yield, nondestructive purification and quantification method for multiwalled carbon nanotubes. .*J. Phys. Chem. B* **2002,** *106* (12), 3087.
37. Secundo, F.; Carrea, G. Mono-and disaccharides enhance the activity and enantioselectivity of Burkholderia cepacia lipase in organic solvent but do not significantly affect its conformation. *Biotechnol. Bioeng.* **2005,** *92* (4), 438.
38. Natalello, A.; Diletta, A.; Brocca, S.; Lotti, M.; Doglia, S. M. Secondary structure, conformational stability and glycosylation of a recombinant Candida rugosa lipase studied by Fourier-transform infrared spectroscopy. *J. Biochem.* **2005,** *385* (2), 511.
39. Tzialla, A. A.; Pavlidis, I. V.; Felicissimo, M. P.; Rudolf, P.; Gournis, D.; Stamatis, H. Lipase immobilization on smectite nanoclays: Characterization and application to the epoxidation of α-pinene. *Biores. Technol.* **2010,** *101* (6), 1587.
40. Raj, S. B.; Ramaswamy, S.; Plapp, B. V. Yeast alcohol dehydrogenase structure and catalysis. *Biochem.* **2014,** *53* (36), 5791.

41. Svensson, S.; Höög, J.-O.; Schneider, G.; Sandalova, T. Crystal structures of mouse class II alcohol dehydrogenase reveal determinants of substrate specificity and catalytic efficiency. *J. Mol. Biol.* **2000,** *302* (2), 441.

42. Abuin, E.; Lissi, E.; León, L. Kinetics of ethanol oxidation catalyzed by yeast alcohol dehydrogenase in aqueous solutions of sodium dodecylsulfate. *Protein J.* **2008,** *27* (4), 247.

43. Cerda-Cristerna, B. I.; Cottin, S.; Flebus, L.; Pozos-Guillén, A.; Flores, H. C.; Heinen, E.; Jolois, O.; Gérard, C.; Maggipinto, G.; Sevrin, C. Poly (2-dimethylamino ethylmethacrylate)-based polymers to camouflage red blood cell antigens. *Biomacromolecules* **2012,** *13* (4), 1172.

44. Wu, L.; Zhang, X.; Ju, H. Detection of NADH and ethanol based on catalytic activity of soluble carbon nanofiber with low overpotential. *Anal. Chem.* **2007,** *79* (2), 453.

45. Du, P.; Liu, S.; Wu, P.; Cai, C. Single-walled carbon nanotubes functionalized with poly (nile blue A) and their application to dehydrogenase-based biosensors. *Electrochim. Acta* **2007,** *53* (4), 1811.

46. Sharifi, E.; Salimi, A.; Shams, E. Electrocatalytic activity of nickel oxide nanoparticles as mediatorless system for NADH and ethanol sensing at physiological pH solution. *Biosens. Bioelectron.* **2013,** *45*, 260.

47. Guo, K.; Qian, K.; Zhang, S.; Kong, J.; Yu, C.; Liu, B. Bio-electrocatalysis of NADH and ethanol based on graphene sheets modified electrodes. *Talanta* **2011,** *85* (2), 1174.

48. Manso, J.; Mena, M. L.; Yáñez-Sedeño, P.; Pingarrón, J. M. Alcohol dehydrogenase amperometric biosensor based on a colloidal gold–carbon nanotubes composite electrode. *Electrochim. Acta* **2008,** *53* (11), 4007.

49. Shan, C.; Yang, H.; Han, D.; Zhang, Q.; Ivaska, A.; Niu, L. Graphene/AuNPs/chitosan nanocomposites film for glucose biosensing. *Biosens. Bioelectron.* **2010,** *25* (5), 1070.

50. Kamin, R. A.; Wilson, G. S. Rotating ring-disk enzyme electrode for biocatalysis kinetic studies and characterization of the immobilized enzyme layer. *Anal. Chem.* **1980,** *52* (8), 1198.

51. Kowalewska, B.; Kulesza, P. J. Toward more efficient bioelectrocatalytic oxidation of ethanol for amperometric sensing and biofuel cell technology. *Anal. Chem.* **2012,** *84* (21), 9564.

Chapter 7: Integrated Bifunctional Electrochemcial Approach for Efficient Bacterial Disinfection*

7.1. Introduction

In recent years there has been an increasing awareness of the dwindling supply of clean potable water on a global scale. Although many improvements have been made to reduce the contamination of water systems and to increase access to clean drinkable water, myriad crises associated with the scarcity of clean potable water persist worldwide. It has been estimated that 1.2 billion people still lack access to safe drinking water; millions of people die annually, including 3,900 children per day from diseases that are transmitted through contaminated water.[1,2] The majority of water related issues are present in poverty stricken areas of the world including some regions of North America. Since the establishment of standardized chlorination for water disinfection, human populations have been protected from bacterial, as well as viral infections for more than 100 years. Mostly adopted current water treatment plans are suffering from high demand of chemical/energy consumption and have need of post-treatment to remove unnecessary chemical by-products.[3] Chlorination comprises one of the most cost effective methods of disinfection; however, it can generate carcinogenic disinfection byproducts (DBPs) (e.g., trihalomethanes (THM) and N-nitrosodiethylamine (NDMA)) during the disinfection process.[4-8] Concerning the safety issues related to chlorination, alternative safe green methods have attracted great interest for water disinfection. To overcome the formation of hazardous DBPs, ultraviolet (UV) disinfection and other physical methods might be employed as

alternatives for water disinfection; however, high energy consumption and the revival of treated bacteria following UV disinfection have constrained the widespread use of these techniques.[9,10]

Photocatalysis and electrocatalysis have been gaining considerable attention owing to their promising applications in water disinfection and hazardous waste remediation.[11] When photocatalysts absorb light, they generate electron-hole pairs, which react with water and dissolved oxygen to produce reactive oxygen species (ROS). These ROSs, such as hydroxyl radicals, peroxides, singlet oxygen, and superoxides, are strong oxidizing agents that can inactivate pathogens by damaging vital macromolecules.[12] For photocatalytic treatment, titanium dioxide (TiO_2) is considered to be one of the most promising photocatalysts due to its low cost, high photocatalytic activity, and chemical stability.[13]

Rapid, energy efficient and green water disinfection technologies are urgently required to address the global challenges for clean potable water.[14-16] With respect to these issues, researchers have been attempting to develop water treatment methods that are more economical and energy efficient than current techniques. We believe that we have taken the initial steps toward the development of a new approach for the treatment of water by integrating photochemistry and electrochemistry. The bifunctional electrode approach has been explored in our group for the remediation of nitrophenols,[17] revealing that photocatalysts and electrocatalysts are combined in a cost-effective manner to improve the efficiencies of both the photochemical and electrochemical processes. The integrated dual processes in a single electrode improves the catalytic performance in a synergistic manner, as the applied potential not only activates the electrocatalyst but also reduces the recombination rate of the photo-generated electrons and holes.[18] In the present study we utilized nanoporous TiO_2 as the photocatalyst in combination with RuO_2 nanoparticles as the electrocatalyst to design a highly efficient bifunctional electrode

for bacterial disinfection, where its disinfection kinetics has been studied in depth. The investigation of bacterial disinfection through this novel bifunctional electrode will advance the environmentally compatible attributes of photochemistry and electrochemistry to an entirely new level.

7.2. Materials and Methods

7.2.1. Design and characterization of bifunctional electrode

Nanoporous titanium dioxide (TiO_2)/ruthenium oxide (RuO_2) bifunctional electrodes (TiO_2/Ti/RuO_2) were fabricated through two steps: TiO_2 nanoporous structures were grown on a titanium substrate via a three step anodization process.[19] The anodization process was carried out in a cell that was designed with a two electrode system, a Ti plate (1.25 cm x 0.8 cm x 0.5 mm) as anode, and a Pt coil as cathode; it contained 0.3 wt% ammonium fluoride; NH4F(Sigma Aldrich) and 2wt% water in ethylene glycol (Sigma Aldrich) under an applied potential of 50V. The initial anodization was carried out for 5h. The as grown rough nanoporous layer was removed with masking tape; the same Ti plate was subsequently anodized for 2 h. The as prepared nanoporous layer was again removed by using masking tape, followed by a third anodization with a duration of 15 min. to fabricate highly ordered nanoporous TiO_2. The newly formed nanoporous TiO_2 plates were incubated at 450°C for 4 h to transform it to an anatase crystal structure. The anatase nanoporous TiO_2 was then electrochemically reduced via a three electrode system (Ag/AgCl as reference electrode, Pt coil as counter electrode, and nanoporous TiO_2 as the working electrode) in 0.1 M H_2SO_4 under an applied negative current of – 5 mA cm^{-2} for stable, reproducible, and high current performance. Ruthenium (III) chloride hydrate ($RuCl_3$.x H_2O; Sigma Aldrich) was employed as an electrocatalyst, which was coated onto a separate bare Ti substrate. A total of 5 coatings of the $RuCl_3$.x H_2O precursor solution were

painted onto the Ti substrate, followed by calcinations at 450 ^{o}C for 2 h in order to obtain the RuO_2 nanoparticles. The bifunctional electrode was subsequently fabricated by interfacing the calcinated nanostructure RuO_2 with the nanoporous TiO_2 electrode. The synthesized nanoporous TiO_2 and RuO_2 were characterized by field-emission scanning electron microscopy (FE-SEM, Hitachi SU 70) combined with an energy dispersive X-ray (EDX) spectrometer (Oxford AZtec operated at 20 kV). The performance of bifunctional, nanoporous TiO_2 and RuO_2 electrodes were assessed through chronoamperometry.

7.2.2. Preparation of bacterial culture

Escherichia coli (ATCC^{R}11775^{TM}) from the American Type Culture Collection were used as a bacterial suspension for all disinfection experiments. Nutrient broth (Sigma Aldrich) and Nutrient agar (Sigma Aldrich) were used as the growth media for the bacteria. All bacterial suspensions for the experiment were prepared from a nearly stationary phase (following 26 hrs of incubation in the broth at 37°C). An initial bacterial population of 2.3 x 10^{-8} colony forming units per milliliter (CFU mL^{-1}) was used for all experiments.

7.2.3. Electrochemical treatment

The electrochemical treatment was carried out through a three electrode system, with Ag/AgCl as the reference electrode, a Pt coil as the counter electrode, and the as prepared bifunctional electrode as the working electrode. An electrochemical chronoamperometry technique with a constant applied potential of 1.2 V was utilized for the treatment process. The UV-visible light (ADAC Systems^{TM} Cure Spot^{TM} 50) with an intensity of 7.4 mW cm^{-2} and 320-450 nm wavelength was employed as the light source for the activation of nanoporous TiO_2 . The light source was introduced into the electrochemical cell through an optic fibre cable. The distance between electrode surface and light source was fixed at 1 cm. The performance of

bifunctional electrode for the photocurrent generation was conducted in a 0.05 M sodium sulfate (Na_2SO_4) solution. All bacterial suspensions for disinfection experiments were prepared in 100 mL of 0.05 M Na_2SO_4 with an initial bacterial concentration of 2.3 X 10^{-8} CFU mL^{-1}. Further, the bifunctional disinfection mechanism was studied through different scavenging chemicals purchased from Sigma Aldrich; 10 mM each of sodium azide, sodium pyruvate, mannitol, and sodium thiosulfate was prepared, and electrochemical treatment was performed under the identical experimental conditions as described above. All of the solutions required for our experiments were prepared using ultrapure water, purified by a Nanopure water system (18.2 MΩ cm).

7.2.4. Culturability estimation through spread plate method

To determine the culturable bacterial density during electrochemical treatment, 100 µl of each sample were collected at regular intervals (every 5 min) from treatment cell and serially diluted 1:10, from 10^{-1} to 10^{-7}. The diluted samples (100 µl) were spread in triplicate on nutrient agar plates using the following standard microbiology procedure. Following overnight incubation at 37°C, the colonies were counted, and colony forming units per milliliter (CFU/mL) were calculated.

7.2.5. Most-Probable Number (MPN) estimation and resuscitation of stressed *E. coli*

Non-pyrogenic sterilized 96 well cell culture microtiter plates (Corning Incorporated, NY, and USA) were used for the MPN analysis. A total of five replicates from each sample were created for five dilutions (10^0-10^{-4}). Nutrient broth, following sterilization, was used as a MPN medium for bacterial growth. A total of 40 µL of each sample was dispensed in a well that contained 190 µL of nutrient broth. Following overnight incubation at 37°C, the turbid well, with a referenced negative and positive control was considered as positive for bacterial growth.

If any survival strategy was adopted by *E. coli* during the electrochemical treatment, the viable but not culturable (VBNC) state of bacteria was assessed through the resuscitation of the treated sample in a nutrient broth containing 30 mM sodium pyruvate. The MPN analysis was performed as described above. The most probable number was determined through the MPN tables referenced from the American Public Health Association.[20]

7.2.6. Estimation of viable bacteria with LIVE/DEAD BacLight

The LIVE/DEAD® *Bac*Light™ bacterial viability kit (Molecular Probes, Invitrogen detection technologies) was used to assess the cell membrane integrity of the treated bacteria. Two fluorescent dyes, SYTO 9 (3.34 mM in DMSO) for green fluorescent and propidium iodide; PI (20 mM in DMSO), were utilized in a 1:2 (SYTO 9:PI) ratio for bacterial cell staining. In a regular interval, 500 µL of each sample (prior to and following electrochemical treatment) were incubated with a 2 µL dye mixture for 15 min at room temperature in the dark. The incubated samples were then immediately filtered through 0.2 µm black membrane filters (Isopore™ membrane filters GTBP02500, Millipore). The membrane filters were transferred to glass slides, which were immediately analyzed through Laser Scanning Microscope Fluoview, version 4.3 FV300 (Olympus FV300 CSLM), and a 60X Plan Apo NA-1.4; oil immersion lens. A HeNe Green (1 mW, 543 nm) laser, and an argon (10 mW, force air cooled, blue 488 nm) laser was used to excite the propidium iodide (ex/em 535/ 617 nm) and SYTO 9 (ex/em 480/500 nm), respectively. Bacteria with damaged cell membranes are considered as being 'dead' and those with integral membranes as 'live'. Live/dead bio-volumes were calculated through PHLIP (Phobia Lasers Image Processing Software-the New Laser Scanning Microscope Image Processing Package).[21]

7.2.7. Scanning electron microscopy (SEM) analysis

The bacterial suspension (1000 µL) was filtered through a 0.22 µm Millipore filter (Millipore Corporation, Bedford, MA) via a sterile vacuum filtration unit. After being air dried, the bacterial sample on filter paper was fixed with 2.5% gluteraldehyde in PBS (Grade I, Sigma Aldrich) for 30 min. Once the bacteria were fixed on filter paper, they were subjected to a series of dehydration steps using 30, 50, 70, 80, and 100 % ethanol. The bacterial sample on the filter paper was subsequently dried by critical point drying, following a modified protocol.[22,23] The prepared sample was then studied through field-emission scanning electron microscopy (FE-SEM, Hitachi SU 70).

7.2.8. Metabolomic analysis during electrochemical treatment

Samples (1000 µL) were taken at regular intervals during the electrochemical treatments and analyzed for total organic carbon (TOC) using a TOC analyzer (Shimazdu, TOC-L, Kyoto, Japan) and further processed for metabolome extraction. The extraction kit and procedure was adopted from the Qproteome^{TM} Bacterial Protein Preparation Kit (QIAGEN, Hilden, Germany) with some modification. The protein content was measured using a Nanodrop instrument (Thermo Fisher Scientific, Massachusetts, USA) at a 280 nm wavelength, and metabolomes were analyzed through ^{1}H NMR (NMR; Bruker AVANCE II 400 MHz, Billerica, MA, USA). After withdrawing sample from the treatment cell, it was initially frozen in liquid nitrogen and then followed the extraction procedure for protein sample analysis. The protein concentrations of the extracted samples (1µL) were measured through a Nanodrops instrument (Thermo Fisher Scientific, Massachusetts, USA) at a 280 nm wavelength. For NMR analysis, we followed the same Qproteome^{TM} Bacterial Protein Preparation Kit procedure without using Benzonase Nuclease, to avoid nucleic acid digestion. The extracted samples were then freeze-dried in a Labconco Freezone (Kansas City, MO, USA) freeze dryer for 2 days to ensure the complete

removal of water residues. Subsequently, the dried samples were dissolved in 500 µL D_2O with tetramethylsilane (TMS) as an internal standard. Thus, the prepared samples were then analyzed for one dimensional (1D) ^1H NMR analysis through nuclear magnetic resonance (NMR; Bruker AVANCE II 400 MHz, Billerica, MA, USA) at room temperature in the Lakehead University Instrumentation laboratory.

7.2.9. Data Processing of NMR analysis

The spectra obtained through ^1H NMR analysis were processed using Spin Works (version 4) software (University of Manitoba, Winnipeg, Canada). The free induction decay (FID) obtained during 1D NMR analysis was employed for data analysis through SpinWorks. Prior to determining the assigned chemical shift (ppm), all spectra were subjected to manual phase and baseline correction. Spectra were edited for 1Hz line broadening (LB) and Gaussian function with 2 bins width. Following the manual calibration in reference to an internal standard (TMS), all of the assigned positions of the spectra chemical shifts were selected through SpinWorks software. The signal positions were then used to search through the *Escherichia coli* Metabolome Database (ECMDB, http://www.ecmdb.ca) for potential metabolites that might be present in the extracted sample.[24,25] The peak assignment for particular metabolites were further verified through the freely available Biocyc (http://biocyc.org) database.[26]

7.2.10. Statistical analysis of NMR data

The processed ^1H NMR spectra were analyzed to compare individually assigned chemical shifts (ppm) among the samples, which were collected during the bifunctional treatment at different time intervals. All of the statistical analyses; correlation matrix, principle component analyses, (PCA) and 3D plots were calculated through XLSTAT version 2016.5 software (University of California, Berkeley, USA).

7.3. Results and Discussion

7.3.1. Characterization of the bifunctional TiO_2/Ti/RuO_2 electrode.

The electrode surface was characterized through field-emission scanning electron microscopy (FE-SEM). Highly ordered nanoporous TiO_2 structures, each approximately 150 nm in diameter, were formed as shown in Figure 7.1A. Each nanopore contained 3-4 smaller nanopores, which were embedded within the structure. These secondary nanopores greatly enhanced the catalytic activity due to a considerable increase in the surface area of the electrode. In order to fabricate the bifunctional electrode, the RuO_2 coating on the Ti substrate was prepared through the thermal decomposition of $RuCl_3.x\ H_2O$. Following thermal decomposition, the uniform RuO_2 nanoparticles of 10-20 nm in diameter were observed, as seen in Figure 7.1B. These dispersed nanoparticles greatly increased the surface area of electrode which ultimately, in combination with nanoporous TiO_2, provided an excellent bifunctional platform with extremely high activity in contrast to the individual platforms on their own. The fabricated electrode underwent further analysis via an energy dispersive X-ray (EDX) spectrometer to verify the nanoporous TiO_2 structure (red) and RuO_2 layer (blue), as depicted in Figure 7.1C. The O: Ti intensity ratio was found to be 2:1, which strongly supported the formation of nanoporous TiO_2 structures. Similarly, the EDX spectra of the RuO_2 layer on the Ti substrate revealed distinct ruthenium and oxygen peaks, which further confirmed the formation of the RuO_2 layer through thermal decomposition.

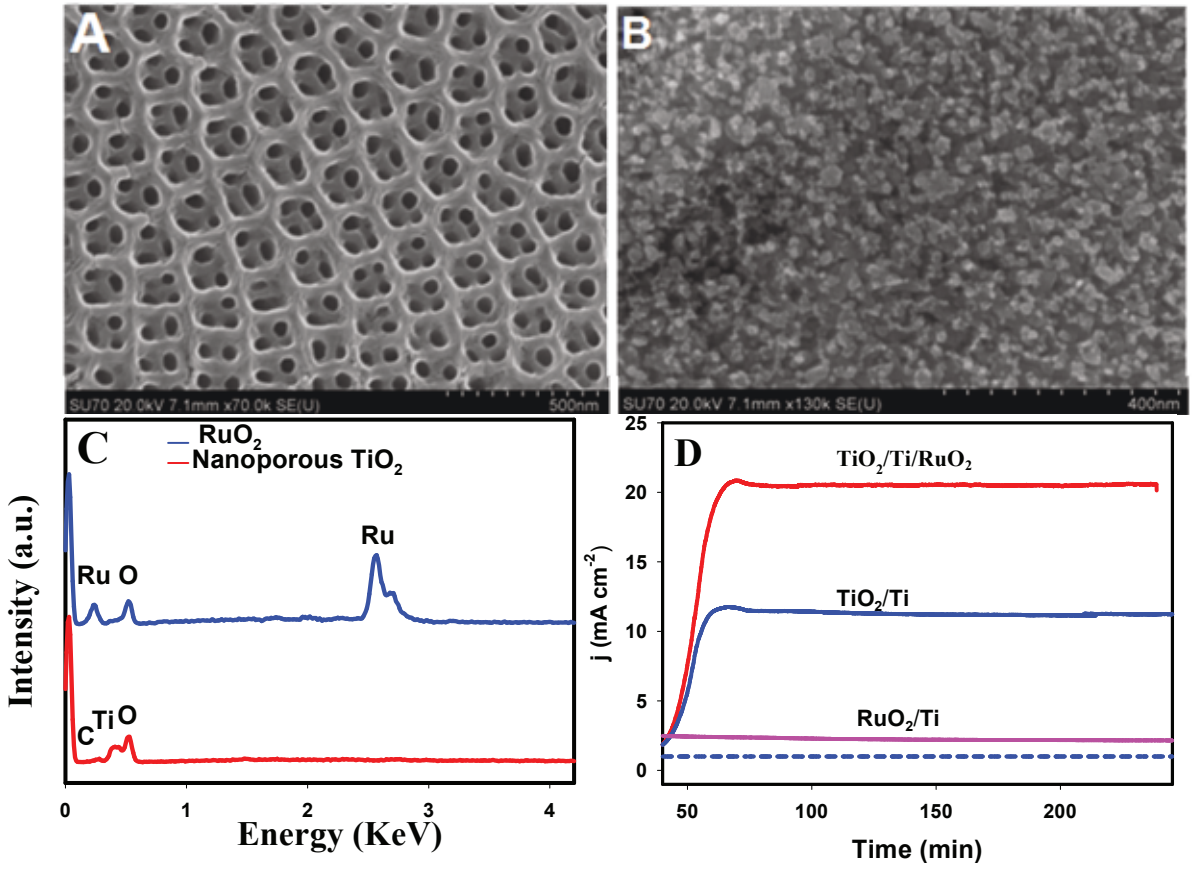

Figure 7. 1. SEM images of the (A) Nanoporous TiO_2; (B) RuO_2 on titanium substrate; EDX spectrum (C) Nanoporous TiO_2 (red) and RuO_2 (blue); (D) Amperometric responses on TiO_2/Ti/RuO_2 (red), TiO_2 (blue) and RuO_2 (pink) in 0.05 M Na_2SO_4, pH 7.0, at a 1.2 V applied potential.

The three electrodes (bifunctional TiO_2/Ti/RuO_2, TiO_2/Ti, and RuO_2/Ti) were further investigated for their activity in 0.05 M Na_2SO_4 through amperometry under an applied potential of 1.2 V. A comparison of the current responses of these electrodes is presented in Figure 7.1D. As expected, the RuO_2/Ti electrode exhibited a higher electrochemical current (2.45 mA cm^{-2}) than the TiO_2/Ti electrode (dashed line; 0.90 mA cm^{-2})). However, under UV-visible light, a high photocurrent (11.45 mA cm^{-2}) was generated by the same TiO_2/Ti electrode. The TiO_2/Ti/RuO_2 bifunctional electrode greatly enhanced the current response (20.55 mA cm^{-2}) over the individual

electrodes under UV-visible light due to the synergistic effects of the integration of the nanoporous TiO_2 photocatalyst and the nanostructured RuO_2 electrocatalyst in a single electrode.

7.3.2. Bacterial disinfection efficiency

The efficiencies of the three electrodes (RuO_2/Ti, TiO_2/Ti, and TiO_2/Ti/RuO_2) in removing culturable *E. coli* were compared in Figure 7.2A. The effects of the photoelectrochemical treatment on *E. coli* with an initial concentration of 2.3 X 10^{-8} CFU/mL in 100 mL of 0.05 M Na_2SO_4 was studied over 60 min through the spread plate method. The combined TiO_2/Ti/RuO_2 electrode demonstrated excellent performance for *E. coli* disinfection as compared to individual TiO_2/Ti and RuO_2/Ti electrodes. A 100% bacterial log reduction of 8.3 was achieved via the nanoporous TiO_2/Ti/RuO_2 electrode within 30 min of treatment, whereas only a 3.79 log reduction (45.66%) was achieved through its counterpart (TiO_2/Ti) (spread plate method shown in Figure 7.3). The performance of RuO_2/Ti was very poor in comparison to the performance of other two electrodes under identical experimental conditions. A control experiment was also conducted to elucidate whether the electrolytes and UV-visible light on their own imparted any bactericidal effect. A very negligible level of bacterial log reduction was observed through the control experiment. The bifunctional electrode that we utilized here had excellent bactericidal properties in comparison to other comparable electrodes. The calculated bacterial disinfection rate of the nanoporous TiO_2/Ti/RuO_2 electrode was 0.62 min^{-1} (R^2= 0.986) under UV visible light, with > 99.999%

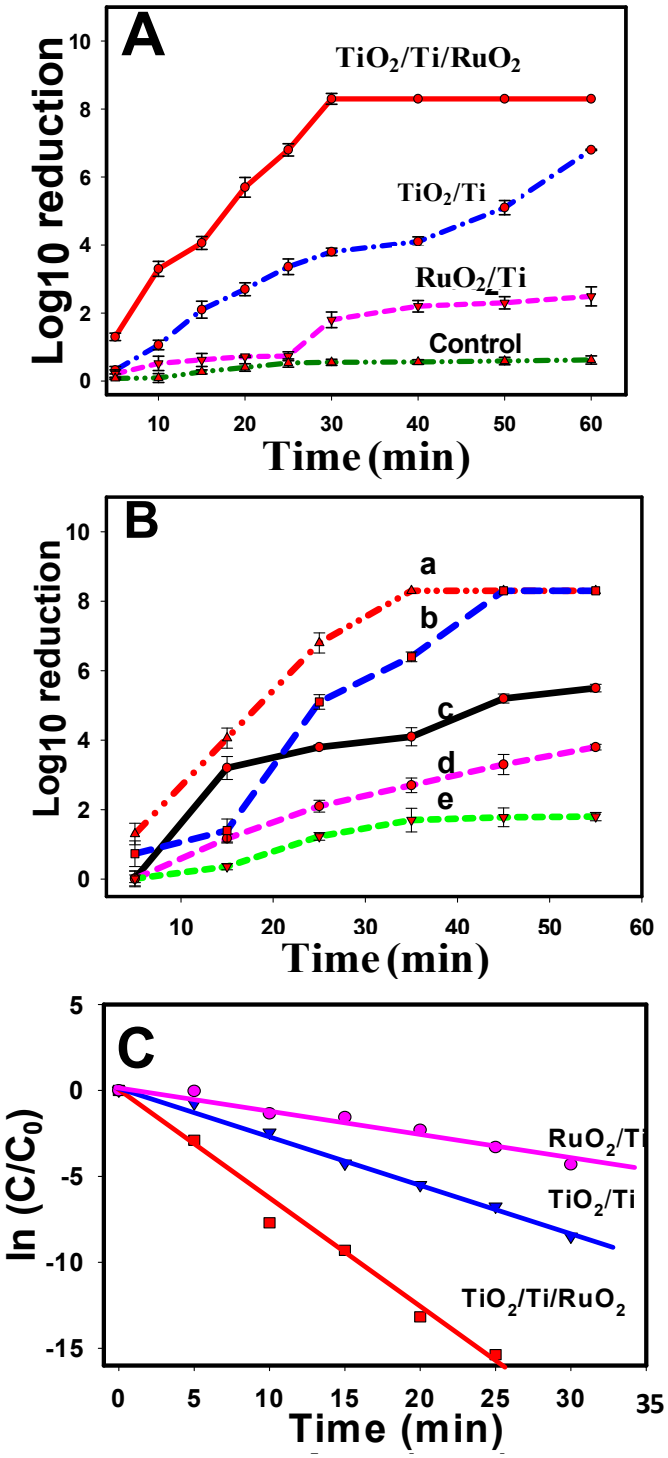

Figure 7. 2. (A) Culturable cell density reduction in logarithm of *E. coli* (initial count 2.3 x 10^8 CFU / mL or Log CFU /mL of 8.3) through the spread plate method on nutrient agar plate through bifunctional (TiO_2/Ti/RuO_2), nanoporous titanium electrode (TiO_2/Ti), electrocatalyst (RuO_2/Ti), and control; (B) ROSs scavenger experiments in bifunctional inactivation system (initial bacterial concentration of logarithm 8.3 CFU/ mL): no scavenging chemicals (a), 10 mM of each sodium azide (b) mannitol (c), sodium pyruvate (d), sodium thiosulfate (e); (C)

Disinfection kinetics of *E. coli* on TiO_2/Ti/RuO_2, TiO_2/Ti, and RuO_2 under identical applied conditions. '*C'* is the concentration of the *E. coli* following the electrochemical treatment, and '*Co'* is the initial concentration of *E. coli* prior to treatment.

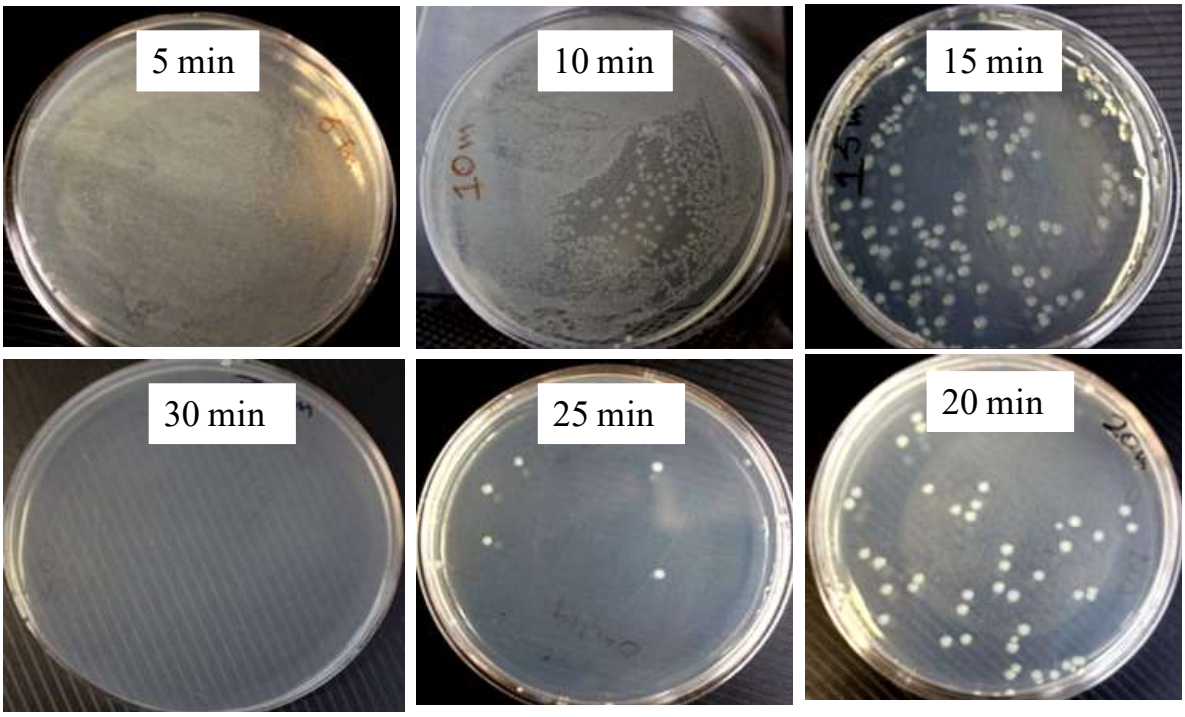

Figure 7. 3. Assessment of disinfection efficiency through spread plate method

bacterial removal within 20 min of treatment, as compared to an only 0.28 min^{-1} and 0.14 min^{-1} disinfection rate with the TiO_2/Ti and RuO_2/Ti electrodes (Figure 7.2C). The combinatory approach, which integrated the photocatalysts and electrocatalysts into a single electrode, demonstrated a significant improvement in performance in contrast to various disinfection strategies described in literature, in terms of time and energy consumption.[27-29] The mechanism behind the bacterial disinfection by TiO_2/Ti/RuO_2 was investigated through a series of reactive oxygen species (ROS) scavenging experiments (Figure 7.2B). Figure 7.2B depicts the ROS scavenging efficiencies of different known scavengers, which were assessed through a spread

plate method. A negligible bacterial log reduction was observed subsequent to the addition of 10 mM sodium thiosulfate followed by sodium pyruvate, mannitol, and sodium azide. It was observed that the bactericidal effect of nanoporous TiO_2/Ti/RuO_2 following the addition of scavenger chemicals was in the order of sodium thiosulfate < sodium pyruvate < mannitol < sodium azide. The reversal of the bacterial log reduction achieved by the bifunctional electrode through the addition of sodium thiosulfate, revealed that the major ROS species generated during the electrochemical treatment were hydroxyl radicals (•OH) and hydrogen peroxide (H_2O_2). Furthermore, there was increased bactericidal activity of the bifunctional electrode following the complete treatment with the addition of sodium pyruvate (3.8 log reduction) followed by mannitol (5.4 log reduction) and sodium azide (8.3 log reduction), which indicated that H_2O_2 was the primary ROS, followed by •OH and $^1O_2$ for bactericidal activity.[30]

7.3.3. Bacterial membrane integrity

Significant *E. coli* cell membrane damage during the bifunctional photoelectrochemical treatment was studied using LIVE/DEAD® BacLight™ stains. Among the two fluorescent dyes used for the stain, SYTO-9 stains only intact cell membrane whereas propidium iodide (PI) will stain only damaged cell membranes. As shown in Figure 7.4A, prior to the photoelectrochemical treatment almost all of the *E. coli* cells were stained with SYTO-9 (green fluorescence), which indicated intact cell membranes, which was also verified by SEM analysis (Figure 7.4E). Immediately following 5 min of electrochemical treatment, a dramatic increase of PI stained (red fluorescence) bacterial cells was observed (Figure 7.4*B*). The PI stained red fluorescent bacteria increased steeply following 30 min of treatment, as shown in Figure 7.4C, which indicated significant damage to the bacterial cell membranes, which was also supported by SEM analysis,

as shown in Figure 7.4F. The decreasing live biovolume vs increasing dead biovolume through the continuous photoelectrochemical treatment as calculated by PHLIP analysis is shown in

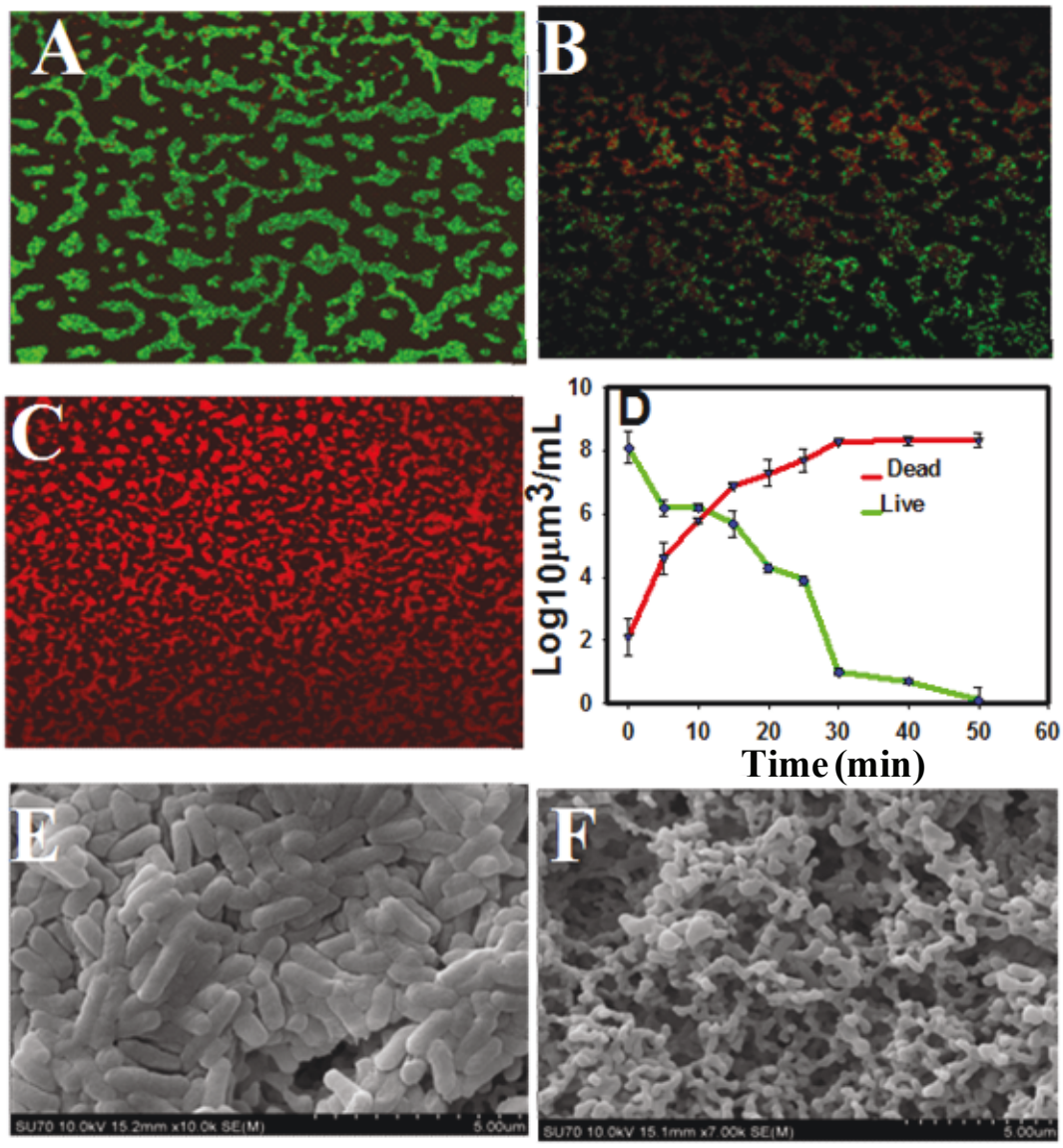

Figure 7. 4. Bacterial cell viability estimation using LIVE/DEAD® BacLight™ stain through confocal scanning laser microscopy during bifunctional treatment: A) 0 min, B) after 5 min, C) after 30 min, D) Biovolume count with PHLIP analysis; SEM analysis of *E. coli*: E) 0 min, F) after 30 min of treatment.

Figure 7.4D. The LIVE/DEAD® BacLight™ stains and biovolume calculation suggested that a certain number of live bacteria were present even after 30 min of treatment, which was shown to be negative by the spread plate method. We assumed that there were two reasons behind the presence of live bacteria even after staining with LIVE/DEAD® BacLight™ stains. Initially, the limit of detection (LOD) through the spread plate method is < 100 CFU/mL for 1/10 dilutions;[31] hence, it might be due to lower number of bacteria than the threshold that was present in the sample, or due to a bacterial survival strategy, which isolated them from the stressed environment through the transformation to a viable but non-culturable (VBNC) state.[32] We further investigated if any live bacteria remained through most probable number (MPN), by suspending sample in a nutrient broth with and without presence of 30 mM sodium pyruvate.

7.3.4. Most probable number (MPN) determination

The MPN was calculated for the samples (after showing a negative result through the spread plate method) at 30-70 min of treatment, as shown in Table 1. Two sets of 96 well microtiter plates; one set of nutrient broth, and another set of nutrient broth with addition of 30 mM of sodium pyruvate for resuscitation; were used to determine bacterial cell viability. As seen in Table 1, average MPN has been calculated from triplicate sets of positive number microtiter plates prior to and following resuscitation. A significant variation in MPN numbers was observed following resuscitation with 30 mM sodium pyruvate (Figure 7.5). The supplementation of the nutrient broth with 30 mM sodium pyruvate in the microtiter plate yielded a positive reaction by resuscitating H_2O_2-damaged *E. coli* cell membranes.[33,34] An MPN of 210 was observed following 30 min of treatment, after which there was a significant decline to 8.6 after 40 min of treatment. Almost nil MPN was observed after 50 min of electrochemical treatment, whereas 5.4

MPN was observed after resuscitation in the same sample. No single positive number was observed for resuscitation of the sample after

Table 7.1. Resuscitation of *E. coli* from the VBNC state during bifunctional treatment as observed in 96 well microtiter plates and average MPN calculation per 100 mL

Time of treatment (minutes)	Nutrient broth (well)		Nutrient broth enriched with 30 mM sodium pyruvate (well)	
	Average MPN	Standard error (n=3)	Average MPN	Standard error (n=3)
30	210	6.3	480	6.3
40	8.6	4.1	18.2	4.1
50	0.66	-	5.4	1.6
60	0	-	0	-
70	0	-	0	-

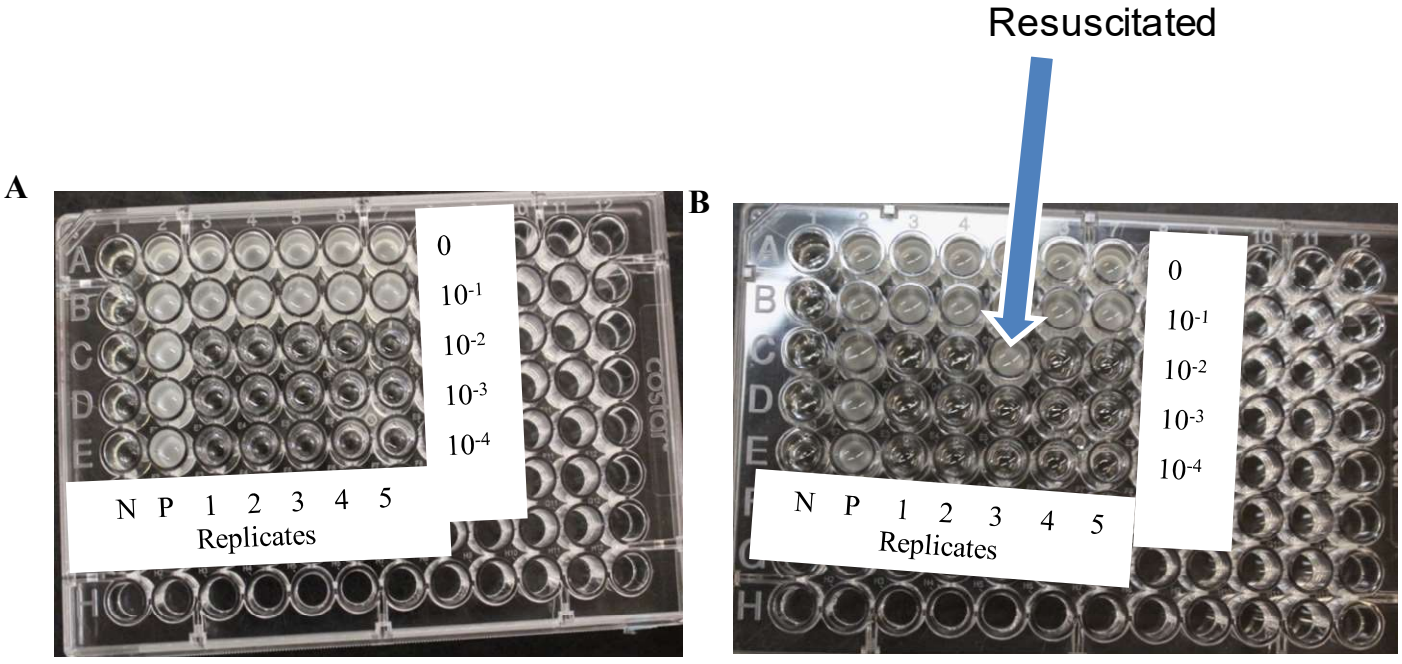

Figure 7. 5. MPN assay through microtiter plate following 30 min of binfunctional treatment for 2.3 X 10^8 CFU mL^{-1} *E. coli*: A) nutrient broth; B) nutrient broth supplemented with 30 mM sodium pyruvate.

60 min of electrochemical treatment. Our results indicated that the VBNC strategy of *E. coli* during photoelectrochemical treatment did not exist for a longer time. Complete bacterial, including VBNC, removal was achieved following 60 min of electrochemical treatment.

7.3.5. Assessment of biomolecule leakage during bifunctional treatment

The damage to cell membranes during the photoelectrochemical treatment was investigated via SEM and confocal laser microscopy. Heavy damage to cell membranes was observed during the course of the photoelectrochemical treatment as shown in Fig. 3. Moreover, the impact of bacterial cell destruction was studied through the leakage of various biomolecules. This biomolecule leakage was determined based on the total organic carbon (TOC) content and protein concentrations. The TOC change during the photoelectrochemical treatment was measured. As shown in Fig. 4A, the TOC content was sharply increased at the onset of the treatment, which continuously increased until the 30-minute treatment. Thereafter, a steady concentration was maintained until 40 min, which was then observed to sharply decrease after 50 min of the treatment, which indicated the onset of the mineralization of the metabolites that were released from the damaged bacterial cells, due to the photoelectrochemical treatment process.[35,36] Protein leakage during the course of the bifunctional treatment was determined by measuring the protein concentration from extracted bacterial samples at different time intervals through Nanodrops,[37,38] as depicted in Figure 7.6B. The figure shows a major drop in protein concentration following 20 min of treatment, which further decreased during the course of the bifunctional treatment.

A bacterial metabolomics study was conducted through 1D ^{1}H (proton) NMR to understand the detailed mechanism of *E. coli* inactivation during the bifunctional treatment. The NMR spectrum was used proton signals to elucidate structural characteristics of specific

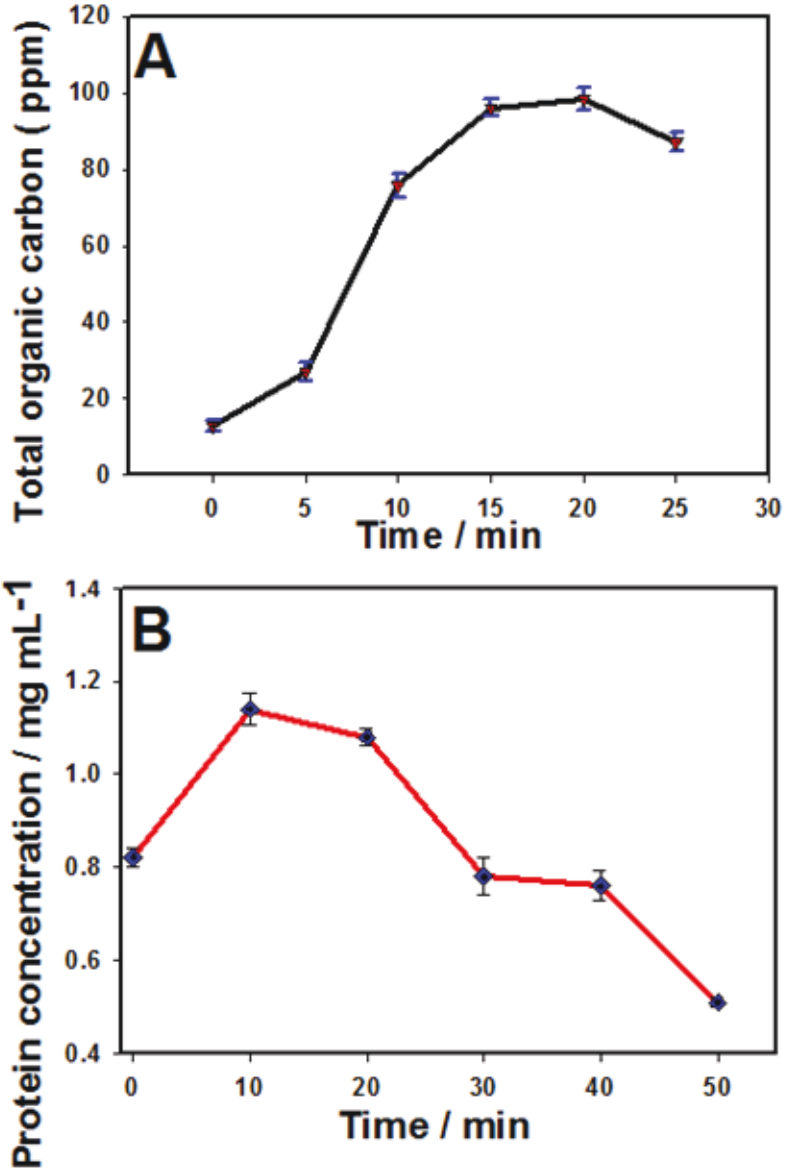

Figure 7. 6. Biomolecule leakage during the bifunctional treatment: A) Total organic carbon (TOC) determination; B) Protein concentration determination.

metabolites through chemical shifts. For this study, we analysed the NMR spectra of samples for different time intervals during the electrochemical treatment, as shown in Figure 7.7. We further analyzed the NMR spectra (assigned chemical shifts)

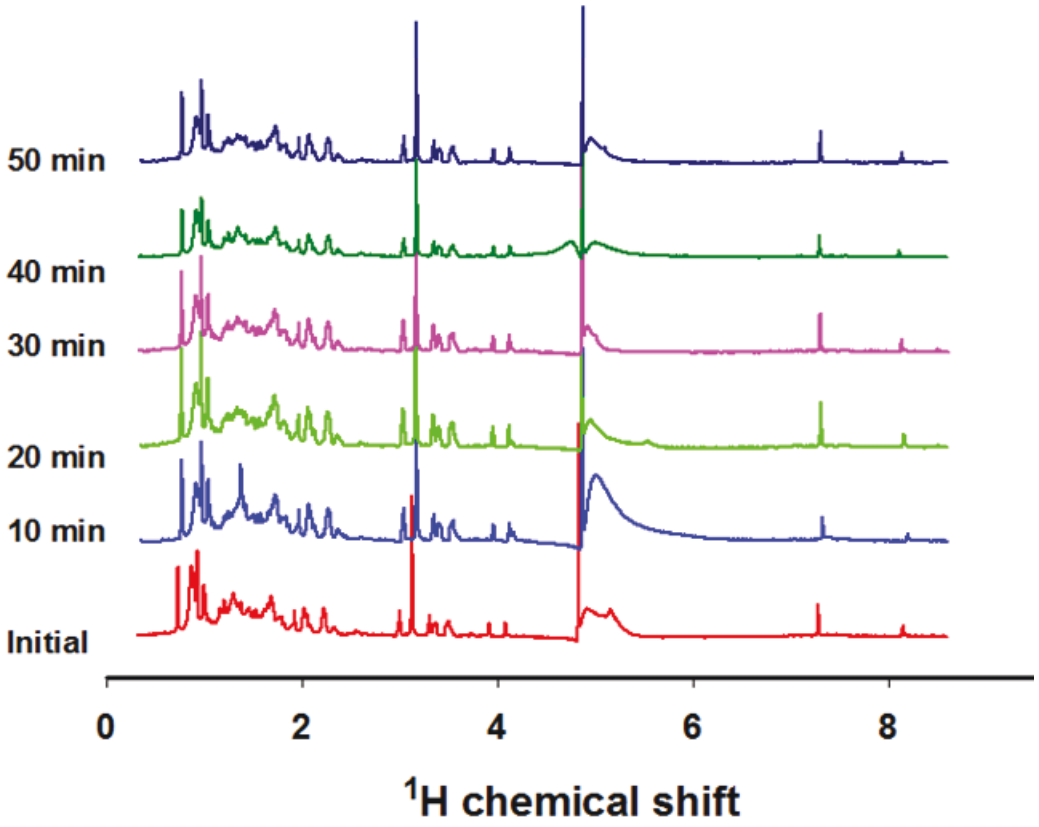

Figure 7. 7. ^{1}H NMR spectra of metabolomes present in sample at different time intervals.

for the sample to illustrate spectral variability through principle component analysis (PCA), as shown in Figure 7.8A, the major factors F1 and F2 contributed almost 63.02%, followed by the minor factors F2 and F3 (Figure 7.8B), which contributed only 41.62% of the total variability among the spectra collected from the electrochemically treated samples. Significant spectral changes were observed from the onset of treatment, to 10 min, and following the treatment time, which was verified by the correlation association between the spectra of treated samples, as presented in Table 2.

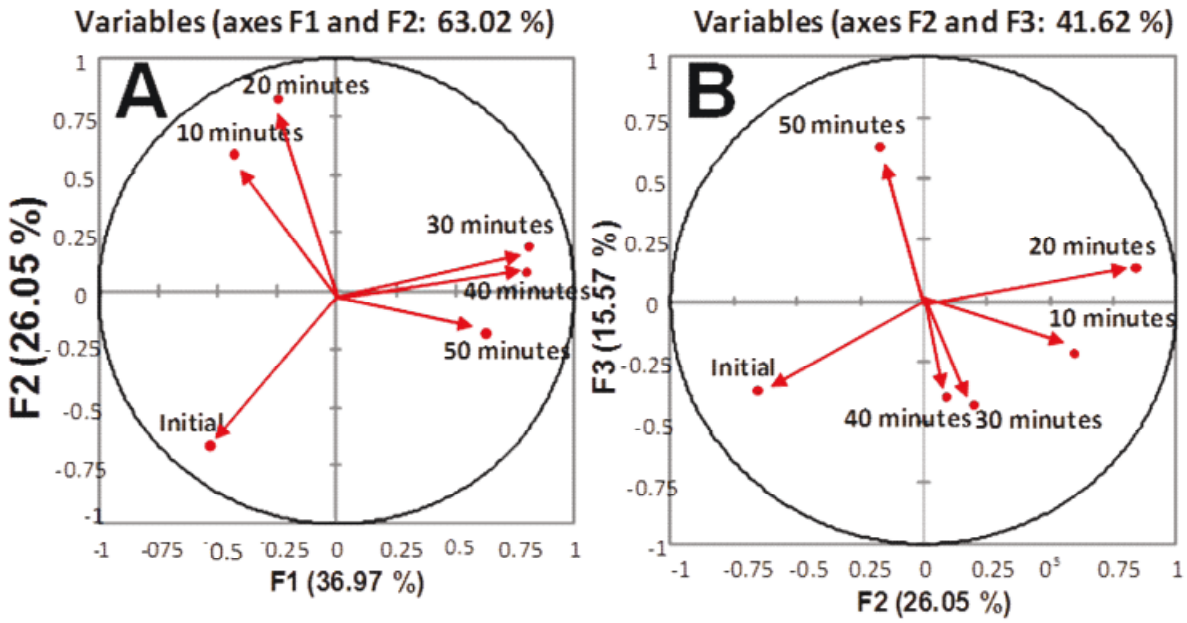

Figure 7. 8. Principle Component Analysis (PCA) of major discriminated factor (F1:F2; A and F2:F3; B) based on ^{1}H NMR spectrum of initial (0 min) followed by 10, 20, 30, 40 and 50 min treated sample of *E. coli* metabolites derived through XLSTAT.

Table 7.2. Correlation matrix (Pearson (n)) calculated during PCA analysis from ^{1}H NMR spectrum obtained through different treated *E. coli* samples.

Variables	Initial	10 minutes	20 minutes	30 minutes	40 minutes	50 minutes
Initial	1	-0.037	-0.363	-0.439	-0.245	-0.340
10 minutes	-0.037	1	0.368	-0.197	-0.144	-0.299
20 minutes	-0.363	0.368	1	-0.109	-0.123	-0.248
30 minutes	-0.439	-0.197	-0.109	1	0.668	0.162
40 minutes	-0.245	-0.144	-0.123	0.668	1	0.325
50 minutes	-0.340	-0.299	-0.248	0.162	0.325	1

Each metabolite possesses a unique ^{1}H NMR spectroscopic fingerprint with a spectral intensity that relies on concentrations and intermolecular interactions.[39,40] To investigate *E. coli* metabolomics, we further explored these NMR spectra for possible metabolic signatures that might have been released during the electrochemical treatment. All of the assigned spectral peaks were processed through the 1D NMR search tool of the ECMDB database. A total of 106 metabolites (Figure 7.9) were determined for the six collected samples. As can be seen in Figure 7.9, a total of 38 primary metabolites were determined from the initial sample, and all other metabolites were altered in accordance with the treatment time. Major metabolite loss was observed following 30 min of electrochemical treatment, as 17 vital metabolites were not detected in the sample. As the result of lacking major metabolites, the majority of *E. coli* cells lost their ability to grow in culture medium after 30 min of electrochemical treatment, which was also confirmed by their inability to grow in NA media through the spread plate method. We noticed a series of metabolic changes in *E. coli* that it employs to adapt to a stressed environment. Accumulation of glycogen; reserved carbohydrates, o-phosphoserine; an important component for glutathione synthesis (an antioxidant) and pseudouridine following 10 min of electrochemical treatment pointed toward the oxidative stress response of *E. coli*.[41-43] Major metabolite loss was observed following 30 min of electrochemical treatment, as 17 vital metabolites were not detected in the sample. As the result of lacking major metabolites, the majority of *E. coli* cells lost their ability to grow in culture medium after 30 min of electrochemical treatment, which was also confirmed by their inability to grow in NA media through the spread plate method. Vital metabolic pathways i.e tricarboxylic acid (TCA) cycle, DNA synthesis, peptidoglycan layer, and the outer and inner membranes of *E. coli* were virtually

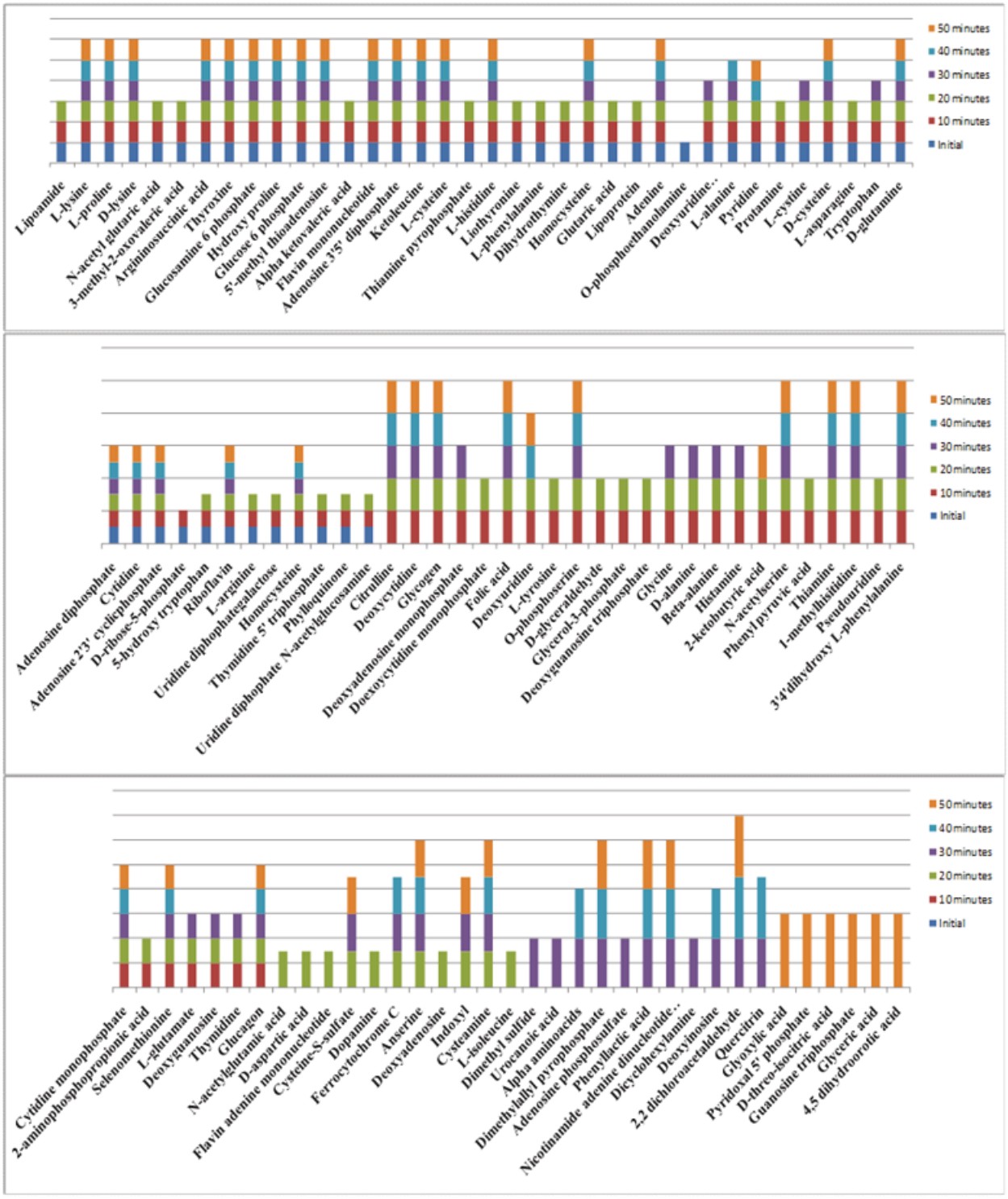

Figure 7. 9. Plot of metabolites identified through ^{1}H NMR analysis during 0, 10, 20, 30, 40, and 50 min following treatment of *E. coli* sample (based on ECMDB data base).

paralyzed due the lack of key metabolites. The lack of key metabolites such as lipoamide, thiamine pyrophosphate, and flavin adenine dinucleotide (as a prosthetic group of pyruvate dehydrogenase complex in the TCA cycle); thymidin-5-triphosphate (as a precursor of DNA synthesis), uridine diphosphate galactose, and uridine diphosphate N-acetlylglucosamine (as a precursor for the synthesis of lipopolysaccharide and peptidoglycan); lipoproteins (as major constituents of both the outer and inner membranes), might responsible to induce the state of cell death in *E. coli*.[44-47]

7.4. Conclusion

An innovative bifunctional strategy for microbial disinfection was investigated by utilizing the synergistic enhancement of the integrated nanoporous TiO_2 photocatalyst and the nanostructured RuO_2 electrocatalyst. The prepared novel bifunctional electrode exhibited a rapid (100%) bacterial log reduction within a 30-minute photoelectrochemical treatment, with a disinfection rate of 0.62 min^{-1} (R^2 = 0.986) in comparison to ~45% (disinfection rate - 0.28 min^{-1}) and 20.6% (0.14 min^{-1}) bacterial log reduction using the nanoporous TiO_2 and RuO_2 electrodes, respectively. Further, we studied any bacterial survival strategy that might have been adopted during the photoelectrochemical treatment through an *E. coli* resuscitation experiment, and LIVE/DEAD staining suggested that no VBNC bacteria survived following 50 min of treatment. The bifunctional electrode exhibited excellent activity over existing electrodes for bacterial disinfection in terms of energy consumption and bactericidal efficiency. In this study, only 1.2 V of energy was required to drive the generation of ROS on the surface of the nanoporous TiO_2/Ti/RuO_2 bifunctional electrode, which is so low that a renewable energy source may be used to power the system.

References

1. Montgomery, M.A.; Elimelech, M. Water and sanitation in developing countries: including health in the equation. *Environ. Sci. Technol.* **2007,** *41* (1), 17-24.

2. Catley-Carlson, M. Water supply: The emptying well. *Nature* **2017,** 542 (7642), 412-413.

3. Lewis, S.R.; Datta, S.; Gui, M.; Coker, E.L.; Huggins, F.E.; Daunert, S.; Bachas, L.; Bhattacharyya, D. Reactive nanostructured membranes for water purification. *Proc. Natl. Acad. Sci.* **2011,** *108* (21), 8577-8582.

4. Mitch, W.A.; Gerecke, A.C.; Sedlak, D.L. A N-nitrosodimethylamine (NDMA) precursor analysis for chlorination of water and wastewater. *Water Res.* **2003,** *37* (15), 3733-3741.

5. Westerhoff, P.; Yoon, Y.; Snyder, S.; Wert, E. Fate of endocrine-disruptor, pharmaceutical, and personal care product chemicals during simulated drinking water treatment processes. *Environ. Sci. Technol.* **2005,** *39* (17), 6649-6663.

6. Lee, W.; Westerhoff, P.; Croué, J.P. Dissolved organic nitrogen as a precursor for chloroform, dichloroacetonitrile, N-nitrosodimethylamine, and trichloronitromethane. *Environ. Sci. Technol.* **2007,** *41* (15), 5485-5490.

7. Tang, X.; Wu, Q.Y.; Du, Y.; Yang, Y.; Hu, H.Y. Anti-estrogenic activity formation potential assessment and precursor analysis in reclaimed water during chlorination. *Water Res.* **2014** 48, 490-497.

8. Sedlak, D.L.; Von Gunten, U. The chlorine dilemma. *Science* **2011,** *331* (6013), 42-43.

9. Guo, M.; Hu, H.; Bolton, J.R.; El-Din, M.G. Comparison of low-and medium-pressure ultraviolet lamps: Photoreactivation of Escherichia coli and total coliforms in secondary effluents of municipal wastewater treatment plants. *Water Res.* **2009,** *43* (3), 815-821.

10. Guo, M.; Huang, J.; Hu, H.; Liu, W.; Yang, J. UV inactivation and characteristics after photoreactivation of Escherichia coli with plasmid: health safety concern about UV disinfection. *Water Res.* **2012,** *46* (13), 4031-4036.

11. Martinez-Huitle, C.A.; Ferro, S. Electrochemical oxidation of organic pollutants for the wastewater treatment: direct and indirect processes. *Chem. Soc. Rev.* **2006,** *35* (12), 1324-1340.

12. Malato, S.; Fernández-Ibáñez, P.; Maldonado, M.I.; Blanco, J.; Gernjak, W. Decontamination and disinfection of water by solar photocatalysis: recent overview and trends. *Catal. Today* **2009,** *147* (1), 1-59.

13. Xu, T.; Cai, Y.; O'Shea, K.E. Adsorption and photocatalyzed oxidation of methylated arsenic species in TiO_2 suspensions. *Environ. Sci. Technol.* **2007,** *41* (15), 5471-5477.

14. Shannon, M.A.; Bohn, P.W.; Elimelech, M.; Georgiadis, J.G.; Marinas, B.J.; Mayes, A.M. Science and technology for water purification in the coming decades. *Nature* **2008,** *452* (7185), 301-310.

15. Liu, C.; Xie, X.; Zhao, W.; Yao, J.; Kong, D.; Boehm, A.B.; Cui, Y. Static Electricity Powered Copper Oxide Nanowire Microbicidal Electroporation for Water Disinfection. *Nano Lett.* **2014,** *14* (10), 5603-5608.

16. Liu, C.; Kong, D.; Hsu, P.C.; Yuan, H.; Lee, H.W.; Liu, Y.; Wang, H.; Wang, S.; Yan, K.; Lin, D.; Maraccini, P.A.; Parker, K.M.; Boehm, A.B.;, Cui Y. Rapid water disinfection using vertically aligned MoS_2 nanofilms and visible light. *Nat. Nano.* **2016,** *11* (12), 1098-1104.

17. Asmussen, R.M.; Tian, M.; Chen, A. A new approach to wastewater remediation based on bifunctional electrodes. *Environ. Sci. Technol.* **2009,** *43* (13), 5100-5105.

18. Chen, X.; Mao, S.S. Titanium dioxide nanomaterials: synthesis, properties, modifications, and applications. *Chem. Rev.* **2007,** *107* (7), 2891-2959.

19. Chang, X.; Thind, S.S.; Tian, M.; Hossain, M.M.; Chen, A. Significant enhancement of the photoelectrochemical activity of nanoporous TiO_2 for environmental applications. *Electrochim. Acta* **2015,** 173, 728-735.

20. Greenberg, A.E.; Clesceri, L.S.; Eaton, A.D. Estimation of bacterial density. *Standard methods for the examination of water and wastewater 18th ed Washington, DC:* American Public Health Association. **1992,** pp 9-49.

21. Mueller, L.N.; De Brouwer, J.F.; Almeida, J.S.; Stal, L.J.; Xavier, J.B. Analysis of a marine phototrophic biofilm by confocal laser scanning microscopy using the new image quantification software PHLIP. *BMC Ecol.* **2006,** *6* (1), 1.

22. Golding, C.G.; Lamboo, L.L.; Beniac, D.R.; Booth, T.F. The scanning electron microscope in microbiology and diagnosis of infectious disease. *Sci. Rep.* **2016,** *6*, 26516.

23. Fischer, E.R.; Hansen, B.T.; Nair, V.; Hoyt, F.H.; Dorward, D.W. Scanning Electron Microscopy. *Curr. Protoc. Microbiol.* **2012,** Chapter unit 2B.

24. Guo, A.C.; Jewison, T.; Wilson, M.; Liu, Y.; Knox, C.; Djoumbou, Y.; Lo, P.; Mandal, R.; Krishnamurthy, R.; Wishart, D.S. ECMDB: the *E. coli* Metabolome Database. *Nucleic Acid Res.* **2013,** *41* (D1), D625-D630.

25. Sajed, T.; Marcu, A.; Ramirez, M.; Pon, A.; Guo, A.C.; Knox, C.; Wilson, M.; Grant, J.R.; Djoumbou, Y.; Wishart, D.S. ECMDB 2.0: A richer resource for understanding the biochemistry of *E. coli*. *Nucleic Acid Res.* **2016,** *44* (D1), D495-D501.

26. Caspi, R.; Billington, R.; Ferrer, L.; Foerster, H.; Fulcher, C.A.; Keseler, I.M.; Kothari, A.; Krummenacker, M.; Latendresse, M.; Mueller, L.A. The MetaCyc database of metabolic pathways and enzymes and the bioCyc collection of pathway/genome databases. *Nucleic Acid Res.* **2016,** *44* (D1), D471-D480.

27. Jia, Y.; Zhan, S.; Ma, S.; Zhou, Q. Fabrication of TiO_2-Bi_2WO_6 binanosheet for enhanced solar photocatalytic disinfection of E. coli: insights on the mechanism. *ACS Appl. Mater. Interfaces* **2016,** *8* (11), 6841-6851.

28. Sun, H.; Li, G.; Nie, X.; Shi, H.; Wong, P.K.; Zhao, H.; An, T. Systematic approach to in-depth understanding of photoelectrocatalytic bacterial inactivation mechanisms by tracking the decomposed building blocks. *Environ. Sci. Technol.* **2014,** *48* (16), 9412-9419.

29. Qi, X.; Wang, T.; Long, Y.; Ni, J. Synergetic antibacterial activity of reduced graphene oxide and boron doped diamond anode in three dimensional electrochemical oxidation system. *Sci. Rep.* **2015,** *5*, 10388.

30. Sun, H.; Li, G.; Nie, X.; Shi, H.; Wong, P.K.; Zhao, H.; An, T. Systematic approach to in-depth understanding of photoelectrocatalytic bacterial inactivation mechanisms by tracking the decomposed building blocks. *Environ. Sci. Technol.* **2014,** *48* (16), 9412-9419.

31. Sutton, S. Accuracy of plate counts. *J. Validation Technol.* **2011,** *17* (3), 42.

32. Zhao, F.; Bi, X.; Hao, Y.; Liao, X. Induction of viable but nonculturable Escherichia coli O157: H7 by high pressure CO_2 and its characteristics. *PloS one* **2013,** *8* (4), 62388.

33. McDonald, L.C.; Hackney, C.R.; Ray, B. Enhanced recovery of injured *Escherichia coli* by compounds that degrade hydrogen peroxide or block its formation. *Appl. Environ. Microbiol.* **1983,** *45* (2), 360-365.

34. Calabrese, J.P.; Bissonnette, G.K. Improved detection of acid mine water stressed coliform bacteria on media containing catalase and sodium pyruvate. *Can. J. Microbiol.* **1990,** *36* (8), 544-550.

35. Jacoby, W.A.; Maness, P.C.; Wolfrum, E.J.; Blake, D.M.; Fennell, J.A. Mineralization of bacterial cell mass on a photocatalytic surface in air. *Environ. Sci. Technol.* **1998,** *32* (17), 2650-2653.

36. Sun, H.; Li, G.; Nie, X.; Shi, H.; Wong, P.K.; Zhao, H.; An, T. Systematic approach to in-depth understanding of photoelectrocatalytic bacterial inactivation mechanisms by tracking the decomposed building blocks. *Environ. Sci. Technol.* **2014,** *48* (16), 9412-9419.

37. Cox, J.; Hein, M.Y.; Luber, C.A.; Paron, I.; Nagaraj, N.; Mann, M. Accurate proteome-wide label-free quantification by delayed normalization and maximal peptide ratio extraction, termed MaxLFQ. *Mol. Cell Proteomics* **2014,** *13* (9), 2513-2526.

38. Skog, J.; Würdinger, T.; Van Rijn, S.; Meijer, D.H.; Gainche, L.; Curry, W.T.; Carter, B.S.; Krichevsky, A.M.; Breakefield, X.O. Glioblastoma microvesicles transport RNA and

proteins that promote tumour growth and provide diagnostic biomarkers. *Nat. Cell Biol.* **2008,** *10* (12), 1470-1476.

39. Nicholson, J.K.; Connelly, J.; Lindon, J.C.; Holmes, E. Metabonomics: a platform for studying drug toxicity and gene function. *Nat. Rev. Drug Discov.* **2002,** *1* (2), 153-161.

40. Nicholson, J.K.; Holmes, E.; Wilson, I.D. Gut microorganisms, mammalian metabolism and personalized health care. *Nat. Rev. Microbiol.* **2005,** *3* (5), 431-438.

41. Ho, C.L.; Saito, K. Molecular biology of the plastidic phosphorylated serine biosynthetic pathway in Arabidopsis thaliana. *Amino acids* **2001,** 20 (3), 243-259.

42. Suzuki, E.; Ohkawa, H.; Moriya, K.; Matsubara, T.; Nagaike, Y.; Iwasaki, I.; Fujiwara, S.; Tsuzuki, M.; Nakamura, Y. Carbohydrate metabolism in mutants of the cyanobacterium Synechococcus elongatus PCC 7942 defective in glycogen synthesis. *Appl. Environ. Microbiol.* **2010,** *76* (10), 3153-3159.

43. Singh, H.; Appukuttan, D.; Lim, S. Hsp20, a small heat shock protein of deinococcus radiodurans, confers tolerance to hydrogen peroxide in *Escherichia coli*. *J. Microbiol. Biotechnol.* **2014,** *24* (8), 1118-1122.

44. Osborn, M.J.; Rosen, S.M.; Rothfield, L.; Horecker, B.L. Biosynthesis of bacterial lipopolysaccharide, I. Enzymatic incorporation of galactose in a mutant strain of Salmonella. *Proc. Natl. Acad. Sci.* **1962,** *48* (10), 1831-1838.

45. Emiola, A.; George, J.; Andrews, S.S. A complete pathway model for lipid A biosynthesis in Escherichia coli. *PloS one* **2015,** *10* (4), e0121216.

46. Cummings, D.J.; Mondale, L. Thymineless death in Escherichia coli: strain specificity. *J. Bacteriol.* **1967,** 93 (6), 1917-1924.

47. Ruiz, N.; Kahne, D.; Silhavy, T.J. Advances in understanding bacterial outer-membrane biogenesis. *Nat. Rev. Microbiol.* **2006***,* 4 (1), 57-66.

Chapter 8: Conclusion and Future work

8.1 Conclusion

The primary aim of this thesis was to investigate new and efficient nanomaterials based electrochemical methods for bioanalysis and bacterial disinfection. In this work, we utilized mainly carbon-based nanomaterials and composites for sensor/biosensor purposes, and TiO_2 nanotubes/RuO_2 for bacterial disinfection purposes. Carbon-based nanomaterials and composites were employed in the design of highly sensitive electrochemical sensors for the detection of biologically and pharmaceutically important compounds. Carbon and its derivatives possess excellent electrocatalytic properties for modified sensors, such as enhanced detection sensitivity, electrocatalytic effects, high conductivity, and reduced fouling. These superior attributes endow SWCNTs, rGO, and their nanocomposites (SWCNT-rGO) with significant advantages for enhanced various sensing and biosensing applications. Among the carbon based nanomaterials tested in this study, SWCNT-rGO nanocomposites were shown to be an excellent platform for incorporation into the core architectures of future sensor/biosensor designs. Carbon nanomaterials and nanohybrids thereof may play a critical role in the future development of advanced electrochemically based point of care (POC) diagnostics. Bacterial contamination constitutes one of the major problems in the distribution of potable water. Due to their green nature, electrochemical methods are attracting tremendous attention for water disinfection. We have utilized a novel bifunctional approach which rapidly and efficiently remove bacterial pathogens from water. Here, we utilized the synergistic effects of photocatalysts (TiO_2 nanotubes array) and electrocatalysts (RuO_2), which were combined in a single electrode.

In Chapter 4, we developed the simple one step simultaneous reduction and deposition of reduced graphene oxide on the electrode surface. A very sensitive graphene based

electrochemical sensor for acetaminophen detection was successfully carried out in this chapter. We showed a very low detection limit and wide linear detection range to cover acetaminophen induced hepatotoxicity. Furthermore, we successfully detected acetaminophen in a serum sample with a very high recovery rate.

In Chapter 5, we evaluated a reduced graphene oxide (rGO) based electrochemical sensor for the detection of individual valacyclovir, and simultaneous detection with acetaminophen. In this study, we explored various parameters of graphene materials i.e. optimized concentration and deposition cycle for optimal catalytic activity on acetaminophen and valacyclovir. We successfully developed a highly sensitive, stable, and reproducible electrochemical sensor. The optimized rGO/GCE sensor demonstrated very high electrocatalytic activity for the simultaneous oxidation of acetaminophen and valacyclovir. The developed rGO/GCE sensor revealed an extremely low detection limit with excellent selectivity for isolated valacyclovir and its combination with acetaminophen, which had been reported in the literature. Due to very low fabrication costs, the developed sensor has great potential for use in the pharmaceutical industry and hospital laboratories for quality control and clinical drug monitoring.

In Chapter 6, we developed a novel facile and effective enzyme entrapment platform using a special cationic polymer, poly (2-(dimethylamino) ethyl methacrylate) (MADQUAT) on a single-walled carbon nanotube and reduced graphene oxide (SWCNT-rGO) nanohybrid thin film. In this study, we developed a new strategy for the immobilization of enzymes utilizing strong electrostatic affinity between MADQUAT as cationic polymer and negatively charged biomolecules. The entrapped ADH was assessed for any conformational changes through secondary structure analysis, which revealed that no structural changes occurred in comparison to the free ADH. The significant synergistic enhancement of the SWCNT-rGO nanohybrid was confirmed, and the ADH entrapped by MADQUAT showed high activity for the detection of

ethanol. The developed ADH-SWCNT-rGO biosensor exhibited high sensitivity with a remarkably low detection limit of 0.16 μM. The wide linear detection range, high stability, and selectivity with a low K_m value make this biosensor a promising candidate for ethanol sensing in both clinical and environmental settings. The SWCNT-rGO nanohybrid and MADQUAT employed in this study not only provided an excellent platform for ethanol detection, but will also have significant impacts in the field, toward the development of high performance enzymatic biosensors for food, clinical, and environmental applications.

In Chapter 7, we studied a novel electrochemical bifunctional approach for microbial disinfection utilizing the synergistic enhancement of photocatalysts (nanoporous TiO_2) and electrocatalysts (RuO_2) in a single platform. The anodic potential bias applied through the bifunctional electrode efficiently suppressed electron-hole recombination on the photocatalysts, while catalyzing the influx of ROS production. In addition, the anodic potential bias enhanced the generation of hydroxyl radicals at the electrocatalyst surface for water splitting, which significantly assisted with improving the performance of the bifunctional electrode. The bifunctional electrode exhibited a rapid (100%) bacterial log reduction within 30 min of electrochemical treatment in comparison to~ 45% and 20.6% bacterial log reduction through nanoporous TiO_2 and RuO_2 electrodes, respectively. We further studied any bacterial survival strategies and metabolomic analysis during the bifunctional treatment. The resuscitation experiment conducted in this study suggested that no VBNC bacteria survived for longer than the treatment exposure period (50 min of treatment). The metabolomic analysis conducted in this study further revealed that the bifunctional treatment significantly instigated the leakage of major metabolites subsequent to 30 min of treatment, and induced inevitable mass bacterial death due to the lack of key metabolites to drive vital biochemical pathways. Protein leakage and TOC

mineralization, following 30 min of treatment, further suggested the promising performance of the bifunctional (TiO_2-Ti-RuO_2) electrode for bacterial disinfection. The nanoporous TiO_2-Ti-RuO_2 bifunctional electrode exhibited excellent activity over existing electrodes for bacterial disinfection in terms of energy consumption and bactericidal time. In this study, only 1.2 V of energy was required to drive the generation of ROS on the surface of the nanoporous TiO_2-Ti-RuO_2 bifunctional electrode, which was sufficiently low that a renewable energy source could power the system.

The electrochemical sensors/biosensors proposed in this thesis have great potential to be used in pharmaceutical quality control, clinical drug monitoring, and bioavailability testing for therapeutic purposes. The successful development of highly sensitive electrochemical approaches for analytical and water treatment devices utilizing a variety of nanomaterials, have desirable manufacturing qualities, such as low cost and quick archetype turnaround times. Furthermore, novel approaches have been utilized for the electrochemical biosensing of ethanol and water treatment. Novel approaches, such as alcohol dehydrogenase entrapment via cationic polymers on a nanohybrid substrate and bifunctional bacterial catalysis for water disinfection, have strong potential as new electrochemical application paradigms.

8.2 Future Work

In this thesis, we developed the facile preparation and deposition of reduced graphene oxide (rGO) on an electrode surface through electrochemical reduction. The developed electrochemical sensors were utilized for the sensitive detection of acetaminophen, valacyclovir, and combinations thereof. These pharmaceutical drugs have great market value and huge investments in research and development. We have shown here a wide linear range and very low detection limit of acetaminophen, valacyclovir, and their mixture. The further exploration of

nanomaterials or graphene based nanocomposite materials might assist in reducing the oxidation potential of both drugs toward the development of energy efficient electrochemical sensors. Graphene based electrochemical sensors also have great potential to be utilized for the detection of other clinically relevant biomolecules and biomarkers. In future, we intend to design these sensors for the electrocatalytic oxidation of other clinically relevant compounds.

Further exploring the potential of rGO for electrocatalytic activity, we have studied its nanocomposite behaviour with single walled carbon nanotubes (SWCNTs) on acetaminophen, valacyclovir and ethanol biosensing. We have studied biocompatibility behaviour of rGO-SWCNTs nanohybrid film and utilized this platform for the enzyme entrapment. Enzyme entrapment is one of the primary techniques for the fabrication of electrochemical biosensors; however, enzyme leakage and sluggish substrate-enzyme electron transfer are major drawbacks. A novel enzyme entrapment strategy utilizing cationic polymers has been utilized in this study for the successful development of an alcohol dehydrogenase based electrochemical biosensor. We employed alcohol dehydrogenase as model enzyme for entrapment, and used this biosensor for the detection of ethanol. In the future, we aim to use same entrapment strategy for variety of bioreceptor molecules for the sensitive detection of other disease biomarkers.

Electrochemical bacterial disinfection is an emerging green water purification method, while TiO_2 nanomaterials have been extensively utilized for photoelectrochemical catalysis. A novel bifunctional approach was used here for the efficient removal of bacteria from water. We utilized TiO_2 nanotubes as photocatalysts and RuO_2 as electrocatalysts in a single electrode system, for the successful and rapid removal of bacteria from water. We have studied the bacterial disinfection efficiency of bifunctional electrode for *E. coli*. Further exploration of bifunctinal catalysis is needed to study the disinfection efficiency on water borne pathogens. The

performance and efficiency of TiO_2 nanotube can be enhanced by reducing its band gap. It would be interesting to further explore the novel metal nanoparticles to dope with TiO_2 nanotube which can significantly reduce the TiO_2 band gap. Once the band gap of the TiO_2 nanotube is reduced, visible light may be used to activate the photocatalyst, thereby greatly reducing the power consumption of the system. Further explorations of highly active electrocatalysts as a component of bifunctional catalysis may assist with increasing its efficiency by enhancing ROS_s production. We also aim to investigate the effects of the electrochemical treatment on electrocatalysts to enhance their activity in bacterial disinfection.

List of publications from my PhD study

- Umasankar, Y., **Adhikari, B.R.**, Chen, A. (2017) Effective immobilization of alcohol dehydrogenase on carbon nanoscaffolds for ethanol biofuel cell. *Bioelectrochemistry*.118: 83-90.

- **Adhikari, B. R**., Schraft, H., and Chen, A. (2017) High-performance enzyme entrapment platform facilitated by a cationic polymer for the efficient electrochemical sensing of ethanol. *Analyst*.142: 2595-2602.

- **Adhikari, B. R.**, Govindhan, M., Schraft, H., and Chen, A. (2016) Simultaneous and sensitive detection of acetaminophen and valacyclovir based on two dimensional graphene nanosheets. *Journal of Electroanalytical Chemistry*. 780:241-248.

- Xie, G., Chang, X., **Adhikari, B.R**., Thind, S., and Chen, A. (2016**)** Photoelectrochemical degradation of acetaminophen and valacyclovir using nanoporous titanium dioxide. *Chinese Journal of Catalysis*. 37: 1062-1069.

- **Adhikari, B. R.**, Govindhan, M., and Chen, A. (2015) Carbon nanomaterials based electrochemical sensors/biosensors for the sensitive detection of pharmaceutical and biological compounds. *Sensors*. 15: 22490 - 22508.

- Govindhan, M.**,** Lafleur T., **Adhikari, B. R.**, and Chen, A. (2015) Electrochemical sensor based on carbon nanotubes for the simultaneous detection of phenolic pollutants. *Electroanalysis*. 27: 902 - 909.

- **Adhikari, B. R.,** Govindhan, M., and Chen, A. (2015) Sensitive detection of acetaminophen with graphene-based electrochemical sensor. *Electrochimica Acta.* 162: 198 - 204.

- Govindhan, M., **Adhikari, B. R.**, and Chen, A. (2014) Nanomaterials-based electrochemical detection of chemical contaminants. *RSC advances*. 4: 63741 - 63760.

- **Adhikari, B. R.**, Thind, S., Schraft, H., and Chen, A. (2017) Integrated bifunctional electrochemical approach for efficient bacterial disinfection. *Submitted.*

Conference presentations

- **Adhikari, B.R**, Schraft, H., Chen, A. (2016) Immobilization of alcohol dehydrogenase on carbon based nanohybrids for enhanced ethanol sensing. 99th Canadian Conference and Exhibition, Halifax, NS. June 5-9.
- **Adhikari, B.R**, Schraft, H., Chen, A. (2016) Graphene-based nanocomposites for the sensitive electrochemical detection of biomedical compounds. 99th Canadian Conference and Exhibition, Halifax, NS (Ryan award presentation). June 5-9.
- **Adhikari, B.R**, Schraft, H., Chen, A. (2016) Design of Graphene nanohybrid-based novel biosensing platform for enhanced electrochemical sensing of ethanol. ECS spring meeting 2016, Saint Mary's University Halifax, NS, Canada. June 10.
- **2-Minute Thesis Presentation** on 'Translation of academic research to the real world application'- Analytical Chemistry Division, Chemical Institute of Canada- AGM 2016, Halifax, NS. June 9.
- **Adhikari, B.R**, Maduraiveeran, G., Chen, A. (2016) Graphen-based nanocomposites for the sensitive electrochemical detection of biomedical compounds. Research and Innovation week, Lakehead University. March 7.
- **Adhikari, B.R**, Maduraiveeran, G., Chen, A. (2015) Graphene-based electrochemical sensor for the sensitive detection of analgesic and antiviral drugs. 98th Canadian Conference and Exhibition, Ottawa, ON. June 9-13.
- **Adhikari, B.R**, Chen, A. (2015). Nanomaterials-based electrochemical sensors/biosensors for medical and environmental applications. 2nd International Conference on Infectious Diseases and Nanomedicine (ICIDN), Kathmandu, Nepal. December 15-18.
- Chen, A., Maduraiveeran, G., **Adhikari, B.R**., Ahmadalinezhad, A., Shah, B. (2015) Nanomaterials-based electrochemical biosensors for medical applications. The 15th Topical Meeting of the International Society of Electrochemistry, Niagara Falls, ON, Canada. April 27 – 30
- **Adhikari, B.R**, Chen, A. (2014) Graphene-Based Electrochemical Sensor for the sensitive detection of acetaminophen. Graduate Student Conference, Research and Innovation week, Lakehead University. March 3.

Honours and awards/scholarships during my PhD study

- **Ryan Award in honor of Douglas E. Ryan**, Analytical Chemistry Division, Chemical Institute of Canada, 2016
- **High Output and Publication Excellence** (HOPE) Award
  Lakehead University, 2016
- **Travel award** for 99th Canadian Chemistry Conference and Exhibition, Halifax, NS
  Analytical Chemistry Division, Chemical Institute of Canada, 2016
- **Attendance Grant** for 2nd International Conference on Infectious Disease and Nanomedicine, Kathmandu, Nepal
  European Society of Clinical Microbiology and Infectious Diseases (ESCMID), 2015
- **NSERC Postgraduate Scholarship-Doctoral Program (PGS D)**
  Natural Sciences and Engineering Research Council of Canada, 2015
- **Ontrario Graduate Scholarship (OGS)-2015 (declined)**